AD NUMBER

AD871583

LIMITATION CHANGES

TO:

Approved for public release; distribution is unlimited.

FROM:

**Distribution authorized to U.S. Gov't. agencies and their contractors;
Administrative/Operational Use; APR 1970. Other requests shall be referred to Air Force Rocket Propulsion Lab., Edwards AFB, CA 93523.**

AUTHORITY

AFRPL ltr 4 Mar 1974

AFRPL-TR-70-49

IMPROVED DESIGN PROCEDURES for THRUST TERMINATION of SOLID PROPELLANT MOTORS

Ralph L. Coates
M. Duane Horton

Brigham Young University
Provo, Utah

TECHNICAL REPORT AFRPL-TR-70-49

April 1970

Air Force Rocket Propulsion Laboratory
Air Force Systems Command
Edwards Air Force Base, California

114

"When U. S. Government drawings, specifications, or other data are used for any purpose other than a definitely related Government procurement operation, the Government thereby incurs no responsibility nor any obligation whatsoever, and the fact that the Government may have formulated, furnished, or in any way supplied the said drawings, specifications, or other data, is not to be regarded by implication or otherwise, or in any manner licensing the holder or any other person or corporation, or conveying any rights or permission to manufacture, use, or sell any patented invention that may in any way be related thereto."

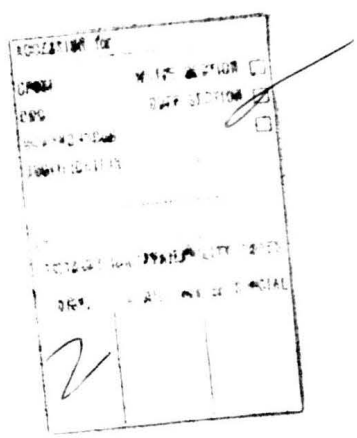

Unclassified

Improved Design Procedures for Thrust Termination of Solid Propellant Motors

Ralph L. Coates
M. Duane Horton

Unclassified

FOREWORD

The work described in this report was performed by R. L. Coates and M. D. Horton, Associate Professors of the Chemical Engineering Department of the Brigham Young University. They were assisted by Robert Bingham and Curtis Morgan, students. The work was sponsored by the Air Force Rocket Propulsion Laboratory under contract No. F04611-69-C-0045, and monitored by Captain Charles E. Payne and by Captain Leigh Stamets, RMPCP. The work was initiated 1 February 1969 and terminated 31 January 1970. This report was submitted for approval 27 February 1970.

This report contains no classified information extracted from other classified documents.

This report has been reviewed and approved.

Leigh E. Stamets, Captain, USAF
Project Engineer

ABSTRACT

The objective of this project was to carry out both experimental and analytical studies leading to improved design procedures for predicting thrust termination of single-chamber controllable solid motors. The experimental work consisted of measuring quantitatively the effects of incident thermal radiation on low pressure burning rates and deflagration limits of typical solid propellants. A technique was developed in which small cylindrical samples of the propellant were burned inside an electrically heated tube furnace. At furnace wall temperatures up to 1500°F, the burning rates were observed to be as much as 50% greater at 10psia than they were when surrounded by room temperature walls. Analytical work was performed using an improved mathematical model of the transient combustion process of a solid propellant. This study led to the conclusion that experimentally characterizing the extinguishability of a propellant in terms of a critical dp/dt provided very little useful design information. On the other hand, characterizing extinguishability in terms of the product $L_f^* \bar{r}_f^2$ was shown to provide a design criteria with the promise of very general applicability.

TABLE OF CONTENTS

LIST OF TABLES

LIST OF ILLUSTRATIONS

I

INTRODUCTION

The accurate prediction of the thrust of a rocket motor during the transient periods that precede or follow steady-state operation is a difficult problem. Even with simplifying assumptions, the mathematics describing the conservation of mass and energy are complex and, more importantly, the burning characteristics of the propellant under transient conditions are not fully understood. Difficulty notwithstanding, obtaining satisfactory solutions to this problem is becoming more critical. This aspect of design is especially important for controllable motors or for conventional motors having thrust termination capabilities. The need for improved design capabilities is indicated most forcefully by the recent failures of scaled-up research motors to completely terminate thrust on command (1). Instead of shutting down as had been predicted on the basis of small-scale data, the motors continued to burn at a low level.

The research reported herein was designed to provide information to improve the ability of the motor designer to accurately predict marginal extinguishment conditions. The work was planned around two important observations: (1) the steady-state low pressure strand burning-rate data that is often used for motor design purposes can be seriously in error because of thermal radiation effects, and (2) correlations can be made which indicate that the extinguishability of a wide variety of propellants increases inversely with the steady-state burning rate. The first observation indicated a need for improved methods for obtaining laboratory data. The second observation indicated a need for analytical work leading to more acceptable general correlations.

The work accomplished can be logically divided into four phases: Experimental Work, Data Compilation and Correlation, Parametric Design Studies, and Recommended Design Procedures.

It should be noted that the analytical work was directed specifically toward applications in the design of single-chamber controllable motors; however, the conclusions regarding low pressure burning rates and the sizing of the nozzle area can also be applied in the design of the aft chamber of a dual-chamber controllable motor. The problem of spontaneous reignition following thrust termination was not considered during this study.

II

EXPERIMENTAL WORK

1. Objectives

One design technique employed to insure extinguishment of single-chamber controllable solid-motors is to size the nozzle throat area such that with the nozzle fully open the motor L* and pressure will both be less than some critical value. The magnitudes of these critical values are determined empirically using test firings of small motors (2).

Problems have been encountered in the use of this technique because the steady-state burning rates determined in small motors or with strand burners, which are used to compute the full-scale nozzle throat area, can be significantly less than the burning rates that occur in the full-size motor (1). This discrepancy in burning rate can lead to continued burning after the nozzle pintle has been withdrawn, rather than extinguishment.

The objective of this phase of the program was to investigate methods for reliably characterizing, in the laboratory, the low-pressure burning rates and deflagration limits that might be expected in full-scale motors. It was reasoned that the principle difference between the combustion process in full-scale motors and in small motors or strand burners was the net supply of thermal radiation to the burning surface of the solid propellant. In the full-scale motor, the surface would be exposed either to additional burning surface or to the hot insulation covering the nozzle and pintle housing. Thus the net supply of thermal radiation incident to the burning surface would be near zero, or positive if the insulation surface were at a higher temperature than the propellant surface. On the other hand, in the strand burner the burning surface would be exposed to the cold walls of the pressurizing container and the net supply of thermal radiation would be negative. In small motors the ratio of burning surface area to the total surface area of the combustion chamber is usually considerably less than it is in full-scale motors, and the exposed area is not so well insulated. Thus, the net incident thermal radiation to the burning surface may also be negative in small motors.

2. Apparatus

The temperature at the surface of burning propellants has been measured by various means (3, 4) and typically has been reported to be near 1000-1100°F (550-600°C). Therefore, if the large motor environment is to be simulated in a laboratory strand burner, the strand should be exposed to inert surfaces heated to

temperatures in this range, or higher, or the propellant sample should be prepared in such a way that the burning surface is exposed principly to additional burning surface.

In exploratory experiments conducted at BYU prior to this program, strands of an ammonium perchlorate-oxidized composite propellant were burned both in the conventional manner and also by placing two strands end to end so that their burning surfaces were opposed. At 1 psia the burning rate of single strands was 0.028 in/sec and the burning rate of the opposed strands was .053 in/sec. This large difference in burning rates could have been partly due to differences in convective heat transfer resulting from the different velocities of the combustion products relative to the burning surfaces. Similar uncertainties were encountered using different sample configurations to simulate motor conditions. It was decided early in the program, therefore, to construct a strand burner with heated walls in order that the effects of incident thermal radiation might be isolated.

Figure 1 shows a diagram of the apparatus that was constructed. The basic part of this apparatus is a tube-furnace, Model No. 423, manufactured by Electro Applications, Incorporated. This furnace is rated at 1200 watts and with an alumina tube can be operated at temperatures up to 2750°F. In initial tests with propellant samples inside the furnace, the alumina tubes fractured due to thermal shock following ignition of the sample. Consequently, the alumina was replaced with a tube made of stainless steel. This tube, which is 2-1/4" O.D. with .065" wall, type 347, has performed satisfactorily. Because of its greater thermal conductivity, however, more heat is conducted to the cooling coils at the sides of the furnace, and the maximum operating temperature is approximately 1500°F.

3. Experimental Procedure

Prior to placing the propellant sample into the heated section of the tube, this section is allowed to reach the temperature specified for the test. Electrical current is supplied to the heating wires of the furnace through an automatic controller which employs a thermocouple sensor inside the heated section. The controller automatically adjusts the electrical current to maintain the desired temperature.

The tube-furnace is connected through a large tank to a high capacity vacuum pump. The pressure in the tank is regulated by controlling air leakage into the tank through a bleed-valve. A small flow of nitrogen is admitted to the tube to provide a continuous purge during the test.

The propellant sample was placed in the heated section with a hand-operated push rod. Immediately after it had reached the proper position, controlled by a pin on the push-rod, it was ignited. Ignition was accomplished with an electrically-heated nichrome wire in contact with propellant surface, the surface previously

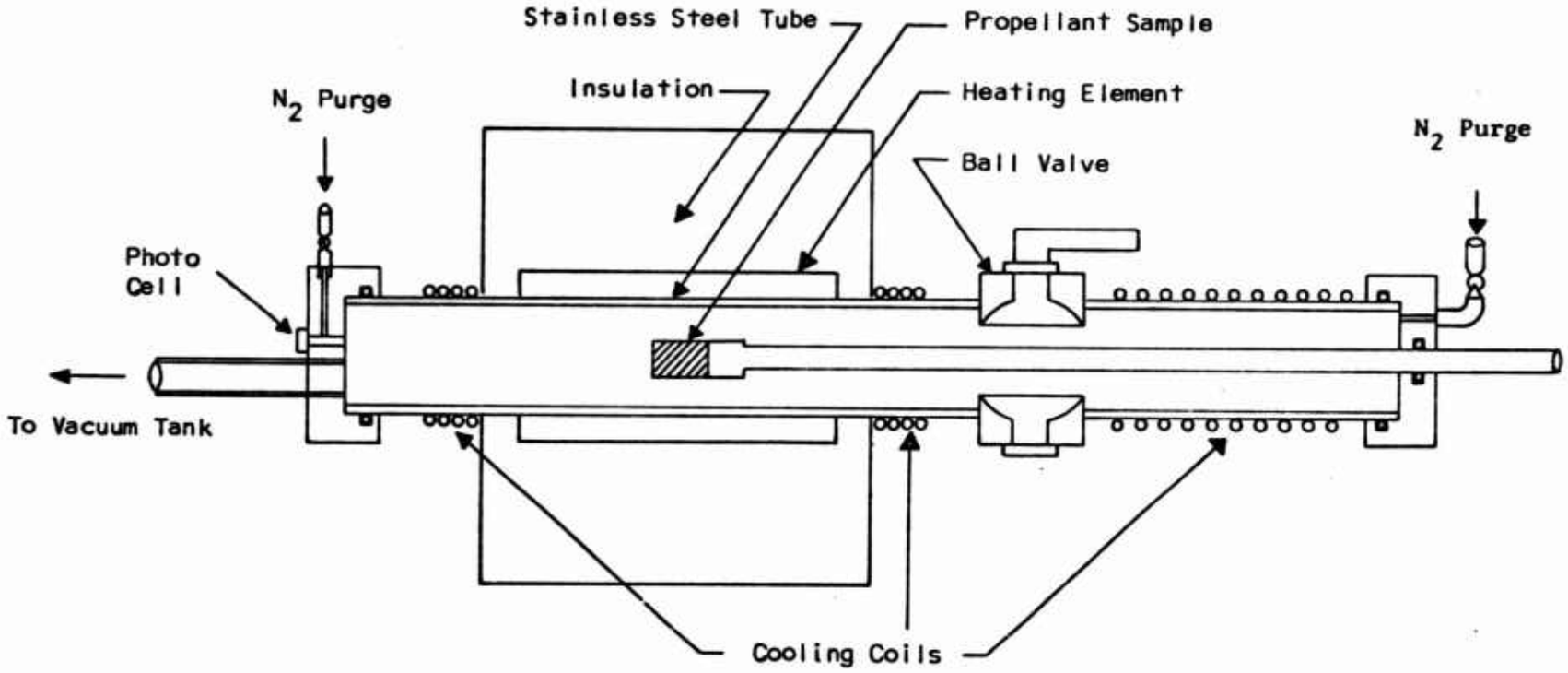

Figure 1. Diagram of tube-furnace apparatus

being coated with a paste consisting of potassium perchlorate, ammonium perchlorate, titanium, boron, and polyisobutylene.

The burning time of the sample was detected with a photocell, Raytheon EM1502, mounted in the end-cap of the tube. The photocell signal, along with the signal from a pressure transducer also mounted in the end-cap, was recorded using a Honeywell Model 1508 Visicorder.

Several different sample configurations were tried. The configuration providing the most reliable data was a solid cylinder, 0.75 inches in diameter, with lengths ranging from 0.1 to 0.6 inches. The ends of these samples were machined to insure that they were parallel and that accurate measurements could be made of the burn distance. The samples burned from one end, the cylindrical surfaces being inhibited with a coating of silicone grease immediately prior to testing. To determine the burning rate at a given pressure and tube temperature, three or more samples of each of three different lengths were prepared. These were then cemented to sample-holders which could be attached to the end of the push rod. The burning times for each of these samples were then measured and the average burning rate computed from the burning time-sample length data. Figure 2 illustrates the type of photocell data that was obtained.

Similar data were also obtained with cylindrical samples inhibited on the end rather than on the cylindrical sides. These samples burned radially. The diameter of these samples was varied, rather than the length, and the burning times measured as a function of radial burn distance.

4. Data Reduction Method

An illustration of the burning time data, plotted versus the sample length, is shown in Figure 3. As indicated by this figure, the burning times can be correlated by an equation of the form $\hat{t} = \hat{a} + \hat{b}L$. The reciprocal of b, or the slope of the lines, represents the burning rate.

The best fit line was determined by the method of least squares for each set of data. An estimate of the reliability of the burning rate was then made following regression analysis procedures (33). According to these procedures, the estimated standard error in time predicted by the best fit equation $t = a - bL$ is

$$S_t = \left[\sum_i (t_i - \hat{t}_i)^2/(N-2)\right]^{1/2} \quad \ldots\ldots\ldots\ldots (2.1)$$

where t_i is the measured time and $\hat{t}_i$ the predicted time for a sample of length L_i, and N is the number of data points. The corresponding standard error in the slope $\hat{b}$ is

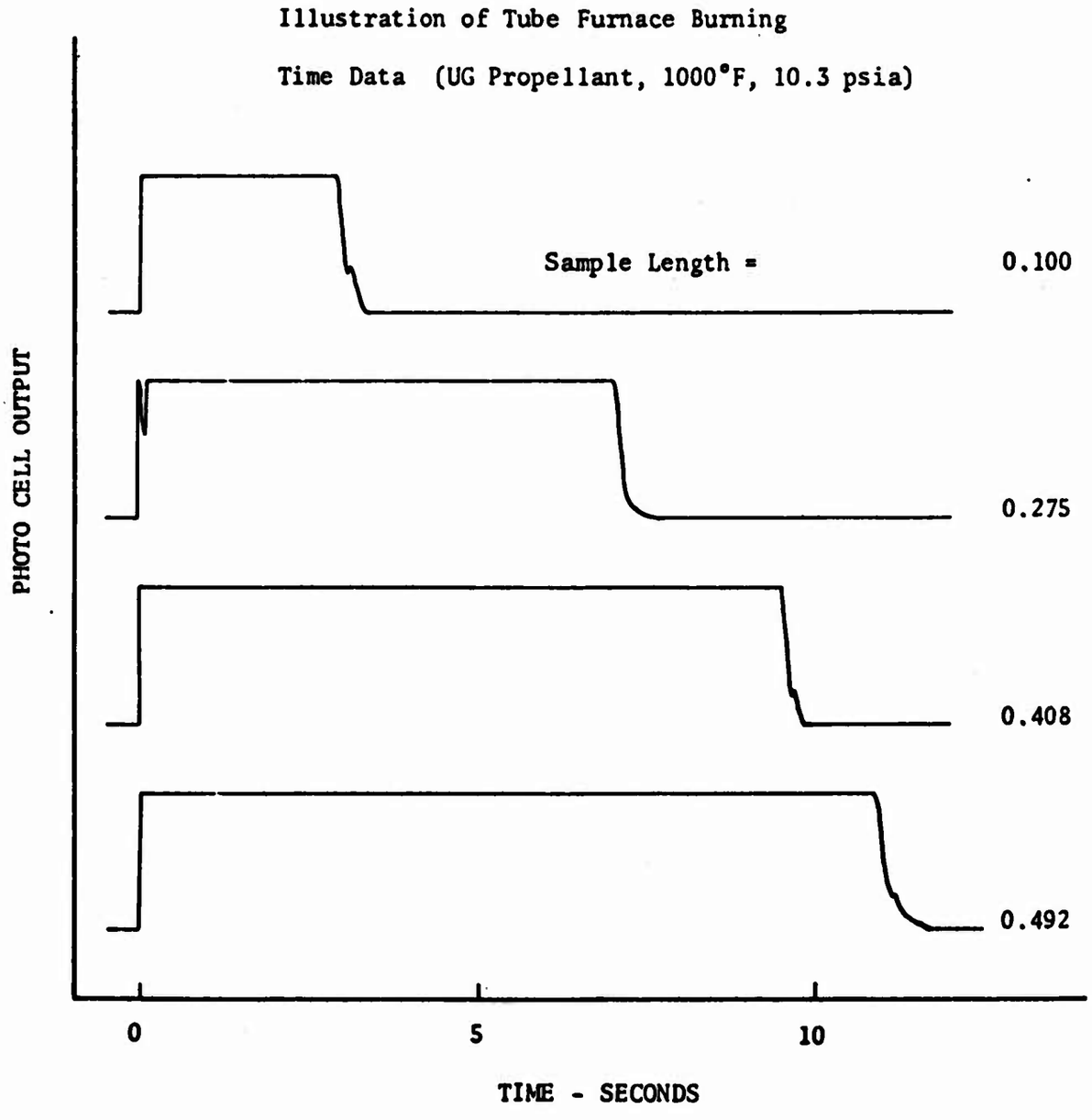

Figure 2. Example of photo cell data used to compute burning rates

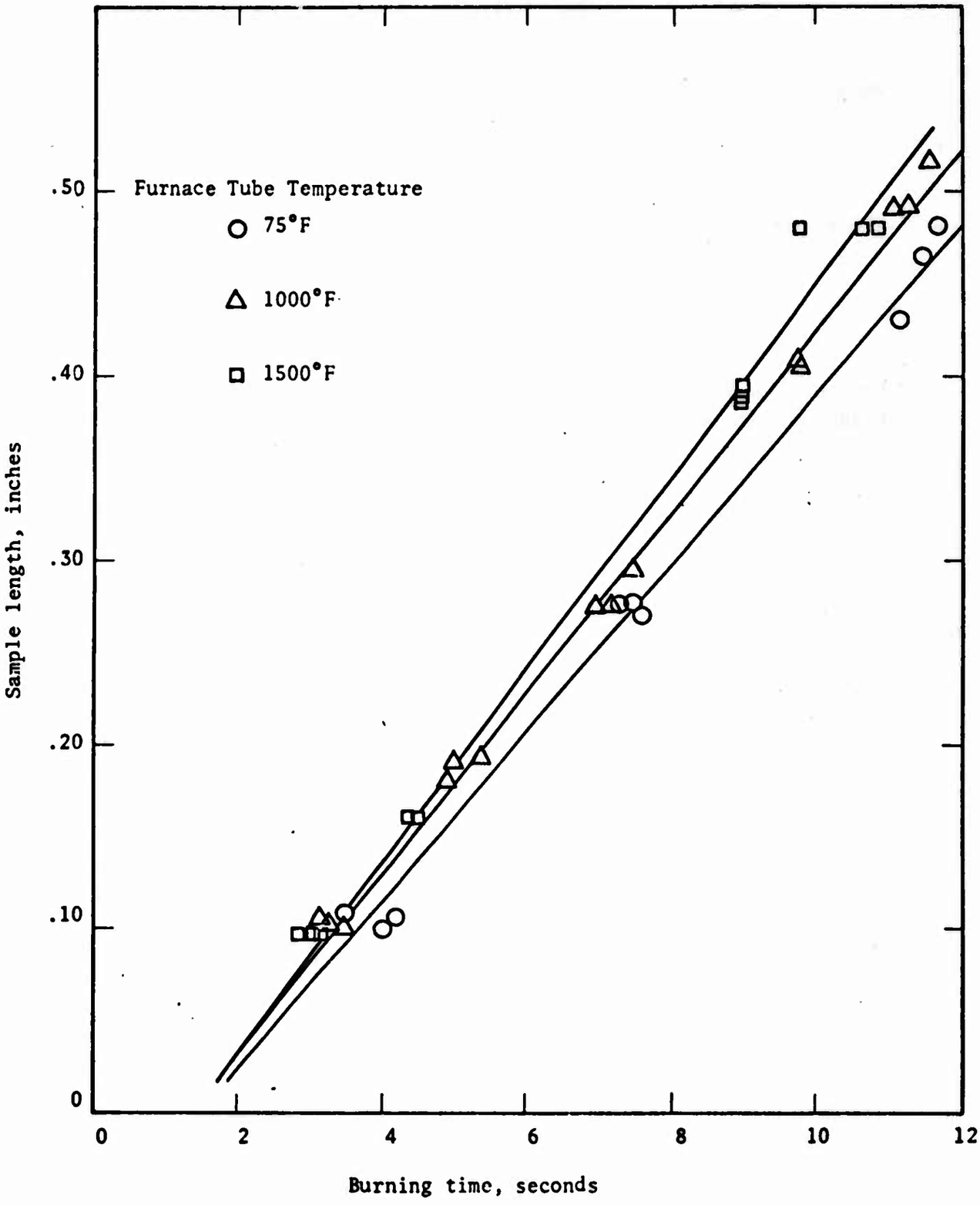

Figure 3. Example of tube-furnace data illustrating effect of thermal radiation on burning times.

$$S_b = S_t / \left[\sum_i (x_i - \bar{x})^2 \right]^{1/2} \quad \ldots\ldots\ldots\ldots\ldots (2.2)$$

where

$$\bar{x} = \sum_i x_i / N \quad \ldots\ldots\ldots\ldots\ldots\ldots (2.3)$$

The 95 per cent confidence limits in $\hat{b}$ would then be given approximately by

$$b = \hat{b} \pm 2S_b \quad \ldots\ldots\ldots\ldots\ldots\ldots (2.4)$$

The corresponding 95 per cent confidence limits on $\hat{r} = 1/\hat{b}$ would then be given to the same degree of approximation by

$$r = \hat{r} \pm 2S_b / (\hat{b})^2 \quad \ldots\ldots\ldots\ldots\ldots (2.5)$$

5. Experimental Results

Table 1 summarizes the experimental burning rate data obtained during this project. The measured burning times and sample lengths for each test are tabulated in the Appendix. Five different propellants were tested during the course of the testing program. All of the propellants were ammonium perchlorate oxidized composites. The propellant designated E-107 has a polyurethane binder with aluminum. Propellant UG consists of 18 per cent polybutadiene-acrylic acid binder with 82 per cent ammonium perchlorate. Propellant AGC 64-1106 has a carboxyterminated polybutadiene binder with aluminum. Propellant A-13 consists of a polybutadiene-acrylonitrile binder and ammonium perchlorate in the ratio 76/24. Propellant AAP-3318 is similar to AGC 64-1106 but with part of the ammonium perchlorate replaced with potassium perchlorate. The test condition variables, in addition to furnace temperature, were sample configuration and furnace pressure.

Effect of furnace temperature. The effect of the furnace tube temperature on the burning rates at 10.3 psia of propellants AGC 64-1106, UG, and E-107 are shown in Figure 4. Approximate incident radiant flux levels corresponding to the measured tube temperatures are shown on this figure. These flux levels were estimated using the equation

$$\dot{q} = F_{12} \sigma (T_s^4 - T_w)^4$$

TABLE 1. Summary of Data Obtained with Tube-Furnace

Propellant Designation	Furnace Temperature of:	Mean Burning Rate, inches/second				Deflagration Limit, psia
		Radial Burning Samples			End Burning Samples	
		2.5 psia	4.9 psia	10.3 psia	10.3 psia	
E-107	75			.016 ± .002		
	1000			.024 ± .002		
	1500					
UG (Ref. 5)	75	.023 ± .004	.027 ± .004	.043 ± .001	.047 ± .003	1.7
	1000		.038 ± .007	.049 ± .001	.049 ± .002	1.5
	1500		.036 ± .002	.067 ± .010	.052 ± .003	
AGC 64-1106 (Ref. 10)	75		.020 ± .002	.028 ± .004	.037 ± .002	2.0
	1000		.026 ± .002	.037 ± .002	.038 ± .003	1.5
	1500		.025 ± .003	.045 ± .005	.045 ± .004	
A-13 (Ref. 18)	75				.039 ± .004	
	1000				.038 ± .004	
	1500				.040 ± .007	
AAP-3318 (Ref. 25)	75				.037 ± .008	
	1000				.032 ± .004	
	1500				.044 ± .007	

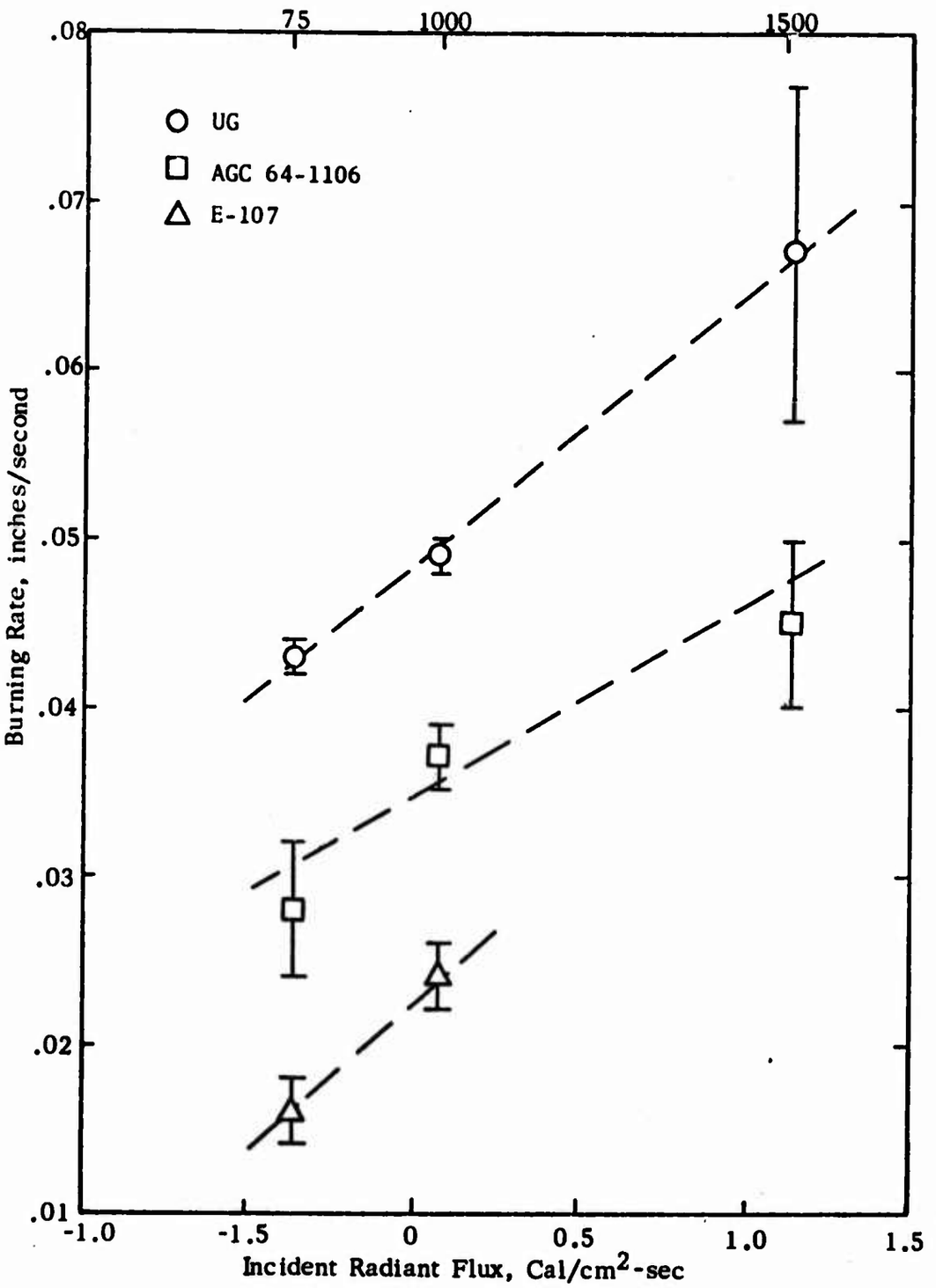

Figure 4. Data showing effect of thermal radiation on burning rates at 10.3 psia.

with F_{12} assumed to be 0.8, T_S assumed to be 450°C (940°F), and T_W the wall temperature. Recent attempts at measuring T_S (5) for similar AP-oxidized propellants have shown it to be in the range of 500-740°C at pressures near 100 psia. The temperature would be expected to be lower at the pressures employed for the furnace tests, assuming an Arrhenius relationship between T_S and burning rate. Consequently, the value of 450°C was selected as a representative value in order to estimate the net radiant flux. It is noted that with these assumptions there is a loss of approximately 0.4 cal/cm^2 sec from the burning surface when the propellant is exposed to room-temperature surroundings.

The data shown in Figure 4 indicate that the burning rates of the UG and AGC propellants were increased by approximately 50 per cent as the furnace tube temperature was increased from room temperature to 1500°F, while for E-107 propellant a 50 per cent increase occurred when the temperature was raised from room temperature to 1000°F. These data clearly indicate a strong effect of thermal radiation on burning rate at this pressure.

Data for A-13 and AAP-3318 propellants illustrated in Figure 5 do not show the same magnitude effect as for the other propellants. Difficulty in igniting these propellants was experienced, however, and the data are somewhat questionable.

Effect of sample configuration. Initial tests with the AGC 64-1106 propellant were made with radial burning cylindrical samples of propellant inhibited on the ends. Subsequent tests made with end-burning cylindrical samples, with the sides inhibited, resulted in substantially higher average burning rates with the furnace at room temperature. The room temperature mean rate for radial burning was .028 inches/sec while the end-burning mean rate was .037 inches/second.

This difference was thought to be due to the proximity of the cold stainless steel tube to the burning surface. The minimum clearance between the burning surface and the tube wall in this configuration was 0.66 inches, whereas in the end-burning configuration the burning surface was perpendicular to the center line of the tube and the motion of the combustion products was unobstructued. To test this hypothesis, tests were made using the radial-burning configuration with the furnace tube replaced by a large-diameter lucite tube. In these tests the clearance between the burning surface and the tube wall was increased to 2.60 inches. The mean burning rate at room temperature was observed to be .030 inches/sec in this configuration, nearly the same as with the small-diameter tube, indicating that the cold wall did not cause the rate to be reduced.

Figure 6 presents a comparison of the data for the different configurations. There appears to be no effect of the configuration when the tube is heated; however, taking into account the uncertainty in the data, the radial-burning configuration appears to result in lower rates for this propellant when the tube is unheated. No suitable explanation for this effect can be given at this time.

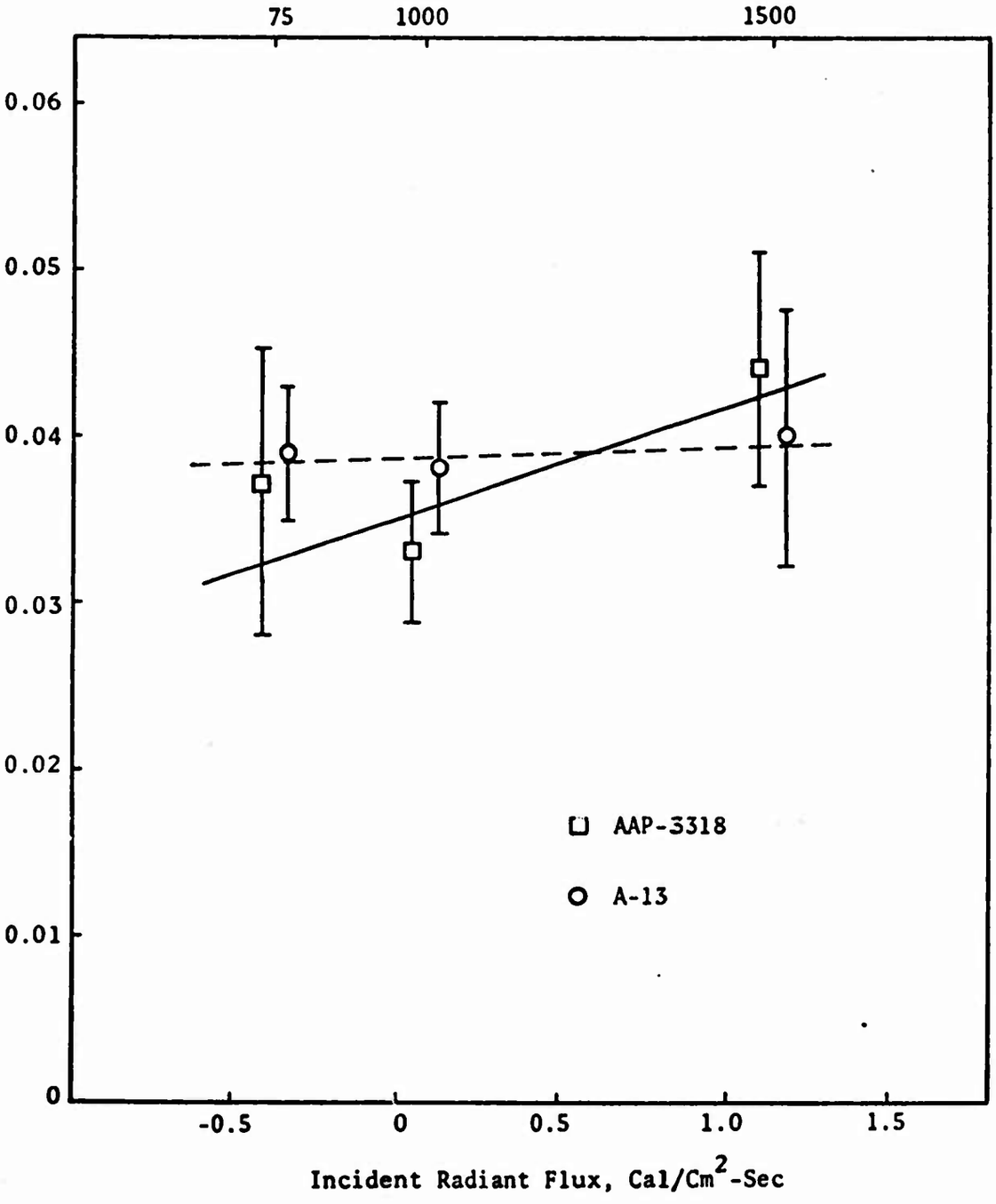

Figure 5. Data showing effect of thermal radiation on burning rates

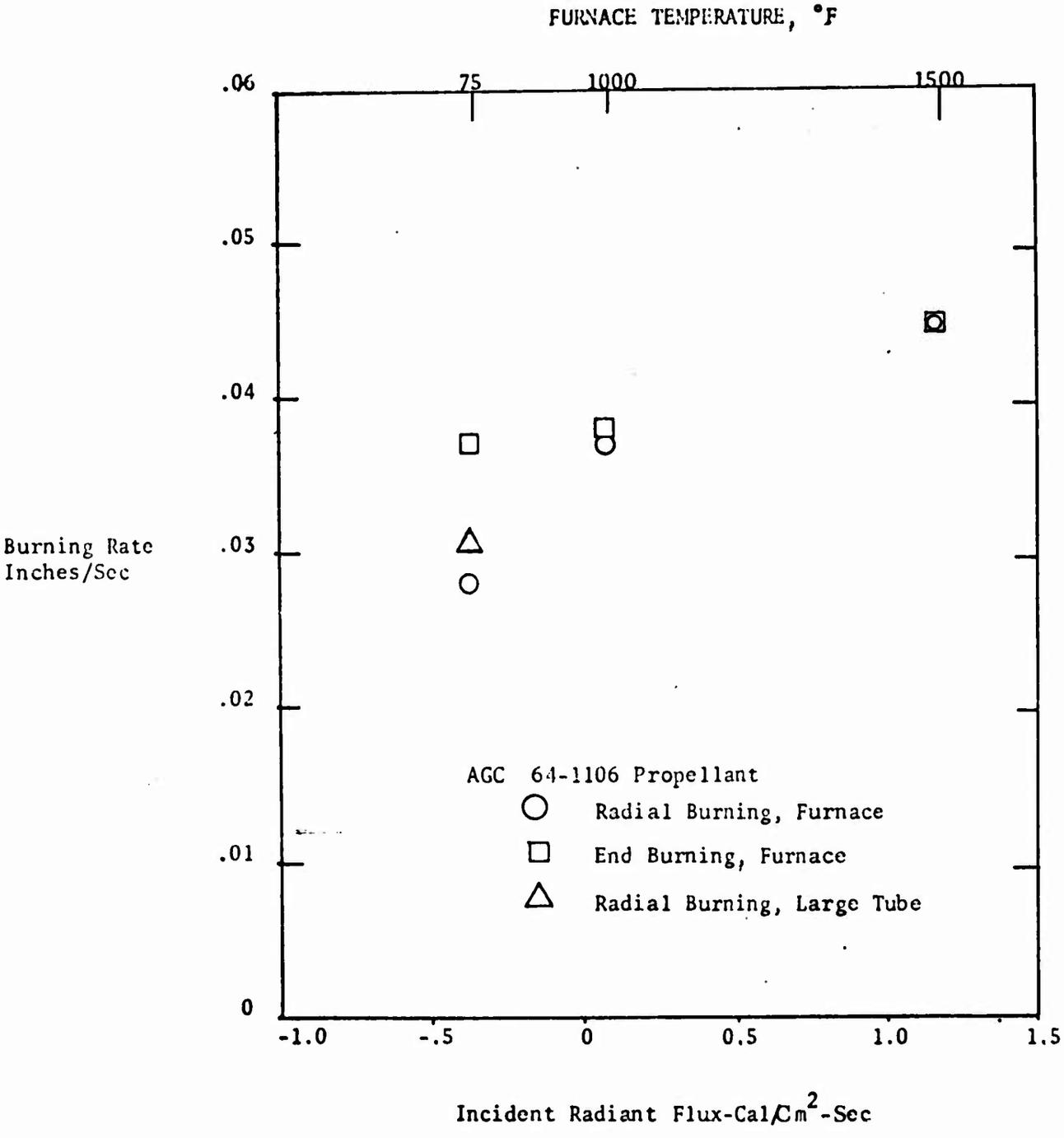

Figure 6. Data showing the effect of sample configuration on measured burning rates

Tests with both radial and end-burning configurations were also made with the UG propellant. For this propellant, the differences in the mean rates were within the uncertainty limits, indicating no significant effect of configuration differences.

Effect of pressure. Figure 7 illustrates the effect of varying the pressure in the tube-furnace. This figure presents data obtained with UG propellant at pressures of 2.5, 4.9, and 10.9 psia. The room temperature (75°F) data is seen to correspond well with conventional strand burner data for this propellant reported by Lockheed Propulsion Company (5).

Effect of radiation on P_{DL}. A limited study was made of the effect of the thermal radiation from the furnace tube on the deflagration limit of the propellant. The results of these experiments are also listed in Table 1.

These experiments were conducted by placing two valves between the tube furnace and the evacuated tank, a metering valve and a fast-acting solenoid valve. Prior to ignition, the pressure in the tube was adjusted to slightly less than atmospheric with the solenoid valve closed. The sample was then ignited and the solenoid valve opened, causing the tube pressure to drop at a rate governed by the metering valve. The deflagration limits were assumed to be indicated by the photocell signal falling off. The sample was withdrawn from the heated tube at this point, the remaining unburned propellant confirming that extinguishment had occurred. To insure that a depressurization effect was not affecting the data, the experiments were repeated at different metering valve settings.

Figure 8 presents data obtained in this manner for the AGC propellant. These data indicate the P_{DL} was reduced approximately from 4 in. Hg to 3 in. Hg, absolute pressure, when the sample was exposed to 1000°F tube walls. Additional data for this propellant and UG propellant are listed in Table 1.

Attempts at measuring the P_{DL} with a tube temperature of 1500°F were unsuccessful. The samples always were consumed even though the photocell indicated extinguishment might have occurred.

Conclusions. These tests show that quantitative measurements can be made in the laboratory which show the effect of incident thermal radiation on solid propellant burning rates. At sub-atmospheric pressures, where the burning rates are low, radiant fluxes corresponding to surrounding walls at 1500°F can cause the burning rates to be as much as 50 per cent greater than those measured under conventional strand burner conditions. This large effect should obviously be considered in the ballistic design of controllable solid propellant motors, and the tube-furnace technique employed in this project can be applied to obtain this data. Additional work should be done to improve the accuracy of the data.

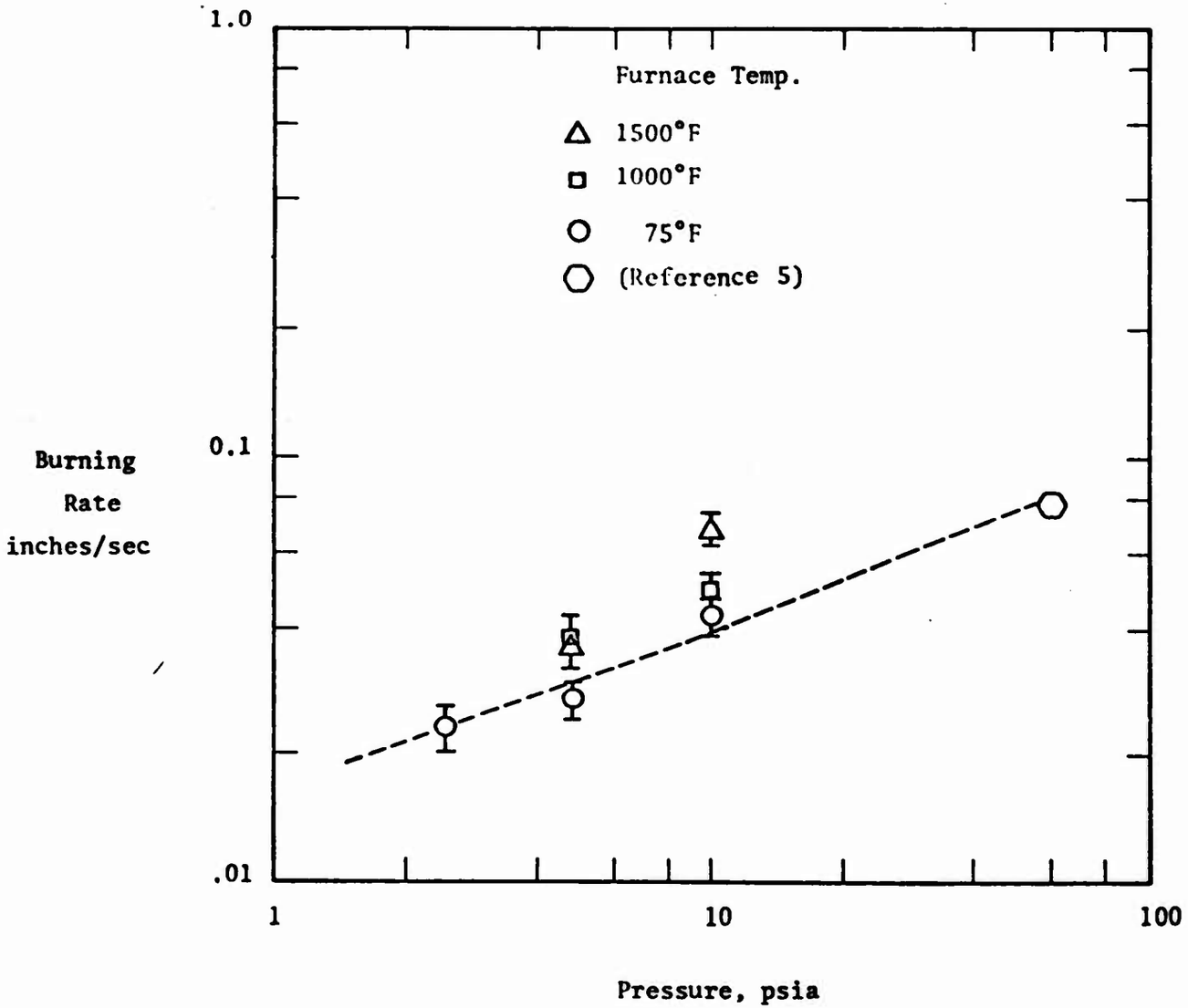

Figure 7. Data showing the effect of pressure on measured burning rates

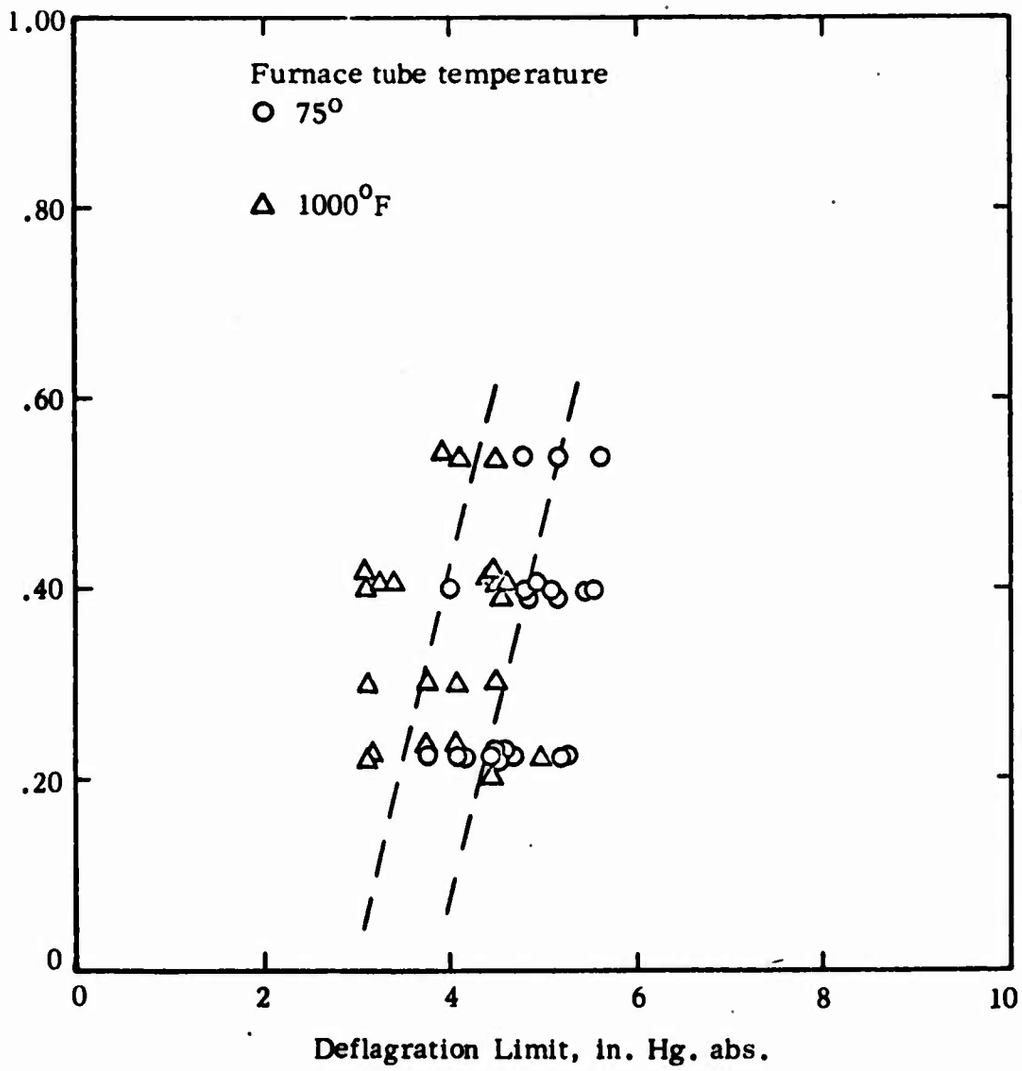

Figure 8. Data showing the effect of thermal radiation on deflagration limit.

III

DATA COMPILATION AND CORRELATION

1. Survey of Published Experimental Data

This survey covers in an historical fashion the work done in the experimental field of propellant extinguishment via rapid depressurization. Data from nine different sources are tabulated in this section. Table 2 lists the nomenclature used in these tables.

References 6, 7, and 8 describe the work of Ciepluch who performed the original set of experiments in this field. The extinguishment experiments were performed by burning a slab of propellant in a specially designed small motor that contained two nozzles. The slab weighed about 1 pound and was placed on the side of the motor so that the gas flow was parallel to the propellant surface. The experimental technique consisted of first igniting the small motor and permitting it to reach a stable operating pressure, one nozzle being closed. At this time, the second nozzle was opened by means of an explosive bolt, causing rapid depressurization. The motor was then examined to determine whether there was any propellant left or whether it had all been consumed. If no propellant remained, the test was classified as a non-extinguishment test. If propellant remained in the motor, extinguishment was said to have occurred. Table 3 summarizes the experimental data reported in these three references.

Marginal extinguishment conditions were expressed in terms of a characteristic depressurization time above which the grain burned out without extinguishment. This characteristic time was defined as that necessary to depressurize the chamber to one-half its initial pressure and was designated as $t_{1/2}$. Later investigators have used both this time and the corresponding average depressurization rate between the initial pressure, P_i, and $P_i/2$. Figure 9, taken from reference 7, illustrates this kind of experimental data.

The Ciepluch technique was followed by nearly all subsequent investigators except that in some cases the propellant configuration was altered and different methods were used to increase the nozzle area.

Reference 9 describes the work conducted by Amcel Propulsion Company. The extinguishment portion of that program was secondary to the major objectives of developing a controllable motor, and only one propellant was tested. Table 4 lists the data for the propellant tested in that program.

In 1964, Aerojet General Corporation began a major program in this area. Table 5 summarizes data extracted from the reports describing the work performed

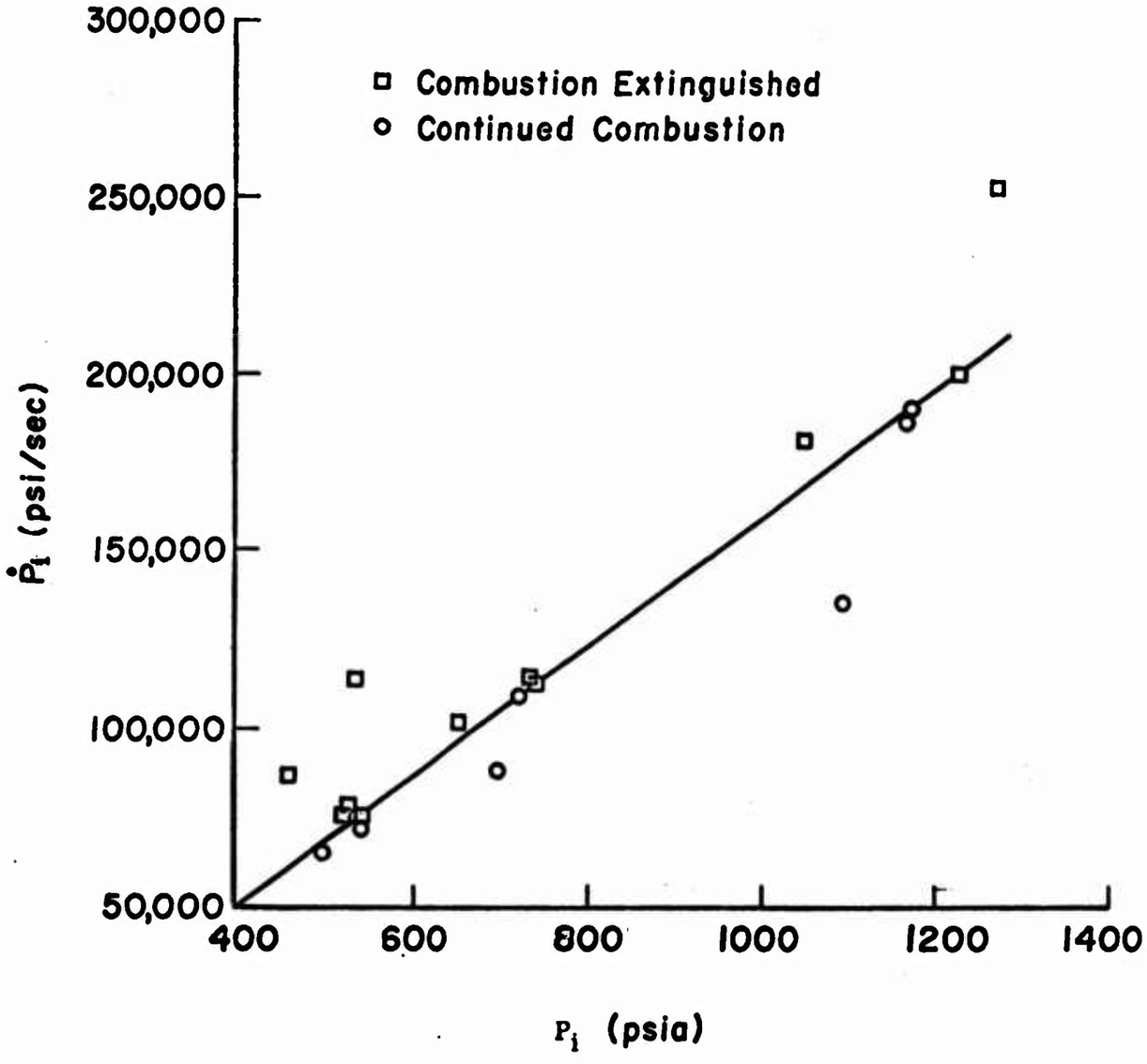

Figure 9. Example of method of correlating $\dot{P}$ extinguishment conditions (Ref. 7)

under several different contracts (2, 10, 11, 12). The test motor geometry used for most of the data reported was very similar to that used by Ciepluch except for the fact that 3" O.D., one-pound, end-burning grains were used rather than side-burning slabs. Some data were also obtained in large motors, however.

Table 6 summarizes the data obtained by Hercules, Inc., at their Bacchus Plant (13). In this investigation they studied the extinguishability of double-base solid propellants and used a motor which was virtually identical to that of Ciepluch's.

Table 7 and Reference 14 present the data and results obtained at the University of Utah. Their experimental procedure was unique in that they used a strand of propellant burning in a very large volume so that a single nozzle was used to control the depressurization. This nozzle was closed at the beginning of a test. Thus, in this experimental technique, the pressure in the chamber would begin to rise very slowly upon ignition of the strand. However, because the strand burning area was small compared with the free volume, the pressure rise rate was negligible. After stable combustion was realized, the nozzle was opened, causing depressurization. With this type of experimental setup, the single nozzle not only controls the depressurization rate but the final pressure if extinction does not occur.

The results of a Stanford Research Institute program are described in Reference 15 and Table 8. Only a limited amount of experimental data were obtained in this program, the effort being largely theoretical. Although differing in some details, the experimental motor and technique were essentially that used in the Aerojet program.

Table 9 and Table 10, respectively, describe the results recently obtained at the United Technology Center as reported in References 16 and 17. In these programs, a very extensive series of propellant formulations were tested for extinguishability characteristics. The extinction technique was similar to that used by Ciepluch. However, several different grain configurations were used in this study, including strands, end-burning grains, slabs, and tubular internal burning grains. Because the data from these programs are presented more completely than those from other programs, Tables 9 and 10 contain the data probably of most use to other investigators.

Reference 18 and Table 11 describe the results of an experimental program carried out at Brigham Young University. The technique used was essentially that of Aerojet except the end-burning grains were only 1-1/4 inches in diameter. Because it has become apparent that the data as reported in Reference 18 were not sufficient for many purposes, the data contained in the present survey have been expanded over that originally presented.

Table 12 describes the results obtained in the program of Atlantic Research Corp. (19). The experimental technique used was essentially that used at the University of Utah in that an extremely large volume of gas made the use of a primary nozzle unnecessary and a single nozzle controlled the entire blowdown. References 20-24 also contain additional experimental data describing the extinguishment of burning solid propellants. However, either the data were taken in a much different manner than described above or are not reported in sufficient detail to permit comparison with the data listed herein.

TABLE 2. Nomenclature Used in Survey Tables (Tables 3-12)

A_{n_f}/A_{n_i}	The area of the secondary nozzle divided by the primary nozzle area
dlnP/dt	$\dot{P}/P_o$
n_i	The exponent in the burning rate law $r=ap^n$ at P_o
$\dot{P}$	The initial depressurization rate when the secondary nozzle opens
P_a	The ambient pressure
P_i	Chamber pressure prior to the opening of the secondary nozzle
P_{dl}	The deflagration limit of the propellant
r_i	Burning rate of the propellant at P_i
$t_{1/2}$	The time required for the chamber to depressurize to $P_i/2$
T_f	Adiabatic flame temperature

TABLE 3. Extinguishment Data, NASA Lewis Research Center
Investigator: Carl C. Ciepluch

Propellant	C1	C2	C3	C4	C5	C6	C7	C8	C9	C10	C11	C12	C13	D
Binder Type	PBAA	PBAA	PBAA	PBAA	PBAA	PBAA	PBAA	PBAA	PBAA	PBAA	PBAA	PBAA	PBAA	PU
Conc. %	24.8	18.8	13.8	18.8	18.8	13.8	18.8	18.8	18.8	15.8	15.8	15.8	15.8	19.0
Oxidizer	AP	AP	AP	AP	AP	AP	AP	AP	AP	AP	AP	AP	AP	AP
Particle Size, μ	70C/30F	70C/30F	70C/30F	70C/30F	77C/23F	70C/30F	85C/15F	100F	100C	70C/30F	70C/30F	70C/30F	70C/30F	77C/23F
Conc. %	75.0	81.0	86.0	79.0	72.0	76.6	65.0	72.0	72.0	81.0	81.0	81.0	81.0	72.0
Additive	MgO	MgO	MgO	MgO	MgO	MgO	MgO	MgO	MgO	MgO	MgO	MgO	MgO	---
Conc. %	0.2	0.2	0.2	0.2	0.2	0.2	0.2	0.2	0.2	0.2	0.2	0.2	0.2	---
Additive	---	---	---	Al	Al	Al	Al	Al	Al	Al_2O_3(F)	Al_2O_3(C)	KF(F)	KF(C)	Al
Conc. %	---	---	---	2.0	9.0	9.4	16.0	9.0	9.0	3.0	3.0	3.0	3.0	9.0
P_i, psia	500	500	1200	500	500	500	1200	500	500	500	500	500	500	500
r_i, in/sec	.221	.263	.315	.355	.278	.263	.350	.31	.24	.643	.246	.364	.387	.315	.319	.260
n_i	.584	.240	---	.251	.294	.337	---	.482	.29	.46	.65	.33	.30	.25	.36	.34
P_a, mm Hg	3.5	3.5	3.5	3.5	3.5	3.5	3.5	3.5	3.5	3.5	3.5	3.5	3.5	3.5	3.5	.8 to 8.8 psia
T_f, ^oK	---	2410	2850	2500	2730	2730	3190	2900	2730	2730	2665	2665	2656	2656	2730

TABLE 3. Continued

Propellant	C1	C2		C3	C4	C5		C6	C7	C8	C9	C10	C11	C12	C13	D
$t_{1/2}$, exting. msec	5.4	3.9	3.2	2.9	4.0	3.7	3.1	2.4	3.7	4.0	5.7	2.7	2.6	5.1	3.7	3 to 9

References: NASA Tech. Note D-1559, December 1962; ARS Journal 31, 11 (1961); (Propellant Data)

TABLE 4. Extinguishment Data, Amcel Propulsion Co.

Propellant	PBO-13
Extinguishment	
$\dot{P}$, 10^3 psi/sec	38
P_i, psia	1000
r_i, in/sec	.27
n_i	.65
P_a, psia	14.7

Reference: Second Annual Report, RRL-PT-4-64-52, September, 1964.

TABLE 5. Extinguishment Data, Aerojet General Corporation
Investigator: R. Lou and L. Landers

Propellant	CTPB Control	ANB 3178	ANB 3177	ANB* 3177	4095A	4095B	ANB 3180	AAB 3179	PU Control	AAB 3194	ANB 3153	ANB 2832	NP Control	BBD	NNOY	AAB* 3220
Binder	CTPB	CTPB	CTPB	CTPB	CTPB	CTPB	CCPB	CTPB	PU	PU	PU	PU	NP	CTPB	NPPU	PBO
P_{dl}, psia	1.5	1.7	2.5	2.5	4.9	2.4	3.0	2.0	1.2	2.0	2.8	.7	1.3	1.3	--	--
P_i, psia	400	600	450	450	400	400	400	400	400	400	400	400	400	400	700	200
r_i, in/sec	.161	.225	.21	.19	.176	.176	.168	.126	.24	.20	.082	.060	.48	.20	.316	.16
n_i	.32	.55	.60	.61	.50	.50	.56	.46	.51	.62	.21	.06	.56	.37	.56	.66
P_a, psia	1	1	1	Vac	1	1	1	1	1	1	1	1	1	1	14.7	--
Extinguish. $t_{1/2}$, msec	4.6	20.4	69.3	51	18	15	18	18	17	18	31	12	16	46	7	51

*Large motors described in the last reference, number 4, below.

References:
1. Aerojet General Corporation, Tech Report No. AFRPL-TR-65-256.
2. Aerojet General Corporation, Final Report on Contract AF04(611)-7889.
3. Aerojet General Corporation, Final Report on Contract AF04(611)-9962.
4. Aerojet General Corporation, Tech Report No. AFRPL-TR-67-300.

TABLE 6. Extinguishment data, Hercules, Inc.

Propellant	CYH		EJC	VHX	VHY	VHW	VHV	VCP	VIR
				(Modified Double Base)					
P_{dl}, psia	1.45		8.2	2.3	1.9	1.9	4.7	2.3	3.0
P_i, psia	512	366	420	360	380	340	400	400	380
r_i, in/sec	.434	.378	.41						
n_i	.55	.55							
P_a, psia	12.5	0.5	0.5-12.5	.5	.5	.5			
Extinguish. $\dot{P}$, 10^3 psi/sec	60	10	9.5	9.5	12	15	7	7	7

Reference: Final Report, Contract No. AF04(694)-127 WS-133A, 1965 PSP Task 8

TABLE 7. Extinguishment Data, University of Utah

Propellant	G	AH	GB	UA	AF	F	UF
Binder	PBAA	PBAA	PBAA	PBAA	PBAA	PBAA	PU
Conc. %	18	25	17	15	15	18	20
Oxidizer	Ap	Ap	Ap	Ap	Ap	Ap	Ap
Conc. %	82	75	80	73	73	80	80
Size, μ	200/15	15	200/15	15	200/15	200/15	200/15
Additive			Carbon Black	CUO_2O_2*	CUO_2O_2	CUO_2O_2	CUO_2O_2
Conc. %			2	2	2	2	
T_f, ^oK	2625	1988	2459				2598
P_{dl}, psia	.7		.92			.49	2.2
P_i, psia	90-175	70-150	90-175	90-175		90-175	90-175
r_i, in/sec	.16-.22	.17-.23	.16-.22	.37-.49		.28-.42	.15-.26
n_i	.5	.56	.50	.55		.38	.78-.31
P_a, psia	12.5	12.5	12.5	12.5	12.5	12.5	12.5
Exting. dlnP/dt	50	50	50	225	600	700	11

Reference: Final Report, Contract AFOSR 67-1901, September, 1966.

*CUO_2O_2 denotes copper-chromite manufactured by Harshaw Chemical Co.

TABLE 8. Extinguishment data, Stanford Research Institute

Propellant	PU174	PU193	PU185
Binder	PU	PU	PU
Conc. %	17.5	20	18.5
Oxidizer	AP	AP	AP
Conc. %	80	80	80
Size, μ			
Additive	Ethyl Siloxane		Fe_2O_3
Conc. %	2.5		1.5
T_f, ^oK	2600		
P_{dl}, psia	3.3	1.0	3
P_i, psia	500	470	750
r_i, in/sec	.19	.32	.37
n_i	.6	.5	.5
P_a, psia	7.8	5.2	6.0
Extinguishment $\dot{P}$, 10^3 psi/sec	19	14	27

Reference: QTR No. 5, Contract NAS 7-389, February, 1967.

TABLE 9. Extinguishment Data, United Technology Center
Investigator: C. E. Jensen

Propellant	9394	9377	9389	9395	9379	9710	9712	9711	9713	9714	9754	9757
Binder	CTPB	PBAN	PU	PEP	UTREZ	UTREZ	UTREZ	UTREZ	UTREZ	UTREZ	UTREZ	UTREZ
Conc. %	16	16	16	16	16	16	16	16	20	24	16	20
Oxidizer	AP	AP	AP	AP	AP	AP	AP	AP	AP	AP	AP	AP
Conc. %	84	84	84	84	84	84	84	84	80	76	84	84
Size, μ	30%8 70%190	30%8 70%190	30%8 70%190	30%8 70%190	30%8 70%190	30%8 70%190	30%8 70%190	30%8 70%190	30%8 70%190	30%8 70%190	30%8 70%400	30%8 70%190
T_f, ^oK	2660	2860	2730	2600	2685	2685	2685	2859	2278	1858	2685	2278
P_i, psia	250	400	225	350	250	400	350	150	300	280	200	200
r_i, in/sec	.18	.25	.21	.28	.14	.17	.16	.17	.12	.087	.10	.11
n_i	.37	.41	.39	.25	.36	.31	.38	.36	.31	.30	-.02	.37
P_a, psia	14.7	14.7	14.7	14.7	14.7	14.7	14.7	14.7	14.7	14.7	14.7	14.7
Exting. $\dot{P}$, 10^3 psi/sec	29	52	12.5	36	12	20	18	18	7.5	4.5	8.5	5

Reference: Final Technical Report, Contract NAS 1-6601, UTC 2243-FR, November, 1967.

TABLE 10. Extinguishment Data, United Technology Center
Investigator: G. D. Jensen

Propellant	UTX 10642		UTX 10645						
Binder	CTPB	CTPB	CTPIB	CTPIB	CTPIB	CTPIB	CTPIB	CTPIB	CTPIB
Conc. %	16	16	16	16	16	16	16	16	16
Oxidizer	AP	AP	AP	AP	AP	AP	AP	AP	AP
Conc. %	84	84	84	84	84	84	84	84	84
Size, μ	$\frac{190}{6}$	$\frac{190}{6}$	$\frac{190}{6}$	$\frac{190}{6}$	$\frac{190}{6}$	$\frac{190}{6}$	$\frac{190}{6}$	$\frac{190}{6}$	$\frac{190}{6}$
T_f, ^oK			2596	2596	2596	2596	2596	2596	2596
P_i, psia	450	100	100	450	275	300	1100	500	825
r_i, in/sec	.22	.11	.13	.18	.16	.16	.20	.18	.19
n_i	.42	.42	.28	.25	.26	.26	.21	.25	.22
P_a	14.7	14.7	14.7	14.7	14.7	14.7	14.7	14.7	14.7
Extinguish. $\dot{P}$ 10^3 psi/sec	40	9	4	25	44	120	430	225	360
Motor	slab	slab	slab	slab	window motor	5" swing nozzle	5" swing nozzle	15"swing nozzle	15" swing nozzle
A_{n_f}/A_{n_i}					5.3	2.6	5.5	2.6	3.1

Reference: "An Experimental Study of Solid Propellant Extinguishment by Rapid Depressurization," UTC Preliminary Final Report on Contract NAS 1-7815.

TABLE 10. Continued

Propellant	UTX 10661						UTX 10691			
Binder	PU	PU	PU	PU	PU	PU	PU	PU	PU	PU
Conc. %	16	16	16	16	16	16	16	16	16	16
Oxidizer	AP	AP	AP	AP	AP	AP	AP	AP	AP	AP
Conc. %	84	84	84	84	84	84	84	84	84	84
Size, μ	$\frac{190}{6}$	$\frac{190}{6}$	$\frac{190}{6}$	$\frac{190}{6}$	$\frac{190}{6}$	$\frac{190}{6}$	$\frac{190}{6}$	$\frac{190}{6}$	$\frac{190}{6}$	$\frac{190}{6}$
T_f, ^oK	2936	2936	2936	2936	2936	2936	2799	2799	2799	2799
P_i, psia	125	375	160	375	160	550	200	800	200	750
r_f, in/sec	.15	.23	.19	.23	.19	.25	.16	.28	.17	.27
n_i	.32	.32	.32	.32	.32	.32	.41	.41	.41	.41
P_a	14.7	14.7	14.7	14.7	vacuum	vacuum	14.7	14.7	vacuum	vacuum
Extinguish. P 10^3psi/sec	6	23	10	35	9	38	17	155	12	90
Motor	slab	slab	window motor	window motor	window motor	window motor	window motor	window motor	window motor	window motor
A_{n_f}/A_{n_i}							4.2	15	4.2	11

TABLE 10. Continued

Propellant	UTX 11339				UTX 10698	UTX 11306		UTX 11315 UTX 11327			
Binder	CTPB	CTPB	CTPB	CTPB	CTPIB	CTPIB	CTPIB	CTPB	CTPB	CTPB	CTPB
Conc. %	16	16	16	16	16	16	16	20	20	20	20
Oxidizer	AP	AP	AP	AP	AP	AP	AP	AP	AP	AP	AP
Conc. %	84	84	84	84	84	84	84	80	80	80	80
Size, μ	$\frac{190}{6}$	$\frac{190}{6}$	$\frac{190}{6}$	$\frac{190}{6}$	$\frac{190}{6}$	$\frac{190}{6}$	$\frac{190}{6}$	$\frac{190}{6}$	$\frac{190}{6}$	$\frac{190}{6}$	$\frac{190}{6}$
T_f, ^oK						2714		2483	2483	2483	2483
P_i, psia	275	840	250	860	325	325	325	275	675	275	675
r_i, in/sec	.21	.33	.20	.34				.16		.16	
n_i	.43	.43	.43	.43				.40		.40	
P_a	14.7	14.7	vacuum	vacuum	14.7	14.7	14.7	14.7	14.7	vacuum	vacuum
Exting. $\dot{P}$ 10^3psi/sec	45	160	25	105	20	20	20	40	100	30	65
Motor	window motor	window motor	window motor	window motor	slab	slab	slab	slab	slab	slab	slab
A_{n_f}/A_{n_i}	8.5		5.8	10	5.8	5.8	6.5	8.3	13.8	5.7	9.6

TABLE 10. Continued

Propellant	UTX 11336				UTX 11317			
Binder	CTPIB	CTPIB	CTPIB	CTPIB	CTPB	CTPB	CTPB	CTPB
Conc. %	16	16	16	16	16	16	16	16
Oxidizer	AP	AP	AP	AP	AP	AP	AP	AP
Conc. %	84	84	84	84	80	80	80	80
Size, μ	$\frac{190}{6}$	$\frac{190}{6}$	$\frac{190}{6}$	$\frac{190}{6}$	$\frac{190}{6}$	$\frac{190}{6}$	$\frac{190}{6}$	$\frac{190}{6}$
Additive					Al	Al	Al	Al
Conc.					4	4	4	4
T_f, ^oK					2931	2931	2931	2931
P_i, psia	400	950	400	900	300	650	320	750
r_i, in/sec	.16	.17	.16	.17	.18	.25	.19	.26
n_i	.05	.05	.05	.05	.4	.4	.4	.4
P_a	14.7	14.7	vacuum	vacuum	14.7	14.7	vacuum	vacuum
Extinguish. $\dot{P}$ 10^3psi/sec	30	85	45	74	30	115	33	90
Motor	slab	slab	slab	slab	window motor	window motor	window motor	window motor
A_{n_f}/A_{n_i}	11.5	14	11.5	14.5	6.3	13	5.9	9.3

TABLE 10. Continued

Propellant	UTX 11325				UTX 11316		UTX 11454					
Binder	CTPB	CTPB	CTPB	CTPB	CTPIB	CTPIB	CTPIB	CTPIB	CTPIB	CTPIB	CTPIB	CTPIB
Conc. %	16	16	16	16	16	16	16	16	16	16	16	16
Oxidizer	AP	AP	AP	AP	AP	AP	AP	AP	AP	AP	AP	AP
Conc. %	78	78	78	78	80	80	78	78	78	78	78	78
Size, μ	$\frac{190}{6}$	$\frac{190}{6}$	$\frac{190}{6}$	$\frac{190}{6}$	$\frac{190}{6}$	$\frac{190}{6}$	$\frac{190}{6}$	$\frac{190}{6}$	$\frac{190}{6}$	$\frac{190}{6}$	$\frac{190}{6}$	$\frac{190}{6}$
Additive	Al	Al	Al	Al	Al	Al	Al	Al	Al	Al	Al	Al
Conc. %	16	16	16	16	4	4	16	16	16	16	16	16
T_f, ^oK	3266	3266	3266	3266	2732	2732	3107	3107	3107	3107	3107	3107
P_i. psia	300	900	450	950	600	600	275	700	275	750	600	1100
r_i, in/sec	.18	.28	.22	.28	.18	.18	.16	.18	.16	.18	.18	.19
n_i	.4	.4	.4	.4	.18	.18	.18	.18	.18	.18	.18	.18
P_a	14.7	14.7	vacuum	vacuum	14.7	vacuum	vacuum	vacuum	14.7	14.7	14.7	14.7
Extinguish. $\dot{P}$ 10^3 psi/sec	35	130	35	95	44	44	10	40	15	60	300	650
Motor	window motor	window motor	window motor	window motor	window motor	window motor	window motor	window motor	window motor	window motor	5"swing nozzle	5"swing nozzle
A_{nf}/A_{n_i}	5.9	9.4	4.7	7.4	8.7	7.4	2.9	5.7	3.3	7.7	2.6	5.1

TABLE 10. Continued

Propellant	UTX11326				UTX 11329			
Binder	CTPB	CTPB	CTPB	CTPB	CTPB	CTPB	CTPB	CTPB
Conc. %	16	16	16	16	16	16	16	16
Oxidizer	AP	AP	AP	AP	AP	AP	AP	AP
Conc. %	83.8	83.8	83.8	83.8	83.8	83.8	83.8	83.8
Size, μ	$\frac{190}{6}$	$\frac{190}{6}$	$\frac{190}{6}$	$\frac{190}{6}$	$\frac{190}{6}$	$\frac{190}{6}$	$\frac{190}{6}$	$\frac{190}{6}$
Additive	Fe	Fe	Fe	Fe	Fe(organ.)	Fe(organ.)	Fe(organ.)	Fe(organ.)
Conc. %	.25	.25	.25	.25	.25	.25	.25	.25
P_i, psia	350	750	300	750	300	650	300	650
r_i, in/sec	.24	.34	.22	.34	.26	.34	.26	.34
n_i	.47	.47	.47	.47	.36	.36	.36	.36
P_a	14.7	14.7	vacuum	vacuum	14.7	14.7	vacuum	vacuum
Extinguish. $\dot{P}$ 10^3psi/sec	55	120	35	85	30	80	30	80
Motor	window motor	window motor	window motor	window motor	window motor	window motor	window motor	window motor
A_{nf}/A_{ni}	6.5	9.5	5.3	8.3	7.5	12	5.3	9.5

TABLE 10. Continued

Propellant	UTX 11333				UTX 11342
Binder	CTPIB	CTPIB	CTPIB	CTPIB	CTPIB
Conc. %	16	16	16	16	16
Oxidizer	AP	AP	AP	AP	AP
Conc. %	83.8	83.8	83.8	83.8	68
Size, μ	$\frac{190}{6}$	$\frac{190}{6}$	$\frac{190}{6}$	$\frac{190}{6}$	$\frac{190}{6}$
Additive	Fe(organic)	Fe(organic)	Fe(organic)	Fe(organic	HYCAT
Conc. %	.25	.25	.25	.25	1
Additive					Al
Conc. %					16
P_i, psia	250	900	250	900	400
r_i, in/sec	.17	.24	.17	.24	.25
n_i	.24	.24	.24	.24	.22
P_a	14.7	14.7	vacuum	vacuum	vacuum
Extinguishment $\dot{P}$ 10^3 psi/sec	15	75	15	75	25
Motor	window motor	window motor	window motor	window motor	window motor
A_{n_f}/A_{n_i}	4.9	10.9	4.4	10.3	3.9

TABLE 11. Extinguishment data, Brigham Young University

Propellant	A-13			A-14		A-15	A-16	A-17	A-18
Binder	PBAN			PBAN		PBAN	PBAN	PBAN	PBAN
Conc. %	24			24		24	24	24	24
Oxidizer	AP			AP		AP	AP	AP	AP
Conc. %	76			76		76	76	76	76
Size, μ	80			15		80	15	80	15
Additive	--			--		CUO_2O_2	CUO_2O_2	LiF	LiF
Conc. %	--			--		1	1	1	1
T_f, ^oK	2100			2100		2100	2100	2100	2100
P_{dl}, psia	.40			.56		.20	.45	.10	.80
P_i, psia	91	164	400	153	280	285	320	169	157
r_i, in/sec	.105	.143	.23	.24	.39	.31	.67	.121	.181
n_i	.51	.51	.51	.61	.61	.53	.56	.42	.57
P_a, psia	12.5	12.5	12.5	12.5	12.5	12.5	12.5	12.5	12.5
Extinguishment $t_{1/2}$, msec	11	10	7.5	7.2	7.2	6.4	1.9	7.3	6.6
A_{n_f}/A_{n_i}	1.99	2.92	4.50	2.39	2.78	4.40	5.15	4.99	2.57

Reference: AIAA Journal, 6, 292-297 (1968).

TABLE 12. Extinguishment data, Atlantic Research Corp.
Investigators: G. Von Elbe, E. McHale

Propellant	Arcite	PBAA	PBAA-Al
Binder	PVC	PBAA	PBAA
Conc. %	20	30	28.5
Oxidizer	AP	AP	AP
Conc. %	80	70	66.5
Size, μ	--	80	80
Additive			Al
Conc. %			13.4
P_i, psia	100	200	200
r_i, in/sec	.174	.109	.178
n_i	.57	.50	.42
P_a, psia	14.7	14.7	14.7
Extinguishment $t_{1/2}$, msec*	20	51	13.4

*Computed from data presented

Reference: AIAA Journal, 6, July 1968, 1417-1419.

2. Correlations of Experimental Data

A first attempt at correlating the data discussed in the previous section utilized the following equation, which was derived independently by Von Elbe (27) and Paul, et al. (28):

$$-(d\ln P/dt)_{ext} = \frac{1}{\lambda}\,\frac{r^2}{n\alpha} \qquad (3.1)$$

or

$$-(\alpha \dot{P}/r^2 P) = \frac{1}{\lambda n}$$

where $(d\ln P/dt)_{ext}$ is the critical logarithmic depressurization rate for extinguishment, r is the burning rate, n is the burning rate exponent, α is the thermal diffusivity, and λ is an empirical correction factor. Figure 10 presents the results of this correlation. To obtain this plot it was assumed that $\alpha = 0.00025$ in^2/sec for all propellants. This assumption was necessary since data for α are not available for most of the propellants. It was further assumed that the pressure decayed exponentially in all cases. The theory leading to Equation (3.1) predicts that extinguishment occurs during the pressure decay transient when this equation is satisfied. Thus the value of r employed in the correlation should be that corresponding to steady-state at the pressure when dlnP/dt satisfied Equation (3.1). Since only average initial decay rates are reported, the time during decay when extinguishment occurred is not known. If the decay is exponential, the value of dlnP/dt is constant during the depressurization and the average initial value will apply approximately throughout the decay. The minimum value of the right-hand side of (3.1) would be that corresponding to the final pressure, since P and hence r would then have their minimum values. For this reason, the correlation was attempted (Figure 10) using the burning rates corresponding to the final pressure. This attempted correlation was clearly unsatisfactory.

Figure 11 presents the results of a second correlation attempt. In this figure the depressurization half-time, which is proportional to dlnP/dt for an exponential decay, is plotted versus the initial steady burning rate. Although the data show a trend consistent with Equation (3.1), the scatter is such that this correlation was also not satisfactory.

As a result of the study discussed in Section IV, it became apparent that the motor L* is an important variable that must be accounted for in any successful correlation of extinguishment data. The importance of this variable is illustrated by the data shown in Figure 12, which were taken from Reference 10. These data show that the marginal initial depressurization rate for extinguishment for a given

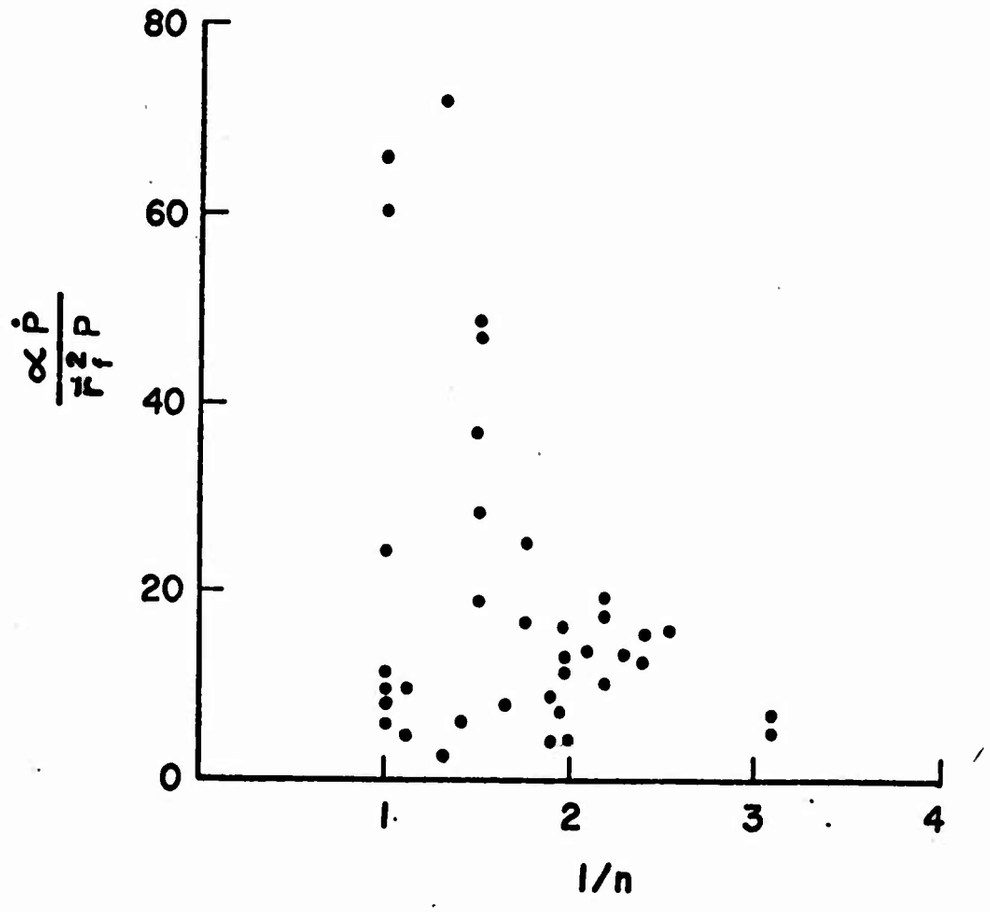

Figure 10. Results of attempt to correlate marginal $\dot{P}$ extinguishment with burning rate exponent

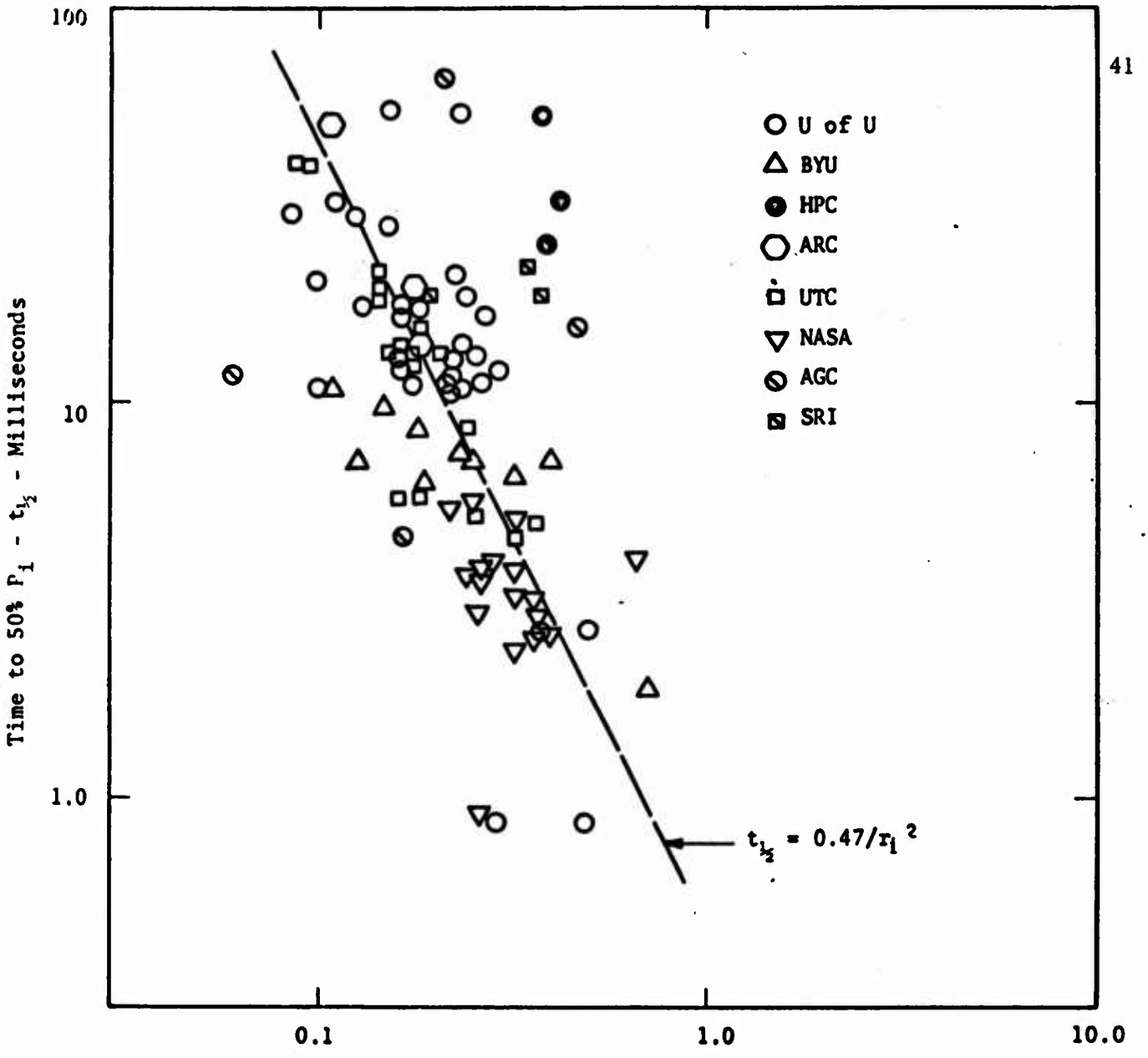

Figure 11. Results of attempt to correlate marginal $\dot{P}$ extinguishment with initial burning rate

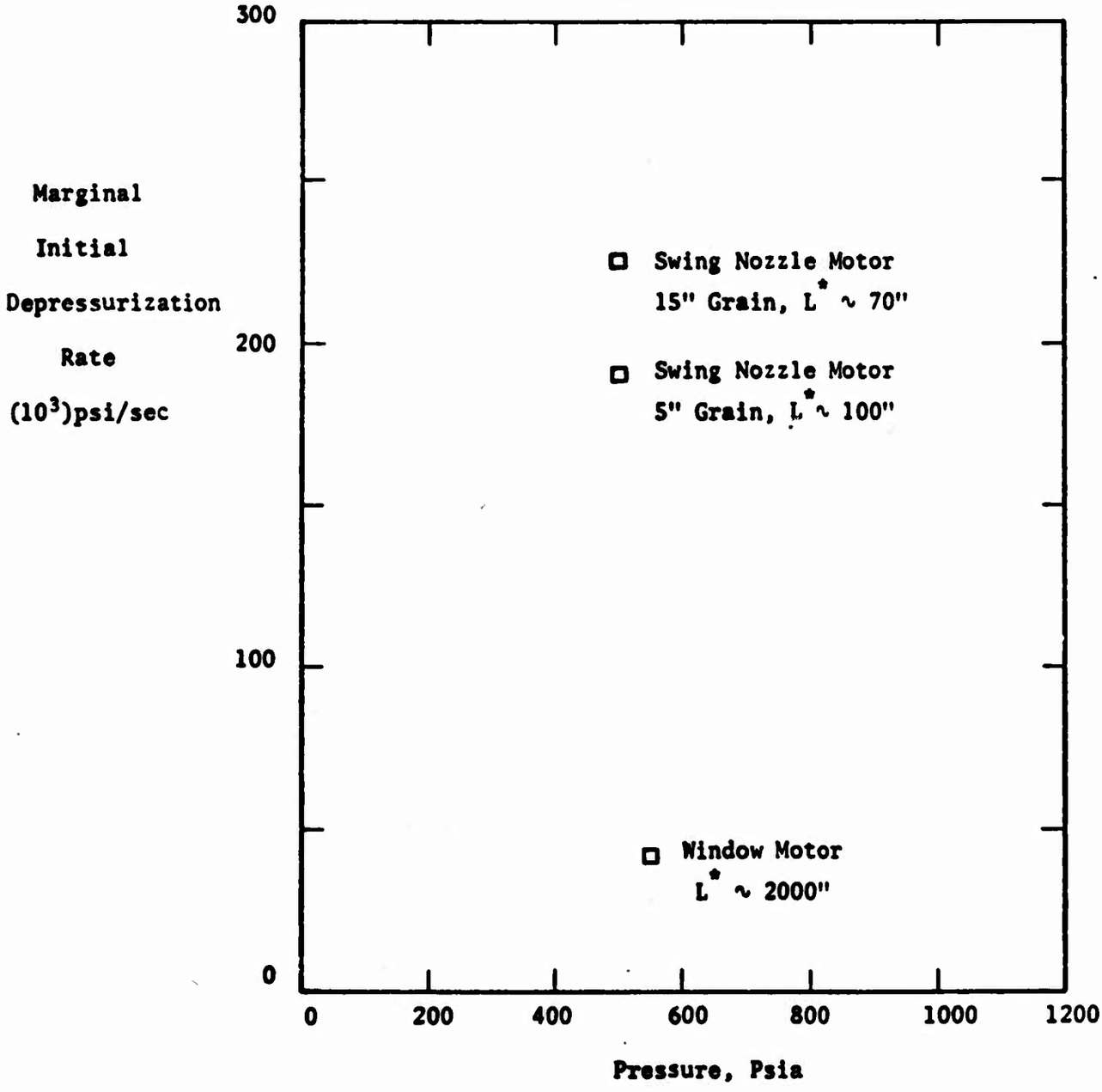

Figure 12.--Data taken from Reference 17 showing the effect of L^* on marginal $\dot{P}$ extinguishment.

propellant can vary by about a factor of 5 depending on the motor used for testing. The critical rate appears to increase with decreasing initial L^* of the test motor.

As discussed in Section IV, the marginal extinguishment conditions predicted theoretically were nicely correlated without regard for depressurization rate using the parameters L_f^* and $\bar{r}_f$. These parameters are the characteristic length of the motor and the burning rate that would be calculated assuming steady-state ballistics apply using the fully opened nozzle area, or using $K_n = A_b/A_{n_f}$. Figure 13 presents the results of the correlation attempt which was made following this approach.

Unfortunately, most of the literature cited previously in this section does not contain sufficient information to permit application of this method of correlation. A notable exception is the recent data reported by the United Technology Center (16, 17), and most of the data points shown in Figure 13 were taken from this reference. In addition to this data, one point was extracted from results reported by Stanford Research Institute (15), one point from full-scale motor testing carried out by Aerojet General Corp. (25), and one from previous tests at BYU. Also included in this figure are theoretical points and lines illustrating the predicted effect of flame temperature. These theoretical results are discussed in Section IV.

It is important to note that the correlations shown in Figure 11 and 13 both suggest that the lower the burning rate of a propellant, the more easily it is extinguished.

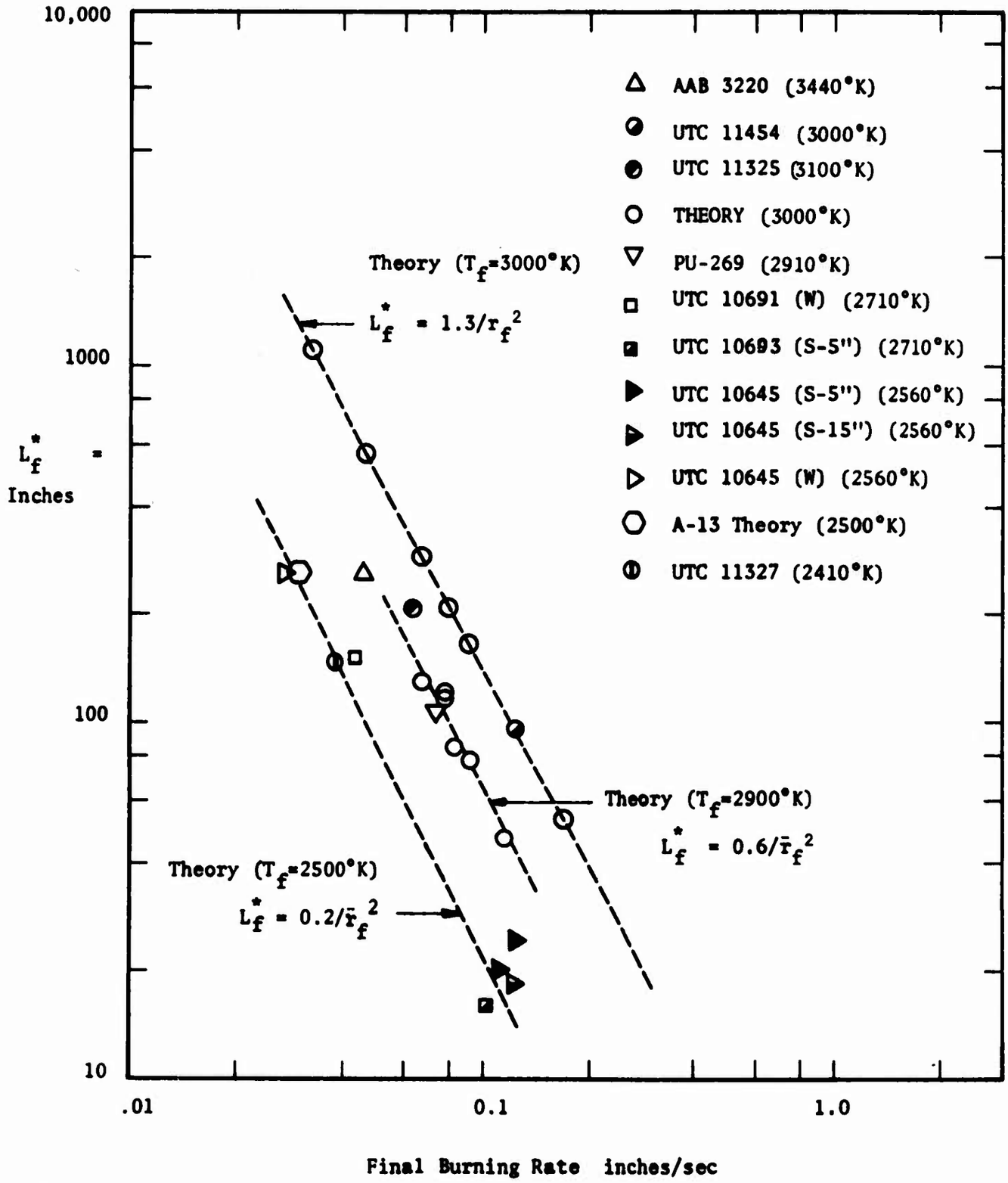
10,000
1000
100
10
.01
0.1
1.0
L_f^* = Inches
Final Burning Rate inches/sec
AAB 3220 (3440°K)
UTC 11454 (3000°K)
UTC 11325 (3100°K)
THEORY (3000°K)
PU-269 (2910°K)
UTC 10691 (W) (2710°K)
UTC 10693 (S-5") (2710°K)
UTC 10645 (S-5") (2560°K)
UTC 10645 (S-15") (2560°K)
UTC 10645 (W) (2560°K)
A-13 Theory (2500°K)
UTC 11327 (2410°K)
Theory (T_f=3000°K)
$L_f^* = 1.3/r_f^2$
Theory (T_f=2900°K)
$L_f^* = 0.6/\bar{r}_f^2$
Theory (T_f=2500°K)
$L_f^* = 0.2/\bar{r}_f^2$

Figure 3.5

IV

PARAMETRIC DESIGN STUDIES

1. Objectives and Approach

The ballistics engineer must make one basic calculation in the design of a single-chamber controllable motor having stop-restart capability. This is the calculation of the minimum area to which the nozzle must be opened in order to cause the propellant to extinguish. Three criteria have been proposed to calculate the required area increase: (1) the depressurization rate resulting from the area change be greater than some critical value ($\dot{P}$ criterion), (2) the predicted steady-state chamber pressure resulting from the change be less than some critical value (P_{DL} criterion), and (3) the L* resulting from the change be less than some critical value (L* criterion).

If there exists a unique deflagration limit, P_{DL}, or minimum pressure below which a propellant will not burn, the nozzle-area increase necessary to reach this P_{DL} can be computed in a straightforward manner using conventional steady-state ballistics. There appears to be a strong effect of the thermal environment on the P_{DL} (26), however, and proven methods have not yet been developed for measuring in the laboratory P_{DL}'s which apply inside full-scale rocket motors. In addition to this problem, the required area changes computed solely on the basis of the P_{DL} criterion, without regard to motor L* effects or $\dot{P}$ effects, tend to be larger than those resulting from employing these alternative criteria. Thus, the area change computed solely on the basis of a limiting P_{DL} may dictate a larger and heavier nozzle than is actually required.

The objective of this phase of the program was to carry out parametric calculations for the minimum nozzle-area change that will lead to extinguishment taking both $\dot{P}$ and L* effects into account. The results of these calculations were then to be graphically presented in a form that would be useful for preliminary design calculations.

The approach that was followed was to develop a mathematical model of the combustion chamber, coupling the gas dynamic equations to the thermal dynamic equations describing the combustion process, and then to compute predicted depressurization transients, varying the operating parameters.

2. Analytical Model

Conventional ballistics equations for a solid propellant rocket motor apply strictly only to the steady-state since steady-state burning rates are assumed to apply. The conditions leading to extinguishment are very non-steady and since

experimental data for non-steady burning rates are difficult to obtain and not readily available, ballisticians have employed theoretical models of the combustion process to predict non-steady behavior. In particular, the rather simple models of Von Elbe (27), Paul (28), and Cohen (34) have been used in controllable motor development programs (25, 26).

These models lead to the $\dot{P}$ criterion mentioned in Section III,

$$-(d\ln P/dt)_{ext} \leq r^2/\lambda n \alpha \tag{4.1}$$

and, as shown by Cohen (34), to the L^* extinguishment criterion:

$$(L^*)_{ext} \leq n r^2 C^* \alpha/r^2 \tag{4.2}$$

As indicated in Section III of this report, Equation (4.1) has limited usefulness in correlating experimental data for different propellants. This is most likely due to the fact that the theoretical basis of these equations employs rather restrictive assumptions. In particular, the rate of heat conduction into the solid is assumed to occur instantaneously, resulting in a temperature profile and heat storage that is a function only of the instantaneous value of the pressure. They also assume the surface temperature to be a constant.

More recent theories for extinguishment have been proposed by Horton (18), Wooldridge and Marxman (15), and Summerfield, et al. (35). In these theories non-steady heat conduction is accounted for using numerical analysis techniques. The recent theories are similar in many respects to theories originally developed for application to combustion instability, for example, the Denison-Baum theory (29).

Predicted responses of the burning rate to imposed pressure transients is illustrated by the curves in Figure 14. This figure shows the type of response predicted by the Von Elbe equation to a ramp or step change in pressure relative to the type of response predicted by the Denison-Baum combustion theory. Using the Von Elbe equation, the assumption of instantaneous heat transfer results in the prediction of a discontinuous burning rate response. The lag and overshoot response predicted by the Denison-Baum theory is certain to be more nearly the kind of response that actually occurs.

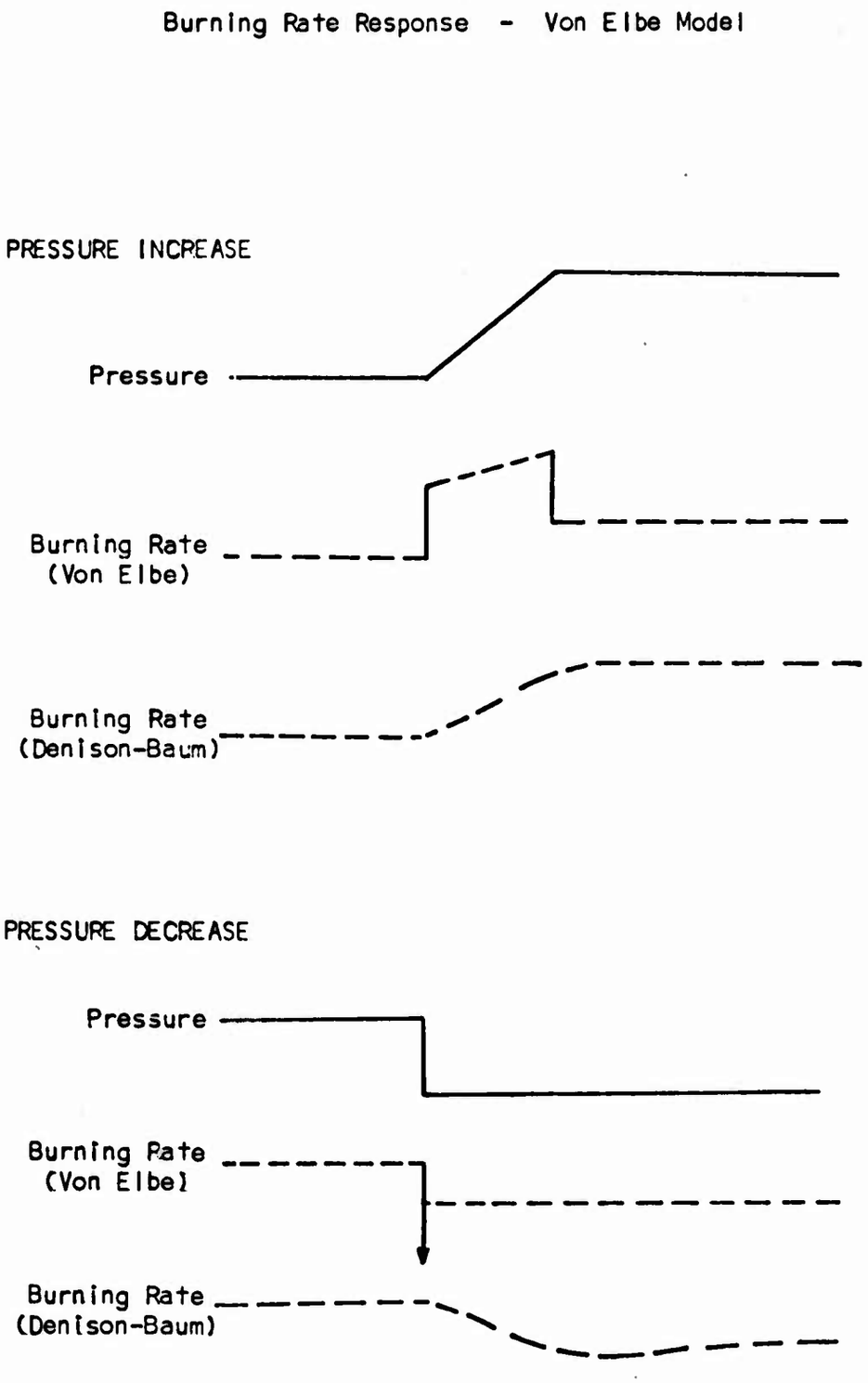

Figure 14. Comparison of burning rate response predicted by Von Elbe equation with Denison-Baum theory.

a. Combustion Model

The combustion model employed in this analysis was developed at BYU under an AFOSR Grant (30). It relies on a previous theory developed by Denison and Baum (29); however, their theory was modified to predict transient deviations from empirical steady-state burning rates. The basic features of this model are described in the following.

The burning process is assumed to be represented by the one-dimensional temperature profile shown in Figure 15. The solid is divided into finite-difference elements as is also illustrated in this figure, and the following energy balance taken on an element of the solid is assumed to describe the transient heat conduction.

$$\frac{dT_i}{dt} = \alpha\left[\frac{T_{i-1}-2T_i-T_{i-1}}{(\Delta x)^2}\right] + r\left[\frac{T_{i+1}-T_{i-1}}{2\Delta x}\right] \qquad (4.3)$$

The instantaneous burning rate is coupled to the surface temperature, pressure, and flame temperature by the following equations:

$$r = \bar{r}_p \exp\left[(-E_s/R)\,(1/T_s - 1/\bar{T}_{s,p})\right] \qquad (4.4)$$

$$r = \bar{r}_p\,(T_f/\bar{T}_f)^{n+1} \exp\left[-(E_g/R)\,(1/T_f - 1/\bar{T}_{f,p})\right] \qquad (4.5)$$

and the heat flux supplied to the solid from the combustion process is given by

$$\left(-k\frac{dT}{dx}\right)_{x=0^+} = r\rho_s\left[C_s(T_s-T_\infty) + C_g(\bar{T}_f-T_f)\right] \qquad (4.6)$$

In these equations

$\bar{r}_p$ = the steady-state burning rate at pressure p
E_s = Activation energy for surface reaction
R = Universal gas constant
T_s = Instantaneous surface temperature
$\bar{T}_{s,p}$ = Steady-state surface temperature at p
T_f = Instantaneous flame temperature
$\bar{T}_{f,p}$ = Steady-state flame temperature at p
n = $d\ln\bar{r}_p/d\ln P$ at P
E_g = Activation energy for gas-phase reaction
ρ_s = Density of solid
C_s = heat capacity of solid
C_g = heat capacity of gas
T_∞ = conditioning temperature of propellant

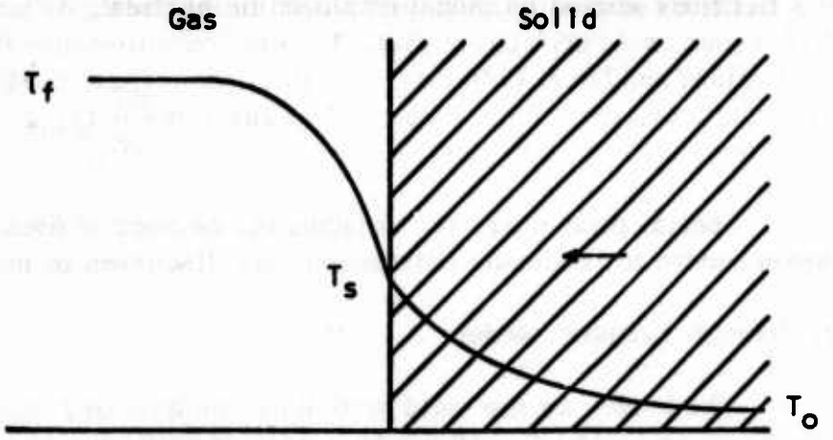

Geometrical Model of Burning Propellant

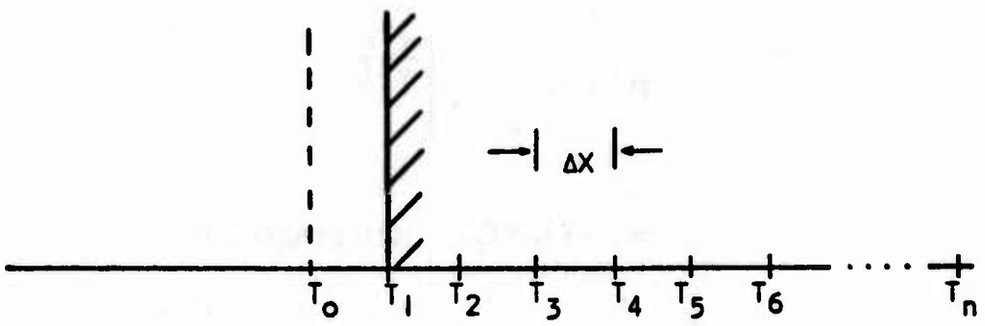

Figure 15. Diagram showing temperature profile during combustion and method of separating solid into finite elements.

The surface flux is incorporated into the finite-difference energy balance equations by the following equation defining T_o, the temperature at a fictitious station immediately above the surface.

$$T_o = T_2 + 2\Delta x \left(-k \frac{dT}{dx} \right)_{x=o^+} \tag{4.7}$$

Special procedures for reducing the number of finite difference elements needed for accurate calculations are discussed in Reference 30.

b. Interior Ballistic Model

The model for the solid propellant combustion process has been combined with equations describing the transient ballistics of a solid rocket motor. Equations expressing conservation of both mass and energy inside the motor cavity have been derived previously (31). In the present study these equations have been used in the following form:

$$\frac{dp}{dt} = \gamma (\bar{p}/\tau_c) (T_c/\bar{T}_{c_1}) \left[(T_f/T_c) (r/\bar{r}_1) - W_n \right] \tag{4.8}$$

$$\frac{dT_c}{dt} = (T_c/p) \frac{dp}{dt} - (T_c/\tau_c) (\bar{p}_1/p) (T_c/\bar{T}_c) \left[(r/\bar{r}_1) - W_n \right] \tag{4.9}$$

where

$$\tau_c = \bar{L}_1^*/\Gamma^2 C^*$$

$$\Gamma^2 = \gamma \left[\frac{2}{\gamma + 1} \right]^{\frac{\gamma+1}{\gamma-1}} \tag{4.10}$$

$$W_n = (\bar{T}_c/T_c)^{1/2} (p/\bar{p}) (A_n/A_{n_i})$$

Prediction of the instantaneous pressure versus time requires the simultaneous numerican integration of these equations along with those presented in the previous section for the solid burning rate. This is accomplished with an integration scheme based on the Adams method (32). The Fortran coding for carrying out these calculations using the BYU Librascope L-3055 computer is presented along with an example of the computed output in the Appendix.

3. Comparison of Predicted and Experimental Transients

The theoretical model which has been described above is based on several simplifying assumptions which can be justified only if the model is useful for correlating experimental data and predicting transient behavior as motor and operating parameters are varied. Evaluating the model for these purposes, of course, depends on the availability of suitable data. Although the developed model allows for the effect of external radiation, this effect was not included in the calculations performed here.

The model requires as input data all of the usual parameters necessary to calculate the steady-state operating pressure of a rocket motor plus several additional motor and propellant parameters. The additional motor parameters are the initial L*, the change in venting area that takes place to terminate thrust, and the time required to change the venting area. The additional propellant parameters are the surface temperature at some specified burning rate, T_{sr}, the steady-state flame temperature, the gas activation energy, E_g, the solid phase activation energy, E_s, the ratio of the solid and gas phase heat capacities, and the thermal diffusivity of the solid. All of these additional parameters can be readily obtained except T_{sr}, E_s, and E_g. These become the curve fitting or correlating parameters. The theory is most useful only if one set of these parameters for a given propellant can be used to predict transient behavior as operating conditions are varied.

The method that has been used to select these parameters is to assume a T_{sr} typical of those measured with very fine thermocouples (600°C) and then to adjust E_s and E_g as required to fit existing experimental data. For convenience, E_s and E_g have been taken to be equal, so that only a single parameter is adjusted to reach agreement with a given set of data. This approach has been satisfactory for correlating two sets of existing data where the initial pressure and ambient pressure were varied; i.e., one set of constants for a given propellant was sufficient to predict the effects on extinguishment conditions observed experimentally as these operating parameters were varied.

The experimental data referred to were taken from a series reported by Horton (18) and from a different series reported by Wooldridge (15) of the Stanford Research Institute. Horton determined the critical depressurization rate necessary to cause extinguishment of a propellant designated as A-13 at initial pressures of 170 and 310 psia. The ambient pressure for these tests was 12.5 psia. The SRI researchers determined the critical vent area-nozzle area ratio necessary to extinguish a propellant designated as PU-269 at ambient pressures of 15 psia and 165 psia, the initial pressure being held constant at approximately 500 psi. Table 13 summarizes the propellant input data, including the activation energies finally selected to correlate the data, and Table 14 summarizes the motor input data and lists the observed and predicted results. As mentioned above, T_{sr} was

TABLE 13. Summary of Propellant Characteristics Employed in Extinguishment Predictions

Propellant Designation	A-13	PU-269
Binder	PBAN/Epoxy 24%	Polyurethane 20%
Oxidizer	Am. Perch. 76%	Am. Perch. 80%
Input Propellant Parameters		
Burning Rate, 100 psi, in./sec.	0.33	.33
Exponent, 1000 psi	0.41	.40
Flame Temperature, ^{o}K	2500	2910
Surface Temperature, 1000 psi, ^{o}C	600	600
Density, lbs/in^3	.061	.062
C_p/C_v, Gas	1.22	1.22
C^*, ft/sec	3070	4500
(C_p) solid/ (C_p) gas	0.75	0.75
Diffusivity, in^2/sec	.00025	.00025
Conditioning Temperature, ^{o}C	25	25
E_s, Kcal/mole	20	21
E_g, Kcal/mole	20	21

TABLE 14. Comparison of Predicted and Experimental Extinguishment Data

Propellant/Laboratory Test Variable	A-13/BYU Initial Pressure				PU-269/SRI Ambient Pressure			
Input Motor Parameters								
Burning Area, inches^2	.859		.859		8.3		8.3	
Burning Area/Throat Area	267		197		238		238	
Initial L*, inches	784		578		316		316	
Initial Pressure, psia	309		167		519		519	
Ambient Pressure, psia	12.5		12.5		15		165	
Vent Opening Time, milliseconds	1.0		1.0		1.5		1.5	
Experimental Results								
Total Vent Area/Throat Area	4.2	4.5	2.8	3.1	3.9	5.6	33.7	74.7
Max. dP/dt, 10^3 psi/sec	24	31	8	11	100	120	370	600
$t_{1/2}$ milliseconds	.2	6	15	11	5	3	1.0	0.6
Extinguish	No	Yes	No	Yes	No	Yes	No	Yes
Theoretical Results								
Total Vent Area/Throat Area	3.0	5.0	2.0	3.0	3.9	5.6	33.7	74.7
Max. dP/dt, 10^3 psi/sec	15	25	6	10	48	77	273	550
$t_{1/2}$ milliseconds	18	8	24	12	8	4	1.2	0.6
Extinguish	No	Yes	No	Yes	No	Yes	No	Yes

assumed to be 600°C for both propellants. The magnitude of $E = E_g = E_s$ was selected by a trial and error approach, noting that increasing E causes extinguishment to occur more readily. The activation energies finally selected were those that correctly predicted marginal extinguishment at both extremes of the operating conditions, i.e., chamber pressures of 170 and 310 psia in the case of A-13 propellant, and ambient pressures of 15 and 165 psia in the case of PU-269 propellant.

Figures 16 and 17 illustrate predicted transients for four of the cases summarized in Table 14. Figure 16, along with the data in Table 14, shows that increasing the vent area/nozzle throat area ratio from 3.9 to 5.6 in the SRI experiments causes a decrease in the depressurization half-time from 8 to 4 milliseconds, causing the burning rate to drop to levels where extinguishment would be expected to occur (burning rates less than about .005 inches/sec are not observed to occur during steady-state and would not be expected during transients). Thus a blow-down half-time $t_{1/2}$ of between 4 and 8 milliseconds is predicted as marginal for extinguishment for this propellant at this particular set of operating conditions. This prediction is in reasonably good agreement with the experimental critical $t_{1/2}$ between 3 and 5 milliseconds observed by SRI under conditions near those assumed for the prediction.

A reasonably severe test of the theory is to determine whether or not it can be employed to predict the observed effects of increasing the ambient pressure from 15 psia to 165 psia without an adjustment being required in the effective activation energies, E_s and E_g. After several trials in which various values of E_s and E_g were used as input data, a value of 21 kcal/mole was found to satisfy the observed effect with reasonable accuracy. Using this value, a critical $t_{1/2}$ of 4-8 milliseconds was predicted for an ambient pressure of 15 psia, as mentioned above, and a critical $t_{1/2}$ of 0.6 - 1.2 milliseconds was found for an ambient pressure of 165 psia; the latter value compares well with the observed value of 0.6 - 1.0 milliseconds.

Figure 17 shows two of the predicted transients made in this series of calculations which illustrate the strong effect of ambient pressure. With ambient pressure of 165 psia extinguishment fails to occur even though $t_{1/2}$ was near 2 milliseconds. With ambient pressure of 15 psia, however, extinguishment occurs with $t_{1/2}$ near 8 milliseconds. Thus the marginal $t_{1/2}$ or dP/dt is predicted to depend strongly on the ambient pressure.

A different, though somewhat less severe, test of the model is to determine if the observed effect of varying the initial pressure can be predicted with a single set of activation energies. This test was made for the BYU experiments of Table 14. As listed in Table 14, the theory predicts the critical $t_{1/2}$ is increased from 8-18 milliseconds to 12-24 milliseconds if the initial pressure is reduced from 309 to 167 psia. These figures bracket the critical times observed in the tests carried out at BYU. This agreement was achieved assuming $E_s = E_g = 20$ kcal/mole, as listed in Table 13.

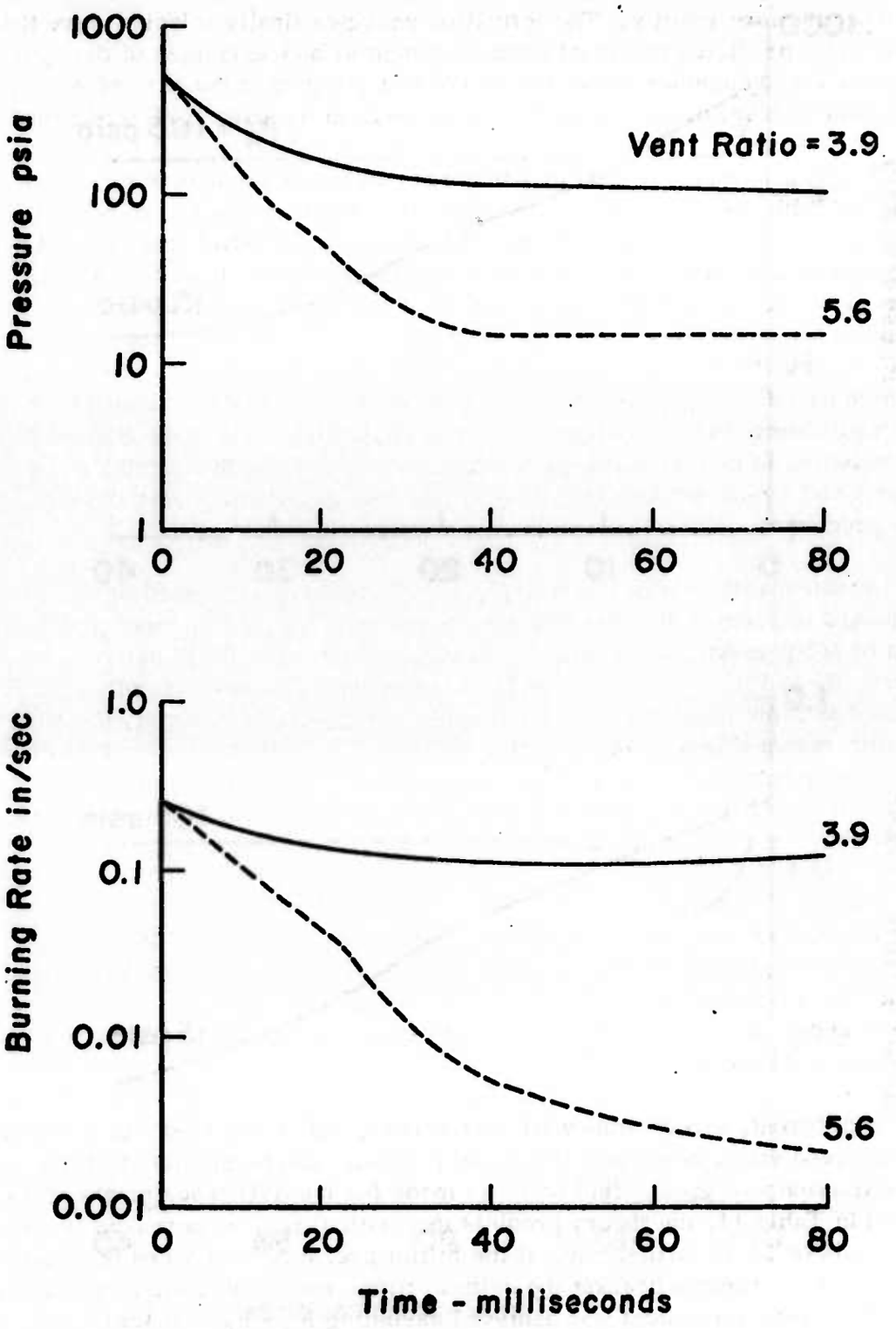

Figure 16. Predicted termination transients for input parameters corresponding to PU-269 propellant (Ref. 15).

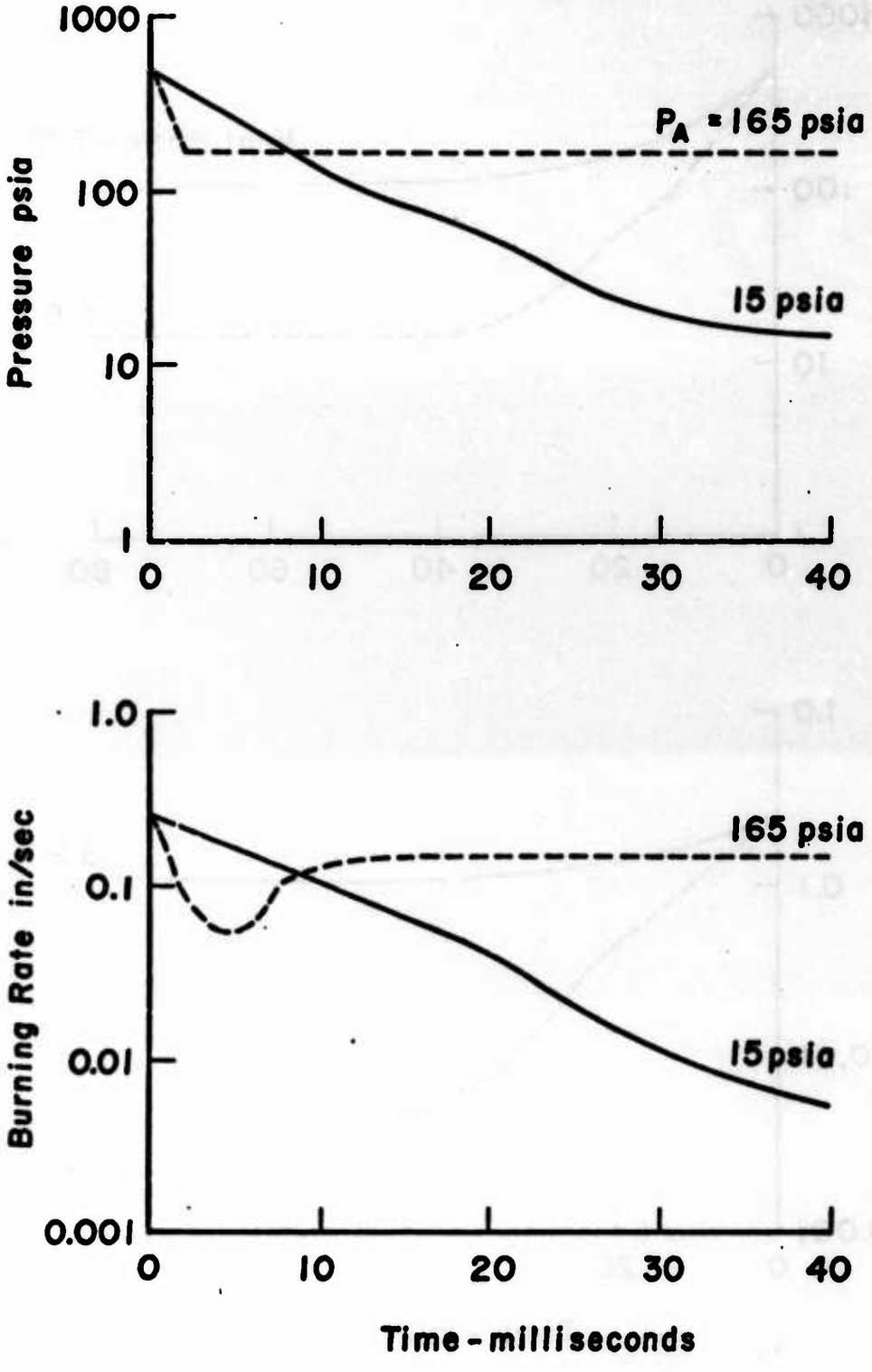

Figure 17. Predicted termination transients for input parameters corresponding to PU-269 propellant (Ref. 15).

4. Results of Parametric Calculations

Because of the large number of input variables that are contained in the mathematical model described above, the effects of varying each parameter were not exhaustively studied during this program. The calculations were limited to those showing the depressurization rates that occur under certain limiting conditions, the overall pressure drop that results if extinguishment does not occur, and the effect on marginal extinguishment conditions of varying initial pressure, initial L*, and nozzle opening time.

a. Limiting Depressurization Rates and Overall Pressure Drop

For the special case of an instantaneous opening of the throat area, Equation 4.8 reduces to Equation 4.11 for the initial depressurization rate.

$$\frac{1}{P}\frac{dP}{dt} = -\frac{12\gamma r^2 C^*}{L_i^*}\left[\frac{A_n}{A_{n_i}} - 1\right] \tag{4.11}$$

where C* has the units of feet/second and L_i^* is the initial L* in inches. Figure 18 shows the initial fractional depressurization rate versus the instantaneous fractional increase in nozzle throat area, with the initial L* as a parameter.

If the nozzle is opened slowly enough, steady-state ballistics apply and the depressurization rate is given by

$$\frac{1}{P}\frac{dP}{dt} = -\left(\frac{1}{1-n}\right)\left(\frac{1}{A_n}\frac{dA_n}{dt}\right) \tag{4.12}$$

for a propellant whose steady-state burning rate can be approximated by $r = aP^n$. Figure 19 shows a plot of these limiting fractional depressurization rates versus the fractional rate of nozzle area increase.

Figures 18 and 19 are useful for bracketing the depressurization rates that may be computed more exactly using the complete set of equations of Section 3.

A third set of curves representing limiting conditions are presented in Figure 20. The curves in this figure represent solutions to the equation

$$\frac{P_2}{P_1} = \left(\frac{A_{n_2}}{A_{n_1}}\right)^{\frac{1}{1-n}} \tag{4.13}$$

which relates the fractional change in steady-state pressure to the fractional

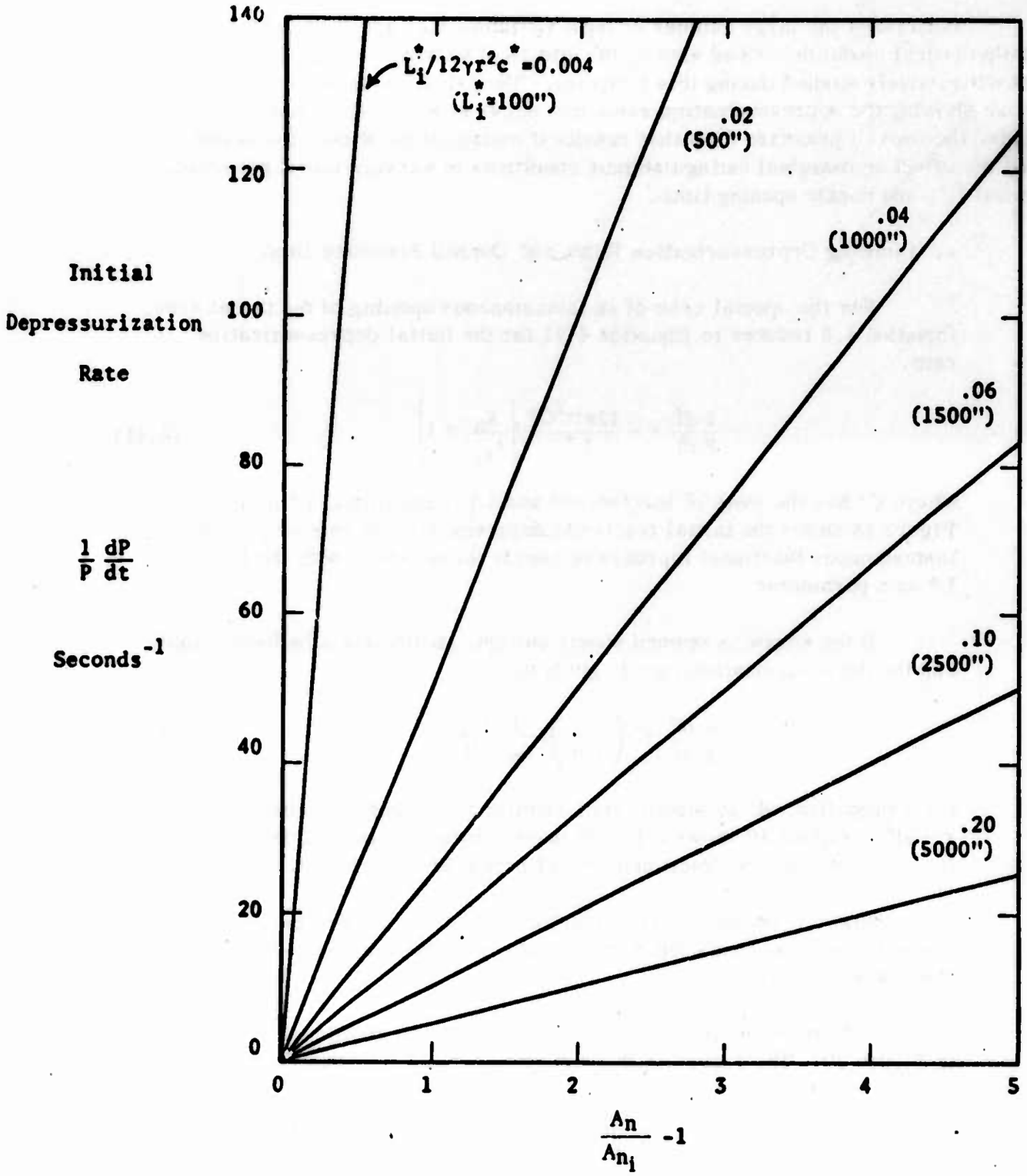

Figure 18. Predicted initial depressurization rates assuming nozzle area is changed instantaneously.

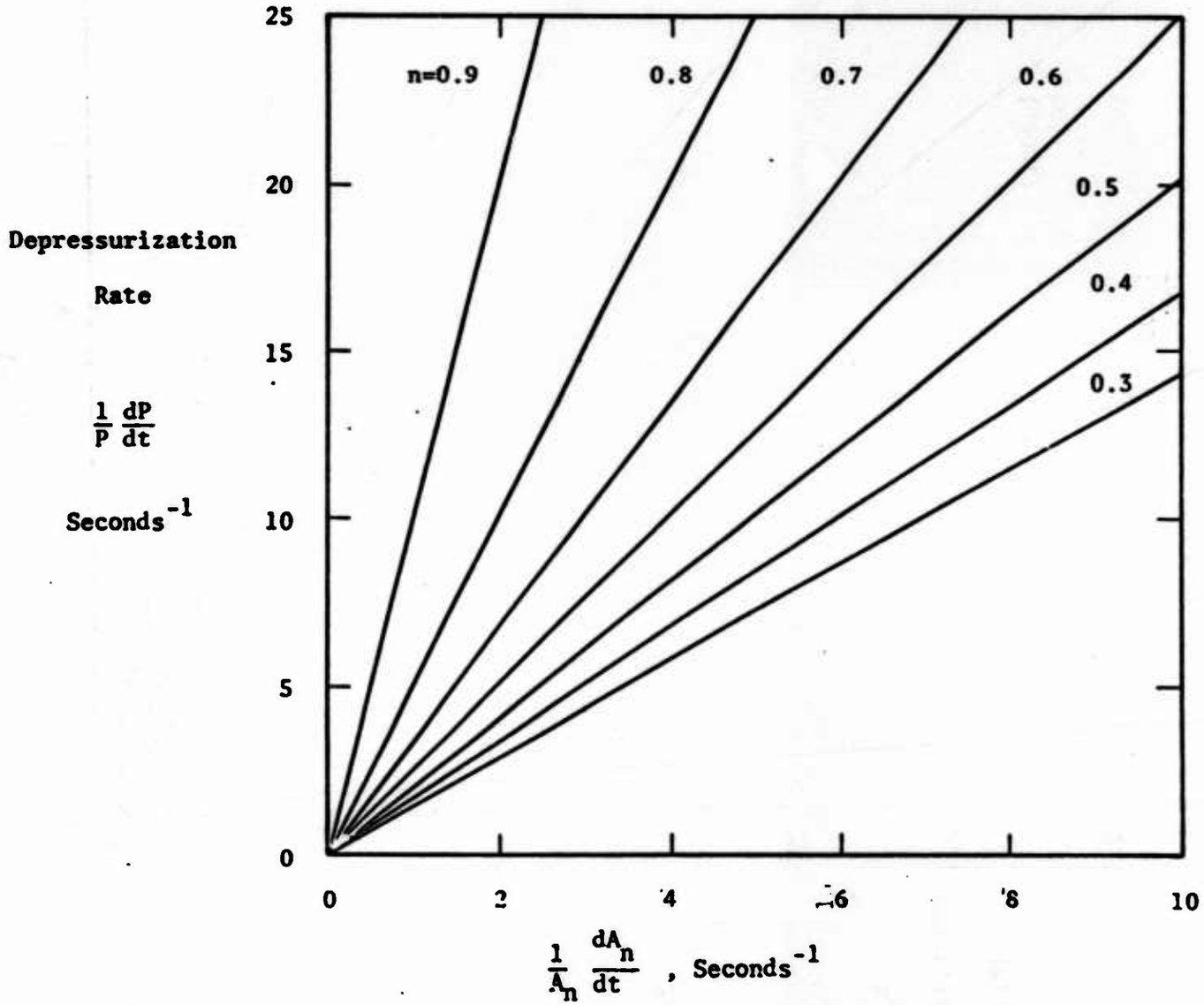

Figure 19. Predicted depressurization rates assuming the burning rates and mass flow in and out of the chamber are at equilibrium.

change in nozzle throat area for a propellant following an $r=aP^n$ burning rate law and for which C* is independent of pressure.

Figures 18 and 20 can be employed to point out an important depressurization relationship, the relationship between initial depressurization rate, initial L_i^* and overall pressure drop. As an illustration of this relationship, consider the following experiment. Five different motors are fired having initial L*'s of 100", 500", 1000", 1500", and 2500". They are at the same initial pressure, 500 psia, and their nozzles are instantaneously opened to the point where the initial depressurization rate is 20,000 psi/second. If extinguishment does not occur, the new steady-state pressures, according to Figures 18 and 20, will range from 345 psia for the 100" L* motor to 9 psia for the 2500" L* motor, as shown in the following table.

Initial L* inches	Fractional Nozzle Increase for $(dP/dt)_i$ = 20,000 psi/sec	Final Steady-state Pressure n = 0.6
100	0.16	345 psia
500	0.80	115
1000	1.60	46
1500	2.40	24
2500	4.00	9

These final steady-state pressures of course apply only for a Vielle propellant ($\bar{r} = aP^n$), but the same trend shown by this exercise should occur for a real propellant; i.e., the nozzle-area changes that will result in the same initial dP/dt can result in drastic differences in the overall pressure drop depending on differences in the initial L*.

If extinguishment results not only as a result of achieving a critical dP/dt but also because of a large overall pressure drop, these calculations show that differences in motor size can have an important effect on marginal extinguishment conditions. The calculations discussed in the following section indicate that, from the ballistic designer's point of view, a critical overall pressure drop is the most important criterion for achieving extinguishment. They show further that expressing extinguishability of a propellant in terms of a critical dP/dt alone is rather meaningless.

b. Basis for Transient Model Calculations

Parametric calculations showing the effect on marginal extinguishment conditions of varying initial pressure, initial L*, and nozzle opening time were all made using a single set of model propellant parameters. The parameters for the model propellant, designated propellant Y, are listed in Table 15.

TABLE 15. Properties of Theoretical Propellant Y

Burning Rate @ 1000 psia, in/sec	0.400
Burning Rate Exponent @ 1000 psia	0.400
Flame temperature, ^{o}K	3000
Burning Surface Temperature at 1000 psia, ^{o}C	600
Density, ρ, lbm/in^3	.060
Ratio of Specific Heats, γ	1.20
Characteristic Velocity, C*, ft/sec	3000
Surface Activation Energy, E_s, Kcal/mole	20
Gas Activation Energy, E_g, Kcal/mole	20
Solid Heat Capacity/Gas Heat Capacity, C_s/C_g	0.50
Solid Thermal Diffusivity, α, in^2/sec	.00025

Its burning rate is shown, plotted versus pressure, in Figure 21. The corresponding K_n curve is also shown. Since the burning rate exponent ($d\ln\bar{r}/d\ln P$) for most propellants is not constant over wide variations in pressure, a Summerfield burning rate law (35) was assumed.

The reference steady-state motor operating conditions were assumed to be 500 psia, which, with the assumed propellant properties, corresponds to a motor K_n of 186.3. The ambient pressure in all cases was assumed to be 1 psia.

To study the effect of initial pressure variation, calculations were made at 100 psia and 1000 psia in addition to the reference pressure of 500 psia. The initial L* was varied between 10 inches and 5000 inches, and the nozzle opening time was varied between 0.2 milliseconds and 413 milliseconds. For each combination of P_i, L_i^*, and nozzle opening time, the minimum nozzle area change resulting in extinguishment was calculated. The results of all of these calculations are summarized in Table 16.

c. Effect of Varying Initial Pressure

The results of the calculations made to illustrate the effect of varying initial pressure are presented in Figure 22, following the procedure which has been employed by others (6) to correlate $\dot{P}$ extinguishment data. For these calculations, the initial L* was 1000 inches and the opening time was 0.2 milliseconds. The marginal initial depressurization rate is shown to increase uniformly with increasing initial pressure, just as observed experimentally, provided a single motor and propellant configuration is used for each test.

d. Effect of Varying Initial L*

Figure 23 presents the results of calculations in which the initial L* was varied between 100" and 5000", the nozzle opening time being 0.2 milliseconds and the initial pressure being 500 psia in all cases. The data are plotted in a similar manner to those in Figure 22 except that interpolated marginal initial depressuration rate is plotted instead of the points for individual calculations. The marginal depressurization rate is shown to increase uniformly with decreasing L_i^*. The similarity between these results and the experimental data of UTC shown in Figure 12 is quite significant.

e. Effect of Varying Nozzle Opening Time

Increasing the nozzle opening time, the overall nozzle-area change and other parameters remaining constant, naturally resulted in a reduction

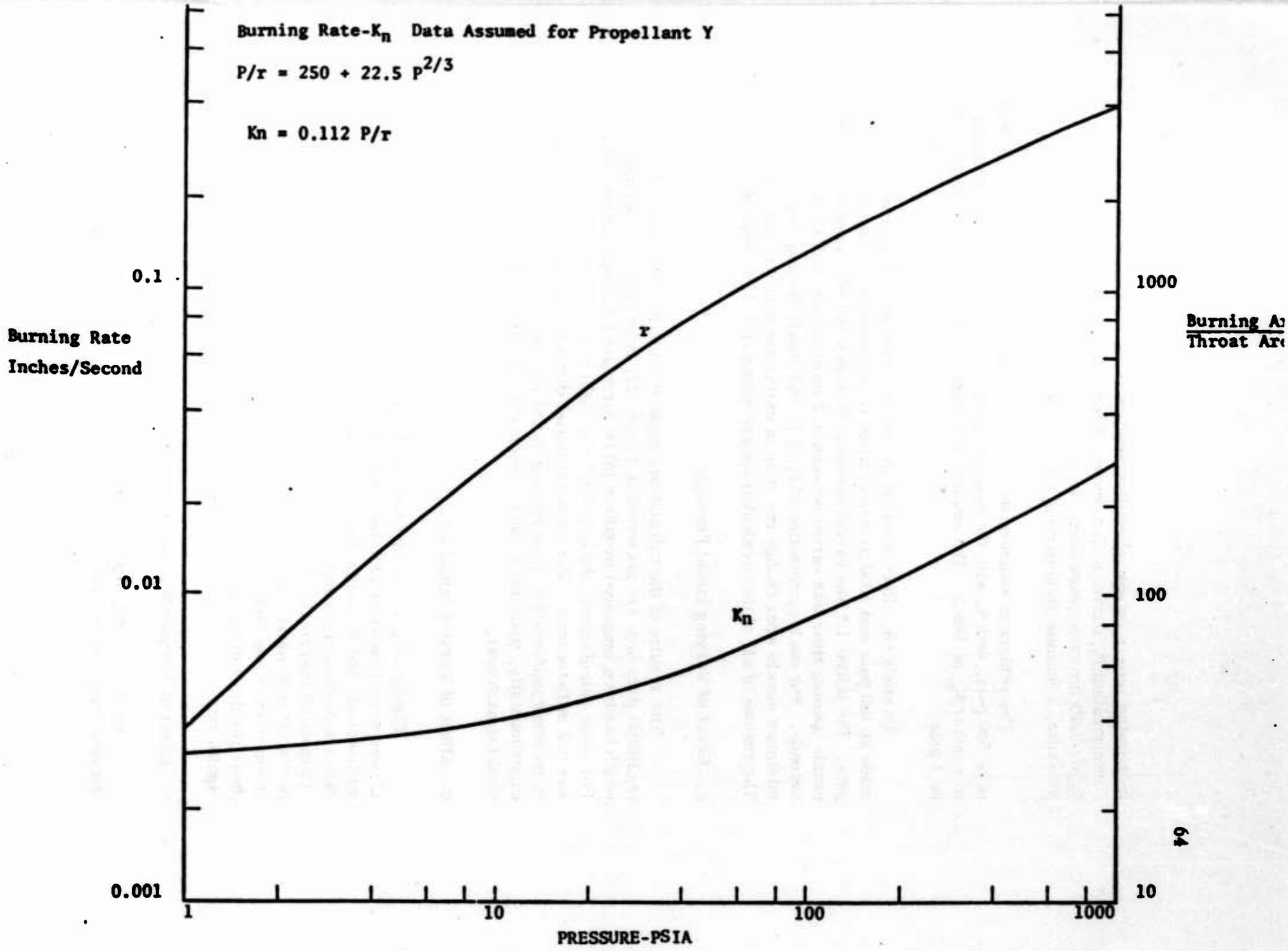

Figure 21. Assumed ballistic properties, K_n and $\bar{r}$ versus pressure, for model propellant Y.

TABLE 16. Summary of Parametric Study Calculations, Propellant Y

Initial L* inches	Opening Time, msec	A_{n_f}/A_{n_i}	L^*_f inches	K_{n_f}	P_f psia	$\bar{r}_f$ in/sec	$(\frac{dlnP}{dt})_i/P_i$	$(\frac{dlnP}{dt})_{max}/P$	Extinguish
				K_{n_i} = 186.3, P_i = 500 psia					
10	0.2	2.0	5.0	93.2	127	.15	1503/98	1500/98	yes
		1.5	6.7	124.3	230	.21	998/200	998/200	yes
		1.2	8.3	155.3	360	.25	375/344	380/344	yes
		1.125	8.8	165.6	400	.27	212/397	310/397	no
	20.4	6.0	1.7	31.1	4	.005	469/387	1050/387	yes
		4.5	2.2	41.4	13	.033	322/418	870/418	yes
		3.375	3.1	55.2	35	.071	209/444	760/444	yes
		2.531	4.0	73.7	75	.114	125/465	550/465	yes
		1.898	5.3	98.2	144	.163	62/480	360/480	yes
		1.423	7.0	130.8	260	.22	16/493	35/493	no
100	0.2	6.0	17.0	31.1	4	.005	870/62	870/62	yes
		4.5	22.0	41.4	13	.033	704/105	700/105	yes
		3.375	30.0	55.2	35	.071	540/163	540/163	yes
		2.531	40.0	73.7	75	.114	357/239	360/239	yes
		2.20	45.0	84.7	104	.138	273/279	340/279	yes
		1.898	53.0	98.2	144	.163	199/323	200/323	no
	20.4	6.0	17.0	31.1	4	.005	116/442	415/47	yes
		4.5	22.0	41.4	13	.033	79/460	359/54	yes
		3.375	30.0	55.2	35	.071	50/474	310/45	yes
		2.531	40.0	73.7	75	.114	29/484	239/46	yes
		1.898	53.0	98.2	144	.163	12/493	66/192	no
	206.5	5.0	20.0	37.3	7.3	.022	24/447	140/447	yes
		3.75	27.0	49.7	26	.057	15/473	130/473	yes
		3.0	33.0	62.1	50	.090	10/489	100/489	yes

TABLE 16. Continued

Initial L^* inches	Opening Time, msec	A_{n_f}/A_{n_i}	L_f^* inches	K_{n_f}	P_f psia	$\bar{r}_f$ in/sec	$(\frac{d\ln P}{dt})_i/P_i$	$(\frac{d\ln P}{dt})_{max}/P$	Extinguish
				K_{n_i} = 186.3, P_i = 500 psia					
250	0.2	6.0	42.0	31.1	1.4	.005	456/190	456/190	yes
		4.5	56.0	41.4	13	.033	335/249	335/249	yes
		3.375	74.0	55.2	35	.071	233/309	233/309	yes
500	0.2	5.5	91.0	33.9	3.5	.012	228/315	230/315	yes
		5.0	100.0	37.3	7.3	.022	205/331	205/331	yes
		4.5	111.0	41.4	13.0	.033	180/348	180/348	yes
		4.0	125.0	46.6	21.0	.049	156/366	156/366	yes
		3.5	143.0	53.3	32.0	.067	130/384	130/384	yes
		3.3	152.0	56.5	39.0	.077	120/393	120/393	yes
		3.1	161.0	60.1	45.0	.084	110/401	110/401	yes
		3.0	167.0	62.1	50.0	.090	105/405	105/405	no
1000	0.2	6.0	167.0	31.1	1.4	.005	134/384	134/384	yes
		5.0	200.0	37.3	7.3	.022	108/404	108/404	yes
		3.75	267.0	49.7	26	.057	75/432	75/434	yes
		3.3	303.0	56.5	39	.077	63/442	63/442	no
		2.812	356.0	66.3	57	.098	50/454	50/454	no
	20.4	6.0	167.0	31.1	1.4	.005	13/494	99/161	yes
		4.5	222.0	41.4	13	.033	9/496	72/223	yes
		3.375	296.0	55.2	35	.071	5/497	50/288	no
	413.0	6.0	167.0	31.1	1.4	.005	2/499	44/12	yes

TABLE 6. Continued

Initial L^* inches	Opening Time, msec	A_{n_f}/A_{n_i}	L_f^* inches	K_{n_f}	P_f psia	$\bar{r}_f$ in/sec	$(\frac{d\ln P}{dt})_i/P_i$	$(\frac{d\ln P}{dt})_{max}/P$	Extinguish
				K_{n_i} = 186.3, P_i = 500 psia					
5000	0.2	6.0	834	31.1	1.9	.005	29/474	29/474	yes
		5.5	909	33.9	5.5	.012	24/391	24/391	yes
		5.0	1000	37.3	7.3	.022	21/401	21/401	yes
		4.0	1250	46.6	21	.049	16/424	16/424	no
				K_{n_i} = 82.0, P_i = 99.8					
1000	1.0	2.0	500	41.0	12	.032	27.9/88	27.9/88	yes
		1.8	556	45.5	18	.047	23.0/99	23.0/99	yes
		1.4	715	58.5	42	.081	11.5/99	11.5/99	no
				K_{n_i} = 280, P_i = 1004					
1000	1.0	5.8	172	48.3	23	.053	136/938	136/938	yes
		5.4	185	51.9	29	.063	125/943	125/943	yes
		5.2	192	53.9	33	.068	101/610	101/610	yes
		4.8	208	58.4	42	.081	96/624	96/624	no
		4.6	217	60.9	48	.088	87/653	87/653	no

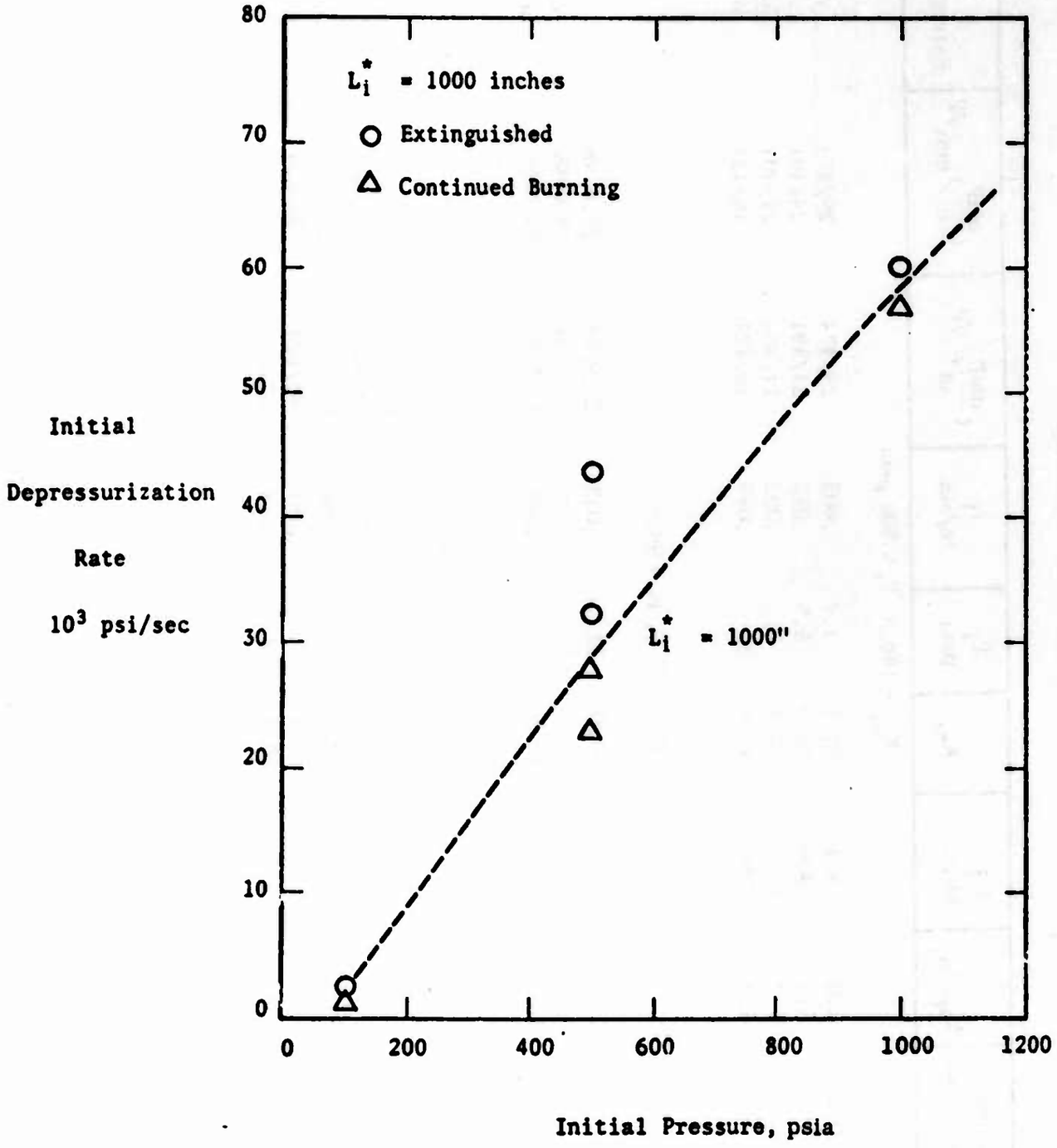

Figure 22. Predicted effect of initial pressure on $\dot{p}$ for marginal extinguishment.

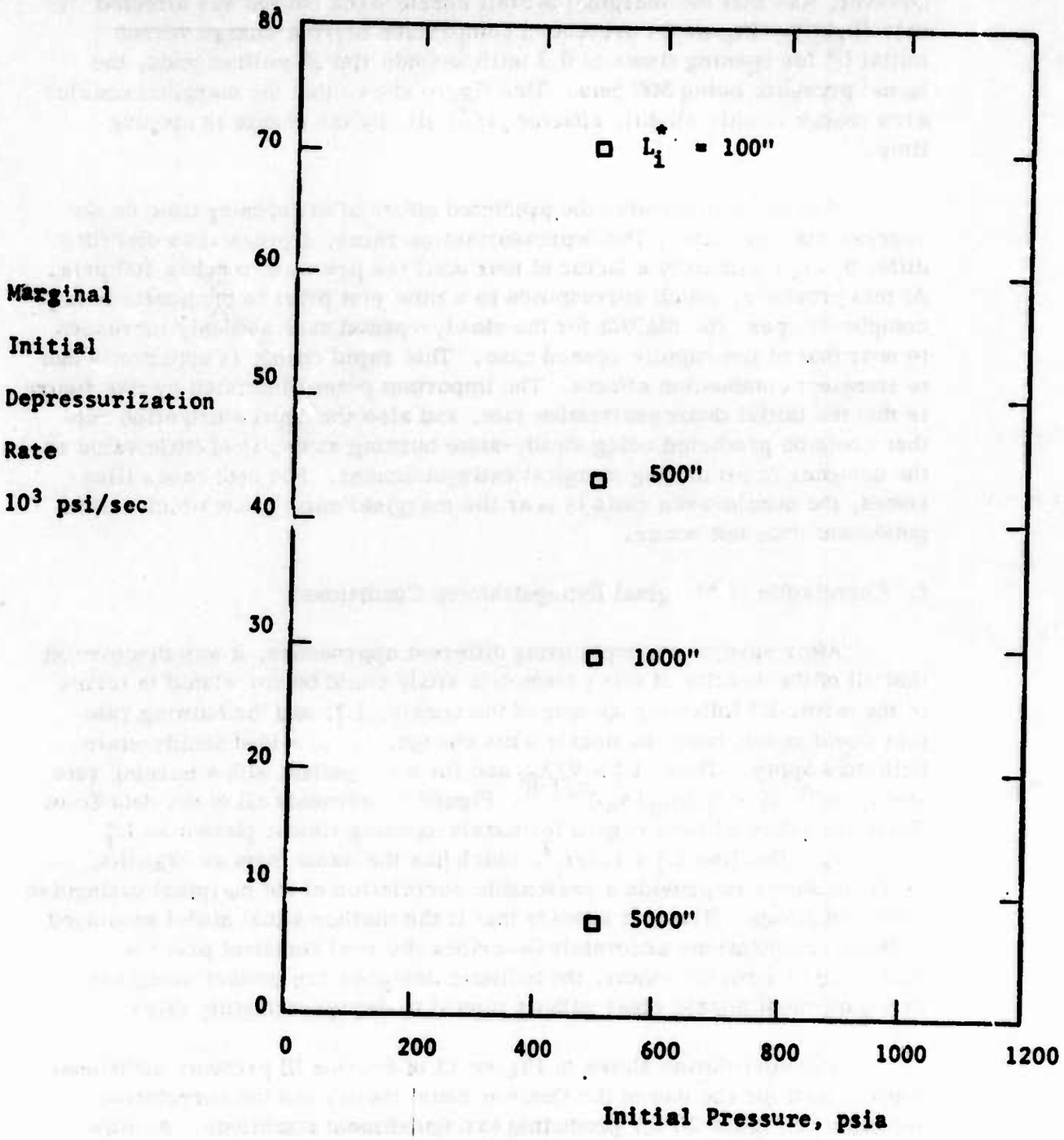

Figure 23. Predicted effect of initial L* on $\dot{P}$ for marginal extinguishment conditions.

in the depressurization rates. The surprising result of these calculations, however, was that the marginal overall nozzle-area change was affected only slightly. Figure 24 presents a comparison of area-change versus initial L^* for opening times of 0.2 milliseconds and 20 milliseconds, the initial pressure being 500 psia. This figure shows that the marginal nozzle-area change is only slightly affected, if at all, by the change in opening time.

Figure 25 illustrates the predicted effect of the opening time on the depressurization rate. The depressurization rates, expressed as dlnP/dt, differ by approximately a factor of four until the pressure reaches 100 psia. At this pressure, which corresponds to a time just prior to the nozzle being completely open, the dlnP/dt for the slowly-opened case suddenly increases to near that of the rapidly-opened case. This rapid change is apparently due to transient combustion effects. The important point illustrated by this figure is that the initial depressurization rate, and also the depressurization rate that would be predicted using steady-state burning rates, is of little value to the designer in predicting marginal extinguishment. For both cases illustrated, the nozzle-area ratio is near the marginal ratio below which extinguishment does not occur.

f. Correlation of Marginal Extinguishment Conditions

After several attempts using different approaches, it was discovered that all of the results of this parametric study could be correlated in terms of the motor L^* following opening of the nozzle, L_f^*, and the burning rate that would result from the nozzle-area change, $\bar{r}_f$, provided steady-state ballistics apply. Thus $L_f^* = V/A_{nf}$ and for a propellant with a burning rate law $\bar{r} = aP^n$, $\bar{r}_f = \bar{r}_i \, (A_{ni}/A_{nf})^{n/1-n}$. Figure 26 presents all of the data from Table 16, taken without regard for nozzle-opening times, plotted as L_f^* versus $\bar{r}_f$. The line $L_f^* = 1.3/\bar{r}_f^2$, which has the same form as Equation (4.2), is shown to provide a reasonable correlation of the marginal extinguishment conditions. Thus, it appears that if the mathematical model employed in these computations accurately describes the real transient process occurring in a rocket motor, the ballistic designer can predict marginal extinguishment nozzle sizes without regard to depressurization rates.

The correlation shown in Figure 13 of Section III presents additional support both for the use of the Denison-Baum theory and the correlative approach of Figure 26 for predicting extinguishment conditions. As was previously noted, Figure 13 contains both theoretically predicted marginal extinguishment conditions and the motor data available with sufficient supporting data. Using the propellant properties of Tables 13 and 15 for the respective flame temperatures, the marginal conditions predicted by the Denison-Baum approach are shown in Figure 13. As delineated by the

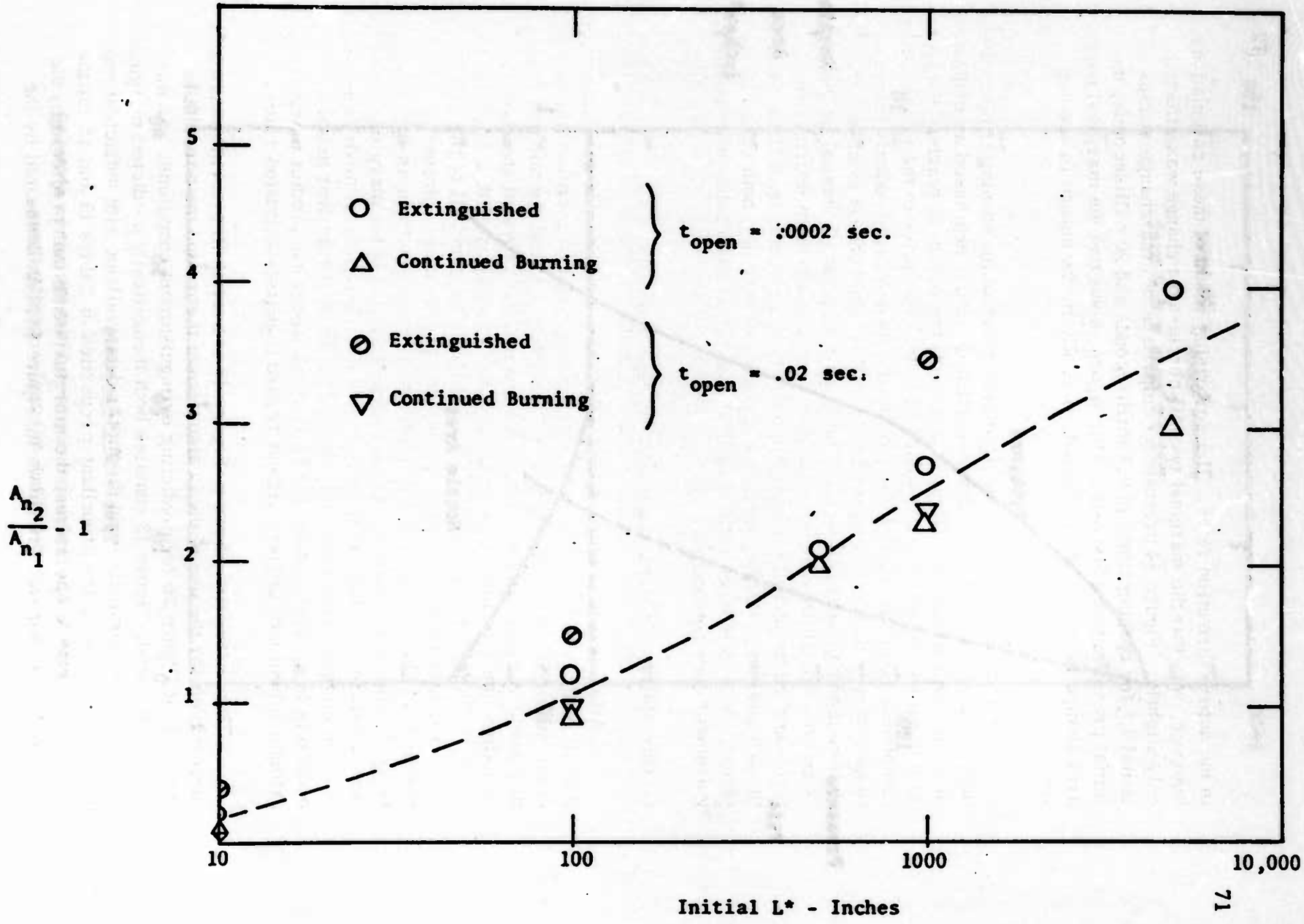

Figure 24. Predicted effect of initial L* and nozzle-opening time on nozzle-area change for marginal extinguishment.

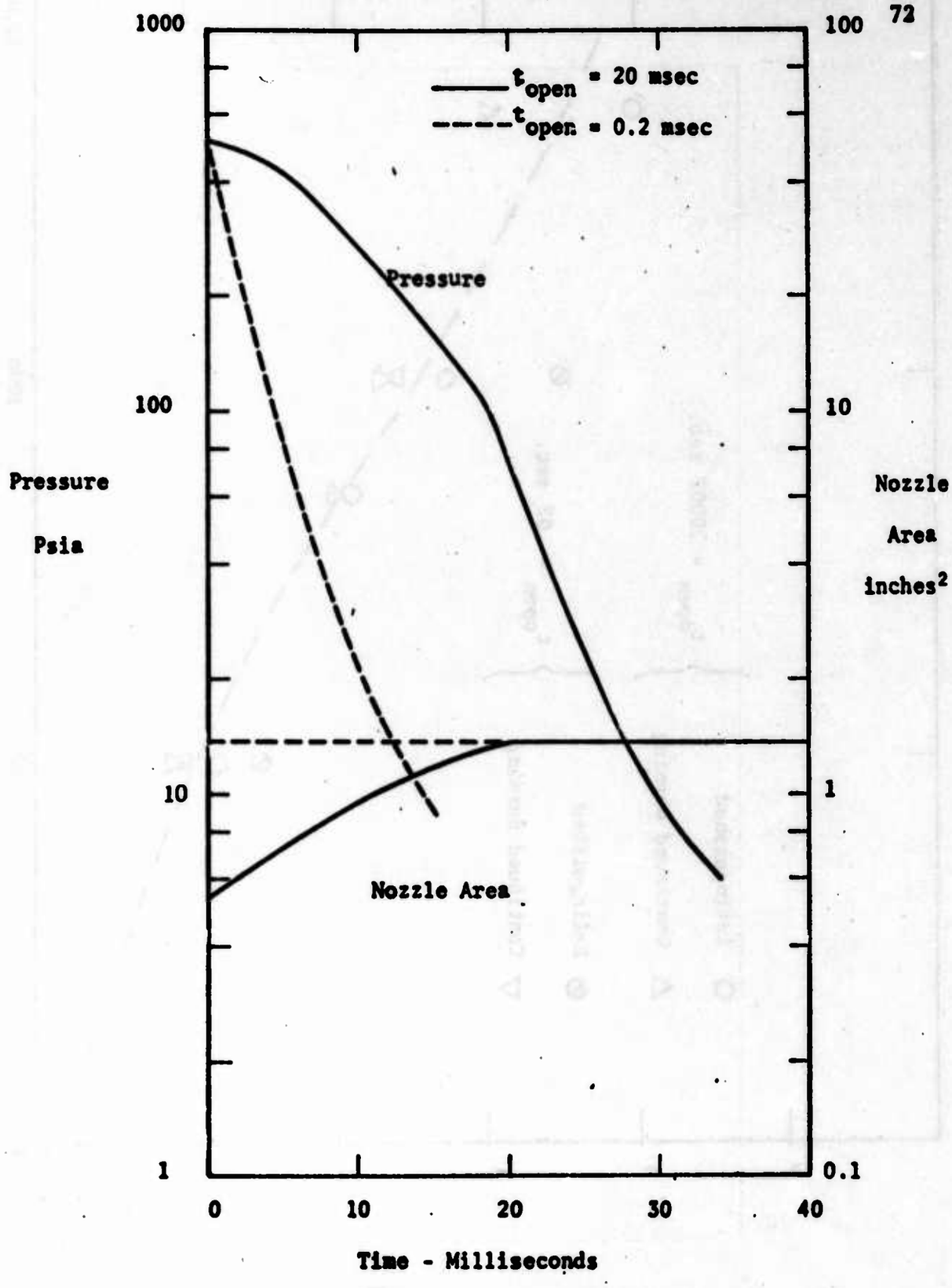

Figure 25. Predicted depressurization curves showing the effect of nozzle-opening times.

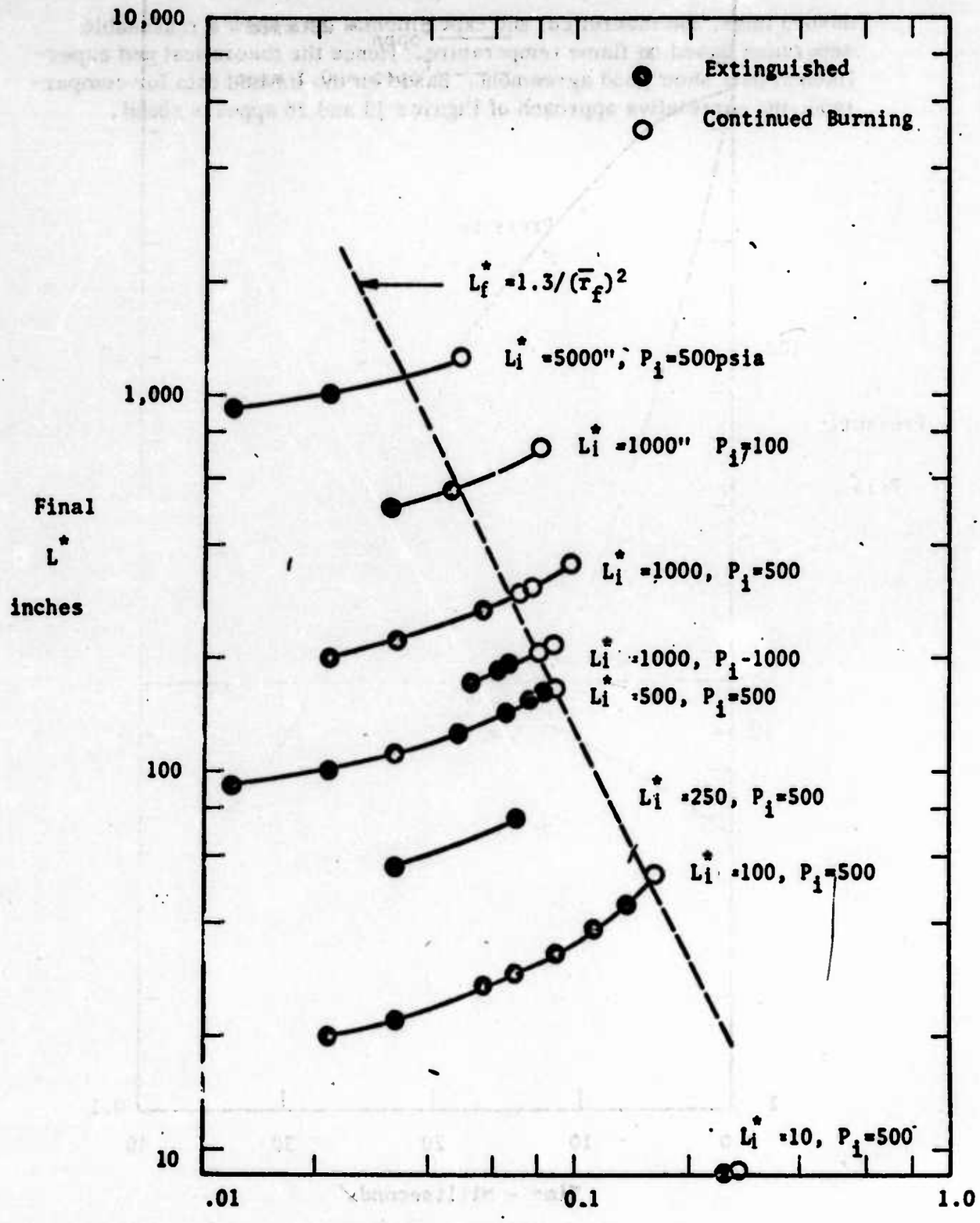

Figure 26. Correlation of parametric study results in terms of steady-state L* and burning rate following the nozzle-area change.

dashed lines, the theoretical and experimental data show a reasonable separation based on flame temperature. Hence the theoretical and experimental data show good agreement. Based on the limited data for comparison, the correlative approach of Figures 13 and 26 appears sound.

V

RECOMMENDED DESIGN PROCEDURES

As a result of the studies carried out during this project, certain recommendations can be made for improving the procedures which have been employed to predict marginal extinguishment conditions in single-chamber controllable motors. These recommendations fall into two categories: (1) those having application to preliminary design calculations, and (2) those having application to experimental development work leading to final designs.

It is cautioned that these recommendations are of a tentative nature. Further parametric studies should be made to investigate the importance of additional operating variables such as conditioning temperature, irregularities in the steady-state burning rates, and the thermodynamic and kinetic properties. More importantly, additional experimental data should be obtained to more fully establish the reliability of the combustion model that has been employed.

It is further pointed out that these recommendations involve only the prediction of marginal extinguishment conditions, and that the problem of reignition following extinguishment has not been considered.

1. Preliminary Design

For carrying out preliminary design studies that include determining optimum operating conditions based on weights of inert motor components, it is recommended that the practice of applying the Von Elbe-Paul theory to define a critical depressurization rate be discontinued. The simple criterion resulting from the study described in Section IV, and applied to existing data in Section III, namely, that extinguishment will occur when

$$L_f^* \bar{r}_f^2 = B \tag{5.1}$$

is recommended. It has shown promise of being applicable regardless of the rate at which the nozzle area is changed, the size and configuration of the motor, and the initial steady-state operating conditions that are imposed. Furthermore, it is extremely easy to apply, requiring only standard steady-state ballistic calculations.

The magnitude of the constant B, which may be interpreted as a parameter characteristic of a given propellant, will typically range from 0.2 to 1.3 when L_f^* is expressed in inches and $\bar{r}_f$ in inches per second, as is shown by the data of Figure 13.

Even though B for different propellants may range from 0.2 to 1.3, the sensitivity of the predicted marginal nozzle-area change to variation in this parameter is rather small, as illustrated in Figure 27. In this Figure the magnitude of the product $L_f^* \bar{r}_f^2$ is plotted versus the corresponding nozzle-area change ratio. The initial pressure for Aerojet General Corp. formulation AAB 3220 is assumed to be 520 psia and the initial L* is taken at 9.55 inches. For this case, the predicted marginal nozzle-area ratio ranges only from 2.8 to 4.0 as B ranges from 0.22 to 1.3. Thus, even assuming the full range uncertainty in B, ignoring flame temperature effects, the uncertainty in the marginal nozzle area ratio is approximately $\pm$20%.

2. Experimental Development Work

The analytical study carried out during this project showed that characterizing the extinguishability of a propellant in terms of a critical initial average depressurization rate provides design information of very limited usefulness.

This kind of marginal extinguishment criterion can be directly applied to full-scale motor design only if the initial L* and pressure of this motor are the same as those used in obtaining the experimental data. A criterion showing promise of much greater generality is given by Equation (5.1). Therefore, it is recommended that the experimental test program be planned with the objective of determining the magnitude of the constant B in this equation.

Using this approach, testing would be carried out in much the same manner as used before to obtain $\dot{P}$ data. However, the important data to be recorded are the burning areas, nozzle areas, combustion chamber volumes, and steady-state pressures.

Since the motor L* appears in the transient ballistic equations along with C*, in the group $L^*/{}^2C^*$, attention should be given to the effective C* that results from small motor tests. If the C* is lower in these firings than anticipated in the full-scale motor, then the B used for the full-scale design should be increased, or

$$B_{FS} = B_{SS} (C^*_{FS}/C^*_{SS})$$

where the subscript FS denotes full scale and the subscript SS denotes sub-scale.

This approach emphasizes the importance of obtaining accurate steady-state burning rate data, particularly at low pressures. A technique to obtain laboratory data more representative of that expected in the full-scale motor is therefore recommended. The tube-furnace approach described in detail in Section II provides useful data and is a recommended technique.

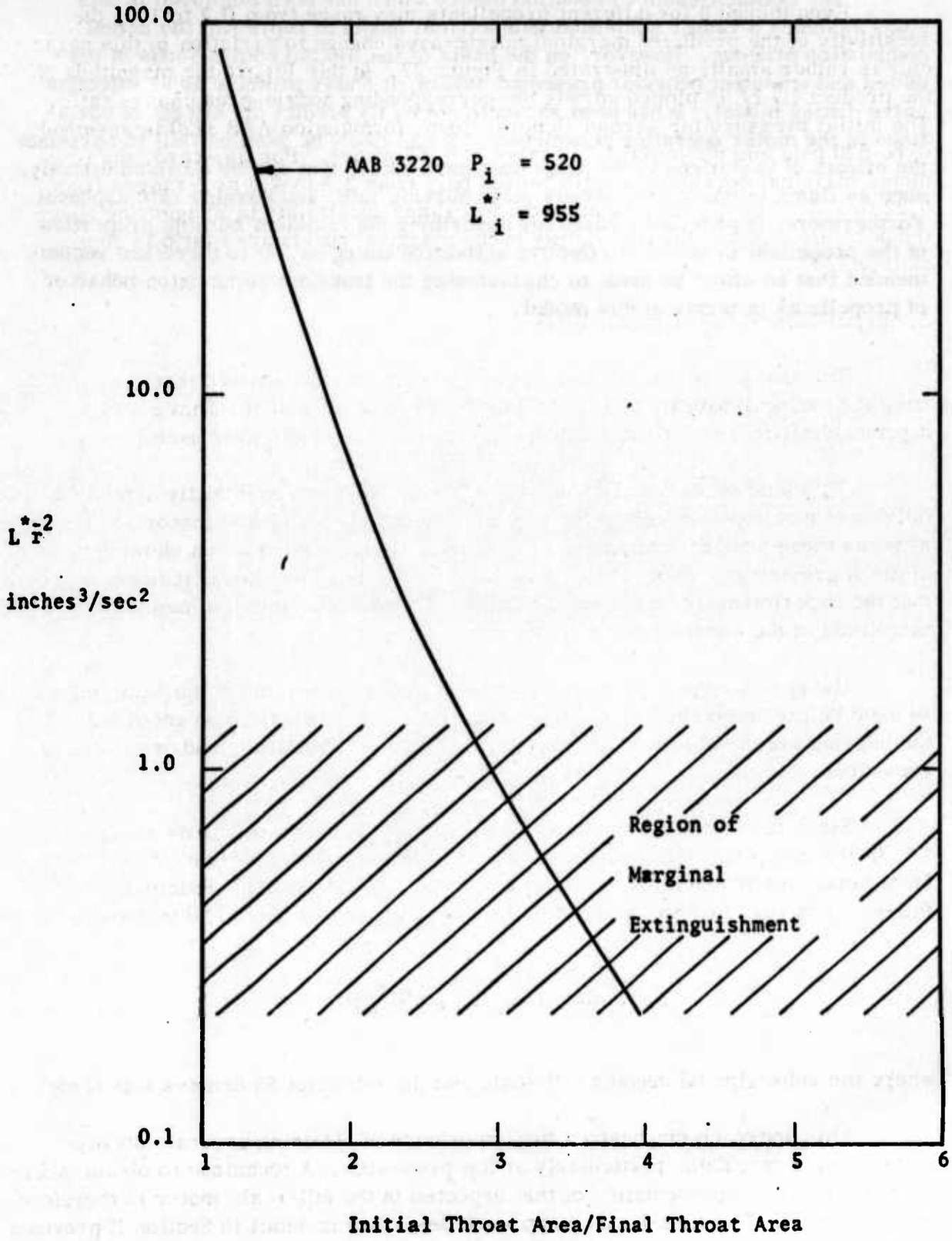

Figure 27. Example showing the variation of the product $L^*\bar{r}^2$ with nozzle-area change illustrating effect of uncertainty in marginal extinguishment criterion.

The Denison-Baum combustion theory which has been employed in this study assumes a rather simplified geometrical model to represent the actual combustion process. However, on the basis of the limited comparisons of predicted and transient behavior presented herein, it shows promise as an effective curve-fitting model. It has been shown to correctly predict the effects of variations in the motor operating parameters. It can likely be used as well to correlate the effects of variations in the propellant parameters that can be obtained directly, such as flame temperature, steady-state burning rate, and burning rate exponent. Furthermore, it provides a basis for describing the transient burning properties of the propellant in terms of effective activation energies. It is therefore recommended that an effort be made to characterize the transient combustion behavior of propellants in terms of this model.

VI

NOMENCLATURE

1. Experimental Data

A_n	Nozzle throat area
B	Constant
C	Heat capacity
C*	Characteristic velocity
E	Activation energy
K_n	Burning area/throat area
k	thermal conductivity
L*	Characteristic length
n	Burning rate exponent = $d\ln\bar{r}/d\ln\bar{P}$
P	Pressure
$\dot{P}$	Rate of depressurization
P_{dl}	Deflagration limit
r	Burning rate
T	Temperature
t	time
$t_{1/2}$	Time to depressurize to $P_i/2$
X	distance
α	Thermal diffusivity
γ	Ratio of specific heats

	Empirical constant
	Density
($\bar{}$)	Bar denotes steady-state

Subscripts

a	Ambient
c	Chamber
f	Flame, final value
g	Gas
i	Initial value
p	Value at pressure p
s	Surface, solid

2. Computer Program

LENGTH Sample length or radius

TIME Measured burn time

ERROR Difference between measured time and time predicted by best fit equation

RBAR Least-squares best fit burning rate

ERROR 95% confidence limit for RBAR (Equation 2.5)

REFERENCES

REFERENCES

1. Levinsky, C. T., "Combustion Problems in Single Chamber Solid Rocket Development," CPIA Publication No. 138, Vol. 1, February, 1967, p.17.

2. "Theoretical and Experimental Study of Extinguishable Solid Propellants," Aerojet General Corporation, Tech. Report No. AFRPL-TR-65-256, 1965-1966.

3. Sabadell, A. J.; Wenograd, J.; and Summerfield, M., "The measurement of Surface Temperatures of Burning Solid Propellants Using Five Thermocouples," AIAA Preprint 64-1106, January, 1964.

4. Powling, J., and Smith, W. A. W., "The Surface Temperature of Burning Ammonium Perchlorate," Combustion Flame, 7, 269-277 (1963).

5. Lockheed Propulsion Co., "Combustion Tailoring Criteria for Solid Propellants," Technical Report AFRPL-TR-69-190, May, 1969, p. 98.

6. Ciepluch, C. C., "Effect of Rapid Pressure Decay on Solid Propellant Combustion," ARS Journal, 31, 1961, pp. 1584-1586.

7. Ciepluch, C. C., "Effect of Composition on Combustion of Solid Propellants Using a Rapid Pressure Decrease," TN D-1559, 1962, NASA.

8. Ciepluch, C. C., "Spontaneous Reignition of Previous Extinguished Solid Propellants," TN D-2167, 1964, NASA.

9. "Controllable Solid Propellant Rocket Motor," Amcel Propellant Company, 2nd Annual Report, RPL DT4 64 52, September, 1964.

10. "Development of an Extinguishable Solid Propellant," Aerojet General Corporation, Final Report, Contract AF04(611)-9889, 1964-1964.

11. "Follow on Propellant Extinguishment Program," Aerojet General Corporation, Contract AF04(611)-9962, 1965-1966.

12. Aerojet General Corporation, Tech Report AFRPL-TR-67-300.

13. Final Report on PSP 10-8, Hercules, Inc., Contract AF 04(694)-127-WS-133A, 1965.

14. Technical Report on Ignition and Combustion of Solid Propellants, University of Utah, AFOSR Final Report, AFOSR 67-1901, September, 1966.

15. "Propellant Combustion Phenomena during Rapid Depressurization," Stanford Research Institute Quarterly and Final Reports, Contract NAS 1-7349, 1965-1967.

16. "A Stop Start Study of Solid Propellants," United Technology Center, Final Report, Contract NAS 1-6601, November, 1967.

17. "An Experimental Study of Solid Propellant Extinguishment by Rapid Depressurization," United Technology Center, Preliminary Final Report, Contract NAS 1-7815, 1969.

18. Horton, M. D.; Bruno, P. S.; and Graesser, E. C., "Depressurization Induced Extinction of Burning Solid Propellants," AIAA Journal, 6 (1968), 292-297.

19. Von Elbe, G., and McHale, E. T., "Extinguishment of Solid Propellants by Rapid Depressurization," AIAA Journal, 6 (1968), 1417-1419.

20. Price, E. W., "Review of Experimental Research on Combustion and Stability of Solid Propellants," Progress in Astronautics and Rocketry, 1st Edition, Academic Press, New York, 1960, pp. 561-602.

21. McCune, C. C., "Solid Propellant Ignition Studies in Shock Propellant Ignition Studies in Shock Tube," unpublished Ph.D. Thesis, University of Utah, Salt Lake City, Utah, 1961.

22. Mitchell, R., "Flame Spread on Solid Propellant," unpublished Ph.D. Thesis, University of Utah, Salt Lake City, Utah, 1963.

23. Donaldson, A. B., "Flame Extinction of Solid Propellants," unpublished Master's Thesis, University of Utah, Salt Lake City, Utah, 1965.

24. "Combustion Instability Studies of Extinguishable Propellants," Hercules, Inc., Quarterly and Final Reports, Contract AF 04(611)-11619, 1967-1968.

25. Levinsky, C. T., "Feasibility Demonstration of a Single Chamber Controllable Solid Rocket Motor, AFRPL-TR-67-300, Aerojet General Corp., January, 1968.

26. McDonald, A. J.; Lamere, G. C.; and Munson, W. D., "Extinguishment and Reignition Analysis of a Large Dual Chamber Propulsion System," Thiokol Report TE9-173-2-9, presented at AIAA 5th Propulsion Joint Specialists Conference, Colorado Springs, Colorado, June, 1969.

27. Von Elbe, G., "Theory of Solid Propellant Ignition and Response to Pressure Transients," Bulletin of the 19th ICRPG Solid Propulsion Conference (CPIA, Silver Springs, Md., 1963), pp. 95-127.

28. Paul, B. E.; Lovine, R. L.; and Fong, L. Y., "A Ballistic Explanation of the Ignition Pressure Peak," AIAA Preprint 64-121, January, 1964.

29. Denison, M. R., and Baum, E., "A Simplified Model of Unstable Burning in Solid Propellants," ARSJ 31, 112-1122 (1961).

30. Brigham Young University, Final Report, AFOSR Grant AF-AFOSR-897-67, March, 1970.

31. Coates, R. L.; Polgien, R. E.; and Price, C. F., "Design Procedures for Combustion Termination by Nozzle Area Variation," J. Spacecraft 3, 419-425 (1966).

32. Conte, S. D., Elementary Numerical Analysis, McGraw-Hill, New York, 1965, pp. 234-238.

33. Draper, N. R., and Smith, H., Applied Regression Analysis, John Wiley and Sons, New York, 1968, p. 19.

34. Cohen, N. S., "A Theory of Solid Propellant Extinguishment by Pressure Perturbation," Proceedings of the Second ICRPG Combustion Conference, Chemical Propulsion Information Agency, Silver Springs, Md., 1963, Publication No. 18, pp. 95-127.

35. Merkle, C. L.; Turk, S. L.; and Summerfield, M., "Extinguishment of Solid Propellants by Rapid Depressurization: Effects of Propellant Parameters," Preprint No. 69-176, AIAA 7th Aerospace Sciences Meeting, New York, January, 1969.

APPENDIXES

APPENDIX I

TABULATION OF BURNING RATE DATA OBTAINED IN THE TUBE-FURNACE APPARATUS

F-107 RADIAL RM TEMP 21 IN HG

LENGTH	TIME	ERROR
0.3950	30.10	2.417
0.3950	28.20	0.517
0.3950	27.10	-0.582
0.3950	27.20	-0.482
0.2400	17.90	0.039
0.2400	16.80	-1.060
0.2400	17.50	-0.360
0.2400	16.40	-1.460
0.2400	16.00	-1.860
0.2400	17.20	-0.660
0.1570	12.40	-0.201
0.1570	15.00	2.398
0.1570	13.50	0.898
0.1570	13.40	0.798
0.1570	12.30	-0.301
0.1570	12.50	-0.101

RBAR = 0.01578
ERROR = 0.00166

E-107 RADIAL 1000 DEG F 21 IN HG

LENGTH	TIME	ERROR
0.3950	16.60	-0.674
0.3950	17.50	0.225
0.3950	17.30	0.025
0.3950	18.30	1.025
0.2400	11.20	0.309
0.2400	10.70	-0.190
0.2400	10.70	-0.190
0.2400	10.70	-0.190
0.2400	10.70	-0.190
0.2400	10.20	-0.690
0.2400	10.30	-0.590
0.1570	6.60	-0.871
0.1570	7.30	-0.171
0.1570	7.60	0.128
0.1570	8.60	1.128
0.1570	6.80	-0.671
0.1570	7.90	0.428
0.1570	7.60	0.128
0.1570	8.50	1.028

RBAR = 0.02427
ERROR = 0.00186

UG RM TEMP 5 IN HG 7/16/69

LENGTH	TIME	ERROR
0.3950	22.00	1.037
0.3950	19.20	-1.767
0.2400	14.20	-0.005
0.2400	15.10	0.894
0.2400	15.80	1.594
0.2400	13.80	-0.405
0.1570	9.30	-1.288
0.1570	11.50	0.913
0.1570	9.70	-0.886
0.1570	10.50	-0.086

RBAR = 0.02294
ERROR = 0.00448

UG 1500 DEG F 10 IN HG RADIAL

LENGTH	TIME	ERROR
0.3950	12.20	-0.306
0.3950	12.50	-0.006
0.3950	12.80	0.293
0.2400	8.20	0.052
0.2400	8.00	-0.147
0.2400	8.30	0.152
0.1570	5.60	-0.212
0.1570	5.60	-0.212
0.1570	6.20	0.387

RBAR = 0.03555
ERROR = 0.00221

UG RM TEMP 15 IN HG RADIAL

LENGTH	TIME	ERROR
0.3950	15.50	-0.044
0.3950	15.80	0.255
0.3950	14.70	-0.844
0.2400	9.70	-0.195
0.2400	10.80	0.904
0.2400	11.00	1.104
0.1570	6.90	0.029
0.1570	5.80	-1.070
0.1570	6.10	-0.770
0.1570	7.50	0.629

RBAR = 0.02743
ERROR = 0.00380

UG RM TEMP 21 IN HG RADIAL

LENGTH	TIME	ERROR
0.3950	9.20	-0.044
0.3950	9.25	0.005
0.3950	9.25	0.005
0.2400	5.60	-0.068
0.2400	5.75	0.081
0.2400	5.75	0.081
0.1570	3.90	0.146
0.1570	3.70	-0.053
0.1570	3.60	-0.153

RBAR = 0.04334
ERROR = 0.00125

UG 1000 DEG F 12 IN HG RADIAL

LENGTH	TIME	ERROR
0.3950	12.00	-0.710
0.3950	11.80	-0.910
0.3950	14.00	1.289
0.2400	9.00	0.351
0.2400	8.70	0.051
0.2400	9.20	0.551
0.1570	6.50	0.026
0.1570	5.90	-0.573
0.1570	6.40	-0.073

RBAR = 0.03815
ERROR = 0.00721

UG 1000 DEG F 21 IN HG RADI.

LENGTH	TIME	ERROR
0.3950	8.70	0.076
0.3950	8.60	-0.023
0.3950	8.50	-0.123
0.2400	5.50	0.033
0.2400	5.50	0.033
0.2400	5.60	0.133
0.1570	3.80	0.023
0.1570	3.70	-0.076
0.1570	3.70	-0.076

RBAR = 0.04910
ERROR = 0.00142

UG (Strand) 1000 DEG F 21 IN HG

LENGTH	TIME	ERROR
0.2950	7.50	0.158
0.2750	7.20	0.265
0.2750	7.00	0.065
0.1050	3.20	-0.276
0.1000	3.30	-0.074
0.1000	3.50	0.125
0.1800	4.90	-0.101
0.1900	5.00	-0.205
0.1930	5.40	0.133
0.4050	9.80	0.221
0.4080	9.80	0.160
0.4920	11.30	-0.048
0.5150	11.60	-0.216
0.4900	11.10	-0.208

RBAR = 0.04915
ERROR = 0.00168

UG 1500 DEG F 21 IN HG RADIAL

LENGTH	TIME	ERROR
0.3950	7.50	0.404
0.3950	6.70	-0.395
0.3950	7.10	0.004
0.2400	4.40	-0.378
0.2400	4.90	0.121
0.2400	5.00	0.221
0.1570	3.70	0.161
0.1570	3.40	-0.138

RBAR = 0.06689
ERROR = 0.01011

UG 150[illegible] DEG F 21 IN HG STRAND

LENGTH	TIME	ERROR
0.2970	3.20	0.064
0.2970	3.00	-0.135
0.2970	2.90	-0.235
0.1600	4.50	0.154
0.1600	4.30	-0.045
0.1600	4.40	0.054
0.3900	9.00	0.237
0.3900	9.00	0.237
0.3900	9.00	0.237
0.4800	10.70	0.209
0.4800	10.40	-0.090
0.4800	9.80	-0.690

RBAR = 0.05206
ERROR = 0.00280

UG RM TEMP 21 IN HG STRAND 9/

LENGTH	TIME	ERROR
0.1060	4.20	0.262
0.0980	4.00	0.232
0.1080	3.50	-0.480
0.2770	7.50	-0.068
0.2700	7.60	0.179
0.2760	7.30	-0.247
0.4810	11.70	-0.200
0.4300	11.20	0.382
0.4650	11.50	-0.000

RBAR = 0.04709
ERROR = 0.00307

GC RM TEMP 10 IN HG RADIAL

LENGTH	TIME	ERROR
0.3950	22.00	-0.030
0.3950	20.50	-1.530
0.3950	23.50	1.460
0.3950	22.30	0.260
0.2400	13.50	-0.901
0.2400	14.70	0.298
0.2400	14.60	0.198
0.1570	10.60	0.288
0.1570	10.10	-0.211
0.1570	10.50	0.188

RBAR = 0.02029
ERROR = 0.00216

AGC 1000 DEG F 21 IN HG RADIAL

LENGTH	TIME	ERROR
0.3950	10.20	-0.461
0.3950	10.70	0.036
0.3950	11.10	0.436
0.2400	6.20	-0.247
0.2400	6.60	0.152
0.2400	6.50	0.052
0.1570	4.10	-0.090
0.1570	4.30	0.109
0.1570	4.20	0.009

RBAR = 0.03677
ERROR = 0.00247

AGC 1000 DEG F 1. IN HG RAD

LENGTH	TIME	ERROR
0.3950	17.00	-0.626
0.3950	18.00	0.373
0.3950	17.70	0.073
0.2400	11.60	-0.093
0.2400	12.30	0.606
0.1570	8.10	-0.416
0.1570	8.60	0.083

RBAR = 0.02612
ERROR = 0.00256

AGC 1500 DEG F 21 IN HG RADIAL

LENGTH	TIME	ERROR
0.3950	10.10	0.561
0.3950	9.70	0.161
0.3950	8.90	-0.638
0.2400	6.10	-0.014
0.2400	6.00	-0.114
0.2400	6.00	-0.114
0.1570	4.40	0.119
0.1570	4.40	0.119
0.1570	4.20	-0.080

RBAR = 0.04526
ERROR = 0.00471

AGC 1500 DEG F 1. IN HG RADIAL

LENGTH	TIME	ERROR
0.3950	17.20	0.434
0.3950	15.50	-1.265
0.3950	16.90	0.134
0.2400	11.50	0.698
0.2400	10.90	0.298
0.2400	11.40	0.798
0.1570	7.00	-0.300
0.1570	6.60	-0.700
0.1570	7.20	-0.100
0.1570	7.10	-0.200

RBAR = 0.02514
ERROR = 0.00284

AGC RM TEMP 21 IN HG STRAND

LENGTH	TIME	ERROR
0.6000	18.70	-0.110
0.6000	18.90	0.089
0.6000	18.50	-0.310
0.4000	13.20	-0.212
0.4000	14.10	0.687
0.4000	13.60	0.187
0.2000	7.70	-0.315
0.2000	8.00	-0.015

RBAR = 0.03705
ERROR = 0.00222

AGC 150[illegible] DEG F 21 IN HG STRAND

LENGTH	TIME	ERROR
0.0970	3.20	-0.085
0.0970	3.10	-0.185
0.1600	4.80	0.114
0.1600	4.90	0.214
0.1600	5.10	0.414
0.3900	8.90	-0.894
0.3900	9.20	-0.594
0.4800	12.00	0.205
0.4800	12.10	0.305
0.4800	12.30	0.505

RBAR = 0.04501
ERROR = 0.00383

AGC 100 DEG F 21 IN HG STRAND

LENGTH	TIME	ERROR
0.5000	14.90	-0.066
0.5000	14.40	-0.566
0.5000	14.70	-0.266
0.3000	10.40	0.700
0.3000	10.20	0.500
0.3000	10.30	0.600
0.1000	4.20	-0.233
0.1000	4.20	-0.233
0.1000	4.00	-0.433

RBAR = 0.03797
ERROR = 0.00297

AGC RM TEMP 21 IN HG PLASTIC TUBE

LENGTH	TIME	ERROR
0.3950	12.80	0.109
0.3950	13.00	0.309
0.3950	12.60	-0.090
0.2500	7.60	-0.388
0.2500	7.60	-0.388
0.2500	8.20	0.211
0.2500	7.90	-0.088
0.2500	7.80	-0.188
0.1570	5.00	0.027
0.1570	5.10	0.127
0.1570	5.10	0.127
0.1570	5.20	0.227

RBAR = 0.03083
ERROR = 0.00148

AGC RM TEMP 21 IN HG STRAND PLASTIC TUBE

LENGTH	TIME	ERROR
0.1300	5.80	-0.369
0.1300	6.40	0.230
0.1300	6.00	-0.169
0.1300	6.20	0.030
0.2130	9.30	0.386
0.2130	8.60	-0.313
0.2130	8.80	-0.113
0.2130	9.00	0.086
0.2800	10.60	-0.528
0.2800	11.50	0.371
0.2800	11.50	0.371
0.2800	11.30	0.171
0.5400	19.80	0.075
0.5400	19.50	-0.224

RBAR = 0.03024
ERROR = 0.00115

A-13 STRAND 100.2 DEG F 21 IN HG

LENGTH	TIME	ERROR
0.5500	17.30	-0.043
0.5500	16.70	-0.643
0.5500	17.10	-0.243
0.3400	12.40	0.593
0.3400	12.30	0.493
0.3400	13.00	1.193
0.1950	7.60	-0.383
0.1950	7.50	-0.483
0.1950	7.50	-0.483

RBAR = 0.03792
ERROR = 0.00458

A-13 STRAND 15.0 DEG F 21 IN HG

LENGTH	TIME	ERROR
0.5500	15.10	-0.729
0.5500	15.40	-0.429
0.5500	15.30	-0.529
0.3400	11.80	1.184
0.3400	11.90	1.284
0.3400	11.70	1.084
0.3400	11.20	0.584
0.1950	6.30	-0.715
0.1950	6.30	-0.715
0.1950	6.00	-1.015

RBAR = 0.04027
ERROR = 0.00723

A-13 STRAND RM TEMP 21 IN HG

LENGTH	TIME	ERROR
0.5500	18.10	0.117
0.5500	17.90	-0.082
0.5500	17.30	-0.682
0.3400	12.90	0.262
0.3400	12.50	-0.137
0.3400	14.10	1.462
0.1950	8.80	-0.146
0.1950	8.40	-0.546
0.1950	8.70	-0.246

RBAR = 0.03928
ERROR = 0.00469

AAP-3318 STRANDS RM TEMP 25 IN HG

LENGTH	TIME	ERROR
0.1950	10.40	-0.002
0.1950	9.40	-1.002
0.1950	9.20	-1.202
0.3900	18.00	2.363
0.3900	16.60	0.960
0.3900	16.70	1.060
0.5860	19.50	-1.457
0.5880	21.50	0.542
0.5880	19.70	-1.257

RBAR = 0.03723
ERROR = 0.00816

AAP-3318 STRANDS 1000 DEG F 25 IN HG

LENGTH	TIME	ERROR
0.1950	6.80	0.128
0.1950	7.30	0.628
0.1950	6.90	0.228
0.3900	12.00	-0.677
0.3900	12.50	-0.177
0.3900	11.40	-1.277
0.5580	17.30	-0.551
0.5580	18.00	0.148
0.5580	19.40	1.548

RBAR = 0.03246
ERROR = 0.00412

AAP-3318 RADIAL 1500 DEG F 25 IN HG

LENGTH	TIME	ERROR
0.2400	6.80	-0.166
0.2400	6.90	-0.066
0.2400	7.20	0.233
0.3950	10.80	0.300
0.3950	10.20	-0.299

RBAR = 0.04386
ERROR = 0.00675

APPENDIX II

FORTRAN CODING AND EXAMPLE OF COMPUTER OUTPUT OF BALLISTICS MODEL CALCULATION

COMPUTER PROGRAM FLOW SHEET

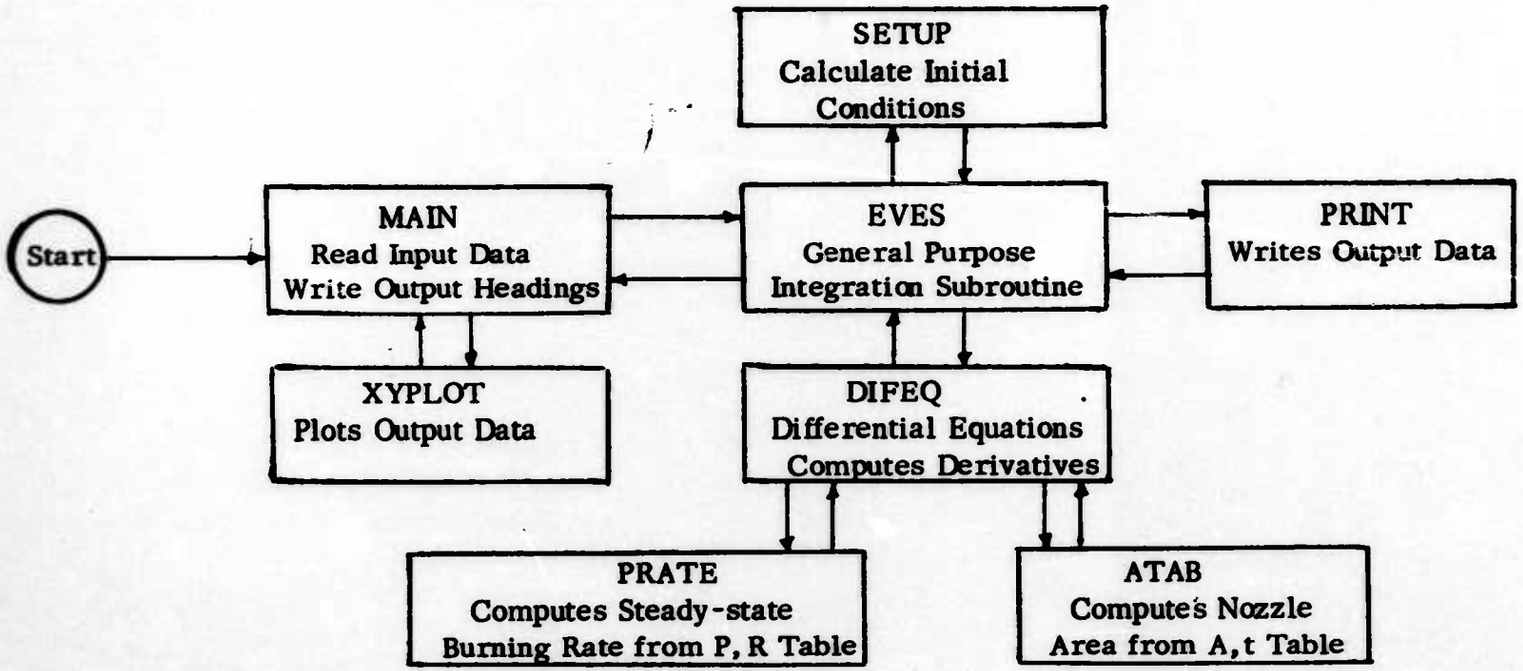

```
      C     MOTOR THRUST TERMINATION
      C      R.L.COATES   REVISED OCTOBER 1969
     1      COMMON TPRNT(6),J1,J2,J3,NPTS,I,
     1     *       TO,PA,AB,XKN,ANR,TOPEN,ELSTAR,EPS,
     1     *       RBAR,RMIN,XNBAR,TFBAR,TSBAR,RHOS,GAM,CSTAR,
     1     *       ES,EG,CSCG,FEXT,ALPHA,
     1     *       CAPGAM,PCRIT,GAMF1,GAMF2,GAMF3,TCHAM,TSOL,BB,DC,TCI,
     1     *       X,P,R,DLPDT,RATE,PRESS,TF,TC,TS,TLAST,DEPTH,AN,XNP,
     1     *       TABLP(8),TABLR(8),RP
     2      COMMON J,TIME(100),PRES(100),TEMP(100),BRATE(100)
     3      DIMENSION NAME(20)
     4      READ(10)0
     5   10 J=0
     6      READ (5,13)NAME
     7   13 FORMAT (20A4)
     8      WRITE(6,16)NAME
     9   16 FORMAT (1H1,20A4)
    10      N=12
    11      READ(5,43) TPRNT(1),TPRNT(2),J1,J2,J3,NPTS
    12   43 FORMAT (2F10.5,4I2)
    13      TPRNT(3)=TPRNT(1)
    14      TPRNT(5)=TPRNT(1)
    15      TPRNT(4)=2.*TPRNT(2)
    16      TPRNT(6)=2.*TPRNT(2)
    17      IF(J2) 45,45,44
    18   44 READ(5,40)TABLP
    19      READ(5,40)TABLR
    20   45 READ (5,40) TO,PA,AB,XKN,ANR,TOPEN,ELSTAR,EPS
    21      READ(5,40) RBAR,RMIN,XNBAR,TFBAR,TSBAR,RHOS,GAM,CSTAR
    22      READ (5,40) ES,EG,CSCG,FEXT,ALPHA
    23   40 FORMAT (8F10.5)
    24      TSOL=ALPHA/(RBAR*RBAR)
    25      DO 30 I=1,6
    26   30 TPRNT(I)=TPRNT(I)/TSOL
    27   41 WRITE (6,42) TO,RBAR,ES,PA,RMIN,EG,AB,XNBAR,CSCG,XKN,TFBAR,FEXT,
    27     *               ANR,TSBAR,ALPHA,TOPEN,RHOS,ELSTAR,GAM ,EPS,CSTAR
    28   42 FORMAT(1H0,10X,'INPUT DATA'//
    28     *       20X,6HTO    =,F10.3,10X,6HRBAR =,F10.3,10X,6HES    =,F10.3/
    28     *       20X,6HPA    =,F10.3,10X,6HRMIN =,F10.3,10X,6HEG    =,F10.3/
    28     *       20X,6HAR    =,F10.3,10X,6HNBAR =,F10.3,10X,6HCSCG =,F10.3/
    28     *       20X,6HKN    =,F10.3,10X,6HTFBAR=,F10.3,10X,6HFEXT =,F10.3/
    28     *       20X,6HANR   =,F10.3,10X,6HTSBAR=,F10.3,10X,6HALPHA=,F10.6/
    28     *       20X,6HTOPEN=,F10.3,10X,6HRHOS  =,F10.3/
    28     *       20X,6HLSTAR=,F10.3,10X,6HGAMMA=,F10.3/
    28     *       20X,6HEPS   =,F10.3,10X,6HCSTAR=,F10.3)
    29      WRITE (6,80)
    30   80 FORMAT-(1H0.3X,'TIME',4X,'PRESSURE',3X,'DLPDT',7X,'RATE',5X,
    30     *'SRATE',5X,'TEMPF',5X,'TEMPC',5X,'TEMPS',6X,'TLAST',4X,'DEPTH',
    30     *4X,'NOZZLE',4X,'EXPONENT')
    31      CALL EVFS (N,TPRNT)
    32      IF(J3) 36,36,34
    33   34 IF(RATE)35,35,36
    34   35 ANR=0.5*ANR
    35      N=12
    36      GO TO 41
    37   36 IF (J1) 60,60,50
    38   50 WRITE (6,16)NAME
    39      CALL XYPLOT (J,50,100,3,TIME,PRES,TEMP,BRATE)
```

```
 40      60  GO TO 10
 41          RETURN
 42          END
```

MESSAGES FOR ABOVE COMPILATION.

VERSION 4 MOD 1

P 026

```
      SUBROUTINE SETUP (T,Y,SIG,N)
      DIMENSION T(2),Y(20),SIG(20)
      COMMON TPRNT(6),J1,J2,J3,NPTS,I,
     *       TO,PA,AB,XKN,ANR,TOPEN,ELSTAR,EPS,
     *       RRAR,RMIN,XNBAR,TFBAR,TSBAR,RHOS,GAM,CSTAR,
     *       ES,EG,CSCG,FEXT,ALPHA,
     *       CAPGAM,PCRIT,GAMF1,GAMF2,GAMF3,TCHAM,TSOL,BB,DD,TCI,
     *       Y,P,R,DLPDT,RATE,PRESS,TF,TC,TS,TLAST,DEPTH,AN,XNP,
     *       TABLP(8),TABLR(8),RP
      COMMON J,TIME(100),PRES(100),TEMP(100),BRATE(100)
C                     REFERENCE PRESSURE IS 1000PSI
C                     REFERENCE RATE IS RATE AT 1000PSI
C                     REFERENCE CONDITIONING TEMP IS 25C
C                     CALCULATE CONSTANTS
      CAPGAM=GAM*(2./(GAM+1.))**((GAM+1.)/(GAM-1.))
      PCRIT=(2./(GAM+1.))**(GAM/(GAM-1.))
      GAMF1=SQRT(2.*GAM/(CAPGAM*(GAM-1.)))
      GAMF2=2./GAM
      GAMF3=(GAM+1.)/GAM
      AA=1.5*(1.0-XNBAR)
      BB=AA/(1.0-AA)
      DD=RHOS*XKN*CSTAR*RRAR/(1000.*32.17)
      TCHAM=ELSTAR/(CAPGAM*CSTAR*12.*DD)
      C1=FG*1000./(2.*1.98)
      I=1
      M=0
      T(1)=0.
C                     CALCULATE APPROXIMATE FLAME TEMP
      TO=TO+273.
      TFRAD=FEXT*CSCG*TO
   10 TF=TFBAR+CSCG*(TO-298.)+TFRAD
      IF(J2) 51,50,52
C                     CALCULATE INITIAL PRESSURE, SUMMERFIELD LAW
   50 XNP=XNBAR
      RT=(TF/TFRAR)**(1.+XNP)*EXP(-C1*(1./TF-1./TFBAR))
      P=(((1.0+BB)*RT*DD-1.)/BB)**1.5
      CC=BB*P**0.667
      XNP=1.0-0.667*CC/(1.+CC)
      RP=P*(1.+BB)/(1.+CC)
      R=RT*RP
C                     ITERATE ON TF
   61 TFRAD=TFRAD/R
      M=M+1
      IF(M-10) 26,26,27
   26 GO TO 10
   27 GO TO 60
C                     CALCULATE INITIAL PRESSURE, VIELLE LAW
   51 XNP=XNBAR
      RT=(TF/TFRAR)**(1.+XNP)*EXP(-C1*(1./TF-1./TFBAR))
      P=RT*DD**(1./(1.-XNP))
      R=P**XNP
      GO TO 61
C                     CALCULATE INITIAL PRESSURE, P,R TABLE
   52 P=1000.
      R=RRAR/DD
   80 CALL PRATE(P,RP,XNP,TABLP,TABLR,NPTS,I)
      RT=(TF/TFRAR)**(1.+XNP)*EXP(-C1*(1./TF-1./TFBAR))
      RP=RT*RP
```

```
      IF(ABS(R-RP)-.0005)  35,35,30
   30 R=RP
      P=1000.*RP*DD/RRAR
      GO TO 80
   35 P=P/1000.
      R=R/RRAR
      GO TO 61
C                    CALCULATE SOLID TEMPERATURES
   60 TSBAR=TSBAR+273.
      TS=TSBAR/(1.-1.98*TSBAR*ALOG(R)/(ES*1000.))
      Y(1)=TS/T0
      T1=1.13393*Y(1)-.13393
      Y(2)=2.*Y(1)-T1
      DO 20 I=3,7
   20 Y(I)=2.*Y(I-1)-Y(I-2)
      Y(8)=(Y(7)+1.)/2.
      Y(9)=P
      Y(10)=R
      Y(11)=TF/TFBAR
      Y(12)=Y(11)
      TCI=TF
      TC=TF
      RETURN
      END
```

MESSAGES FOR ABOVE COMPILATION.

```
C15,T=10  COATES                          FORTRAN DECK 'PRATE    '        10/24/69

    1           SUBROUTINE PRATE(P,RP,XNP,TABLP,TABLR,NPTS,I)
    2           DIMENSION TABLP(8), TABLR(8)
    3         1 IF (TABLP(I)-P) 2,4,4
    4         2 I=I-1
    5           IF (I-1) 3,3,1
    6         3 I=1
    7           GO TO 7
    8         4 IF (TABLP(I+1)-P) 8,5,5
    9         5 I=I+1
   10           IF (I-NPTS)10,6,6
   11         6 I=NPTS-1
   12           GO TO 7
   13        10 IF (TABLP(I+1)-P) 7,5,5
   14         7 XNP=ALOG(TABLR(I+1)/TABLR(I))/ALOG(TABLP(I+1)/TABLP(I))
   15         8 RP=TABLR(I)*(P/TABLP(I))**XNP
   16           RETURN
   17           END


0 MESSAGES FOR ABOVE COMPILATION.

FEQ                                                          026
```

```
      SUBROUTINE DIFEQ (T,Y,DYDX,N,TPR)
      DIMENSION T(2),Y(20),DYDX(20)
      COMMON TPRNT(6),J1,J2,J3,NPTS,I,
     *       TO,PA,AB,XKN,ANR,TOPEN,ELSTAR,EPS,
     *       RBAR,RMIN,XNBAR,TFBAR,TSBAR,RHOS,GAM,CSTAR,
     *       FS,EG,CSCG,FEXT,ALPHA,
     *       CAPGAM,PCRIT,GAMF1,GAMF2,GAMF3,TCHAM,TSOL,BB,DD,TCI,
     *       X,P,R,DLPDT,RATE,PRESS,TF,TC,TS,TLAST,DEPTH,AN,XNP,
     *       TABLP(8),TABLR(8),RP
      COMMON J,TIME(100),PRES(100),TEMP(100),BRATE(100)
      X=T(1)*TSOL
      P=Y(9)
      R=Y(10)
      RATE=RBAR*Y(10)
      PRESS=1000.*Y(9)
      TF=TFBAR*Y(11)
      TC=TFBAR*Y(12)
C                     CALCULATE NOZZLE AREA
      IF (X-TOPEN) 30,30,40
   30 AN=AB/XKN*(1.0+(ANR-1.0)*X/TOPEN)
      GO TO 41
   40 AN=AB/XKN*ANR
   41 A=AN/(DD*AB/XKN)
C                     CHECK FOR EXTINGUISHMENT
      IF (RATE-RMIN) 10,10,20
   10 RATE=0.
      N=0
      CALL PRINT(T,Y,DYDX,N,TPR)
      RETURN
   20 CONTINUE
C                     CALCULATE SURFACE FLUX
      FS=P*(Y(1)-1.+CSCG*(TFBAR+TO-298.-TF)/TO)+FEXT
C                     CALCULATE SURFACE TEMP CHANGE
      T1=Y(2)+0.26786*FS/R
      DYDX(1)=56.*R*R*(T1-2.0*Y(1)+Y(2))
C                     CALCULATE RATE CHANGE
      C2=1000.*FS/(1.98*TO)
      DR=R*C2*DYDX(1)/(Y(1)*Y(1))
C                     CALCULATE PRESSURE CHANGE
      RNC=SQRT(TF/TCI)*P*A
   60 PRAT=PA/PRESS
      IF(PRAT-PCRIT) 55,55,48
   48 PRATF=PRAT**GAMF2-PRAT**GAMF3
      IF (PRATF) 49,49,50
   49 RS=0.
      GO TO 51
   50 RS=RNC*EPS*GAMF1*SQRT(PRATF)
      IF (RS-RNC) 51,51,55
   51 RN=RS
      GO TO 70
   55 RN=RNC
   70 DP=TSOL/TCHAM *GAM*TC/TCI*R*(TF/TC-RN/R)
C                     CALCULATE CHAMBER TEMP CHANGE
      DTC=(TSOL/TCHAM)*TC/P*TC/TCI*R*(GAM*TF/TC-1.+(1.-GAM)*RN/R)
      IF(J2) 75,76,77
C                     CALCULATE RP,XNP  SUMMERFIELD LAW
   76 CC=RR*P**0.667
      XNP=1.0-0.667*CC/(1.+CC)
```

```
819,T=10  COATES                          FORTRAN DECK 'DIFEQ   '        10/24/69

   45          RP=P*(1.+BR)/(1.+CC)
   46          GO TO 80
               C                    CALCULATE RP,XNP   VIELLE LAW
   47        75  XNP=XNBAR
   48          RP=P**XNP
   49          GO TO 80
               C                    CALCULATE RP,XNP   R,P TABLE
   50        77  P=1000.*P
   51          CALL PRATE(P,RP,XNP,TABLP,TABLR,NPTS,I)
   52          RP=RP/RRAR
   53          P=P/1000.
   54            GO TO 80
               C                    CALCULATE FLAME TEMP CHANGE
   55        80  ETA=1.+XNP+1000.*EG/(3.96*TF)
   56          DTF=TF/ETA*(DR/R-XNP*DP/P)
               C                    CALCULATE SOLID TEMP CHANGE
   57          DYDX(2)=42.*R*R*(Y(1)-2.*Y(2)+Y(3))-0.4615*(Y(3)-Y(1))*DR/R
   58          DYDX(3)=30.*R*R*(Y(2)-2.*Y(3)+Y(4))-0.8442*(Y(4)-Y(2))*DR/R
   59          DYDX(4)=20.*R*R*(Y(3)-2.*Y(4)+Y(5))-1.1323*(Y(5)-Y(3))*DR/R
   60          DYDX(5)=12.*R*R*(Y(4)-2.*Y(5)+Y(6))-1.3020*(Y(6)-Y(4))*DR/R
   61          DYDX(6)= 6.*R*R*(Y(5)-2.*Y(6)+Y(7))-1.3114*(Y(7)-Y(5))*DR/R
   62          DYDX(7)= 2.*R*R*(Y(6)-2.*Y(7)+Y(8))-1.0619*(Y(8)-Y(6))*DR/R
   63          DYDX(8)=.091*R*R*(Y(7)-2.*Y(8)+1.) -0.2357*(1.0-Y(7))*DR/R
   64          DYDX(9)=DP
   65          DYDX(10)=DR
   66          DYDX(11)=DTF/TFRAR
   67          DYDX(12)=DTC/TFRAR
   68          RETURN
   69          END

NO MESSAGES FOR ABOVE COMPILATION.

PRINT                                                          026
```

```
15,T=10  COATES                          FORTRAN DECK 'PRINT  '          10/24/69

  1           SUBROUTINE PRINT (T,Y,DYDX,N,TPR)
  2           DIMENSION T(2),Y(20),DYDX(20),TPR(2)
  3           COMMON TPRNT(6),J1,J2,J3,NPTS,I,
  3          *       TO,PA,AB,XKN,ANK,TOPEN,ELSTAR,EPS,
  3          *       RBAR,RMIN,XNBAR,TFBAR,TSBAR,RHOS,GAM,CSTAR,
  3          *       ES,EG,CSCG,FEXT,ALPHA,
  3          *       CAPGAM,PCRIT,GAMF1,GAMF2,GAMF3,TCHAM,TSOL,BB,DD,TCI,
  3          *       X,P,R,DLPDT,RATE,PRESS,TF,TC,TS,TLAST,DEPTH,AN,XNP,
  3          *       TABLP(8),TABLR(8),RP
  4           COMMON J,TIME(100),PRES(100),TEMP(100),BRATE(100)
  5           TS=TO*Y(1)-273.
  6           TLAST=TO*Y(8)-273.
  7           DEPTH=ALPHA/RBAR*2.593/R
  8           DLPDT=DYDX(9)/(P*TSOL)
  9           SRATE=RP*RBAR
 10      14   WRITE (6,15) X,PRESS,DLPDT,RATE,SRATE,TF,TC,TS,TLAST,DEPTH,AN,XNP
 11      15   FORMAT (F10.5,F10.2,3F10.4,2F10.1,2F10.2,2F10.5,F10.4)
 12           TSTOP=TPRNT(2)*TSOL
 13           IF (X.GE.TSTOP)  N=0
 14           J=J+1
 15           TIME(J)=X
 16           PRES(J)=P
 17           TEMP(J)=Y(12)
 18           BRATE(J)=R
 19           RETURN
 20           END


MESSAGES FOR ABOVE COMPILATION.

 VERSION 4 MOD 1
```

Unclassified
Security Classification

DOCUMENT CONTROL DATA - R & D

(Security classification of title, body of abstract and indexing annotation must be entered when the overall report is classified)

1. ORIGINATING ACTIVITY (Corporate author) Brigham Young University Chemical Engineering Dept. Provo, Utah 84601	2a. REPORT SECURITY CLASSIFICATION unclassified 2b. GROUP

3. REPORT TITLE
Improved Design Procedures for Thrust Termination of Solid Propellant Motors

4. DESCRIPTIVE NOTES (Type of report and inclusive dates)
Scientific, Final, 1 Feb. 1969 to 1 Feb. 1970.

5. AUTHOR(S) (First name, middle initial, last name)
Ralph L. Coates
M. Duane Horton

6. REPORT DATE	7a. TOTAL NO. OF PAGES	7b. NO. OF REFS
1 May, 1970	97	32

8a. CONTRACT OR GRANT NO.	9a. ORIGINATOR'S REPORT NUMBER(S)
F04611-69-C-0045 new b. PROJECT NO. c. d.	9b. OTHER REPORT NO(S) (Any other numbers that may be assigned this report)

10. DISTRIBUTION STATEMENT
This document is subject to special export controls and each transmitted to foreign governments or foreign nationals may be made only with prior approval of (AFRPL/STINFO), Edwards, California 93523

11. SUPPLEMENTARY NOTES	12. SPONSORING MILITARY ACTIVITY
	Air Force Rocket Propulsion Lab. RPMCP Edwards, California 93523

13. ABSTRACT

The objective of this project was to carry out both experimental and analytical studies leading to improved design procedures for predicting thrust termination of single-chamber controllable solid motors. The experimental work consisted of measuring quantitatively the effects of incident thermal radiation on low pressure burning rates and deflagration limits of typical solid propellants. A technique was developed in which small cylindrical samples of the propellant were burned inside an electrically heated tube furnace. At furnace wall temperatures corresponding to the interior surfaces of a rocket motor, the burning rates were observed to be as much as 50% greater at 10psia than they were when measured in the conventional strand burner configuration. Analytical work was performed using an improved mathematical model of the transient combustion process of a solid propellant. This study led to the conclusion that experimentally characterizing the extinguishability of a propellant in terms of a critical dp/dt provided very little useful design information. On the other hand, characterizing extinguishing in terms of the product $L^*r_c^2$ was shown to provide a design criteria with the promise of very general applicability.

DD FORM 1 NOV 68 1473

Security Classification

14. KEY WORDS	LINK A		LINK B		LINK C	
	ROLE	WT	ROLE	WT	ROLE	WT
Solid Propellant						
Combustion						
Rocket Motor						
Characteristic Length						
Burning Rate						
Extinquishment						
Depressurization						
Depressurization						
Deflagration Limit						
Nozzle Area						